

PhD dissertation

Jakub Wawrzyniak

Laser modification of the titania-based electrodes for energy conversion

Supervisor

Katarzyna Siuzdak, PhD, DSc

Associate professor IMP PAN

Gdańsk 2022

Funded by the Polish National Science Centre via grant no. 2017/26/E/ST5/00416



NATIONAL SCIENCE CENTRE
POLAND

Table of contents

List of acronyms and abbreviations	5
Abstract	6
Abstrakt	7
Aims and objectives	8
Chapter one	9
Anodization and oxide growth	9
Work one: The geometry of free-standing titania nanotubes as a critical factor controlling their optical and photoelectrochemical performance.....	15
Chapter two	30
Laser interactions with matter	30
Work two: Formation of the hollow nanopillar arrays through the laser-induced transformation of TiO ₂ nanotubes	32
Chapter three	45
Electrochemical water-splitting.....	45
Work three: Spectacular Oxygen Evolution Reaction Enhancement through Laser Processing of the Nickel-Decorated Titania Nanotubes	47
Work four: Nanostructure of the laser-modified transition metal nanocomposites for water splitting	55
Summary	65
List of references	68
Statements of contribution	75
Scientific contribution of the candidate	89
Research papers.....	89
Conference appearances	91
Patents and utility models	91
Stipends and awards	91

List of acronyms and abbreviations

ACL	– anion-contaminated layer
E _{bg}	– energy bandgap
HER	– hydrogen evolution reaction
NTs	– nanotubes
OER	– oxygen evolution reaction
SEM	– scanning electron microscope
TEM	– transmission electron microscope
TiO ₂	– titanium dioxide
TiO ₂ NTs	– titanium dioxide nanotubes
XPS	– X-ray photoelectron spectroscopy
XRD	– X-ray diffraction

Abstract

The following dissertation contains a comprehensive study of the synthesis steps necessary to create electrodes for water electrolysis based on titania nanotubes using scalable processing and modification techniques. The presented work is divided into three chapters, each outlining one of the crucial steps of the process. The first chapter delves into the mechanism of the formation of titania nanotubes, as well as the analysis of parameters critical for their growth. It further analyzes the size-dependent effects of the nanotubes based on the experimental data. Chapter two discusses the interactions of the pulsed nanosecond laser with the matter, and consequently, with the titania nanotubes. The impact of three different laser wavelengths is analyzed and the physical changes in the material are noted. Moreover, the novel method for creating titania capsules from the nanotubes is described. The final chapter discusses the basis of electrochemical water-splitting and the requirements for the electrode materials. The obtained, laser-treated electrodes covered with transition metal species are evaluated for hydrogen- and oxygen evolution reactions. Moreover, the theory encompassing the role of the particular metal species as well as the effects of the laser treatment is derived from the experimental results and literature data. The findings of this dissertation can be used to design and produce more efficient electrodes while utilizing commonly available technologies.

Abstrakt

Poniższa rozprawa zawiera kompleksowy opis procesu wytwarzania wydajnej elektrody do rozkładu wody bazując na modyfikowanym metalami przejściowymi tlenku tytanu z użyciem impulsowej wiązki laserowej. Ze względu na szerokość poruszanych zagadnień, praca została podzielona na trzy rozdziały, z których każdy opisuje konkretny etap wytwarzania. W pierwszym rozdziale opisany został mechanizm anodyzacji folii tytanowej i wyznaczone zostały najistotniejsze parametry wpływające na jej przebieg. Bazując na danych eksperymentalnych, opisany został wpływ geometrii otrzymanych nanostruktur na ich właściwości fizyczne i chemiczne. Drugi rozdział skupia się na oddziaływaniach nanosekundowego lasera z podłożem z warstwą uporządkowanych nanorurek tlenku tytanu. Porównane jest oddziaływanie trzech różnych długości fali na podstawie zmian w geometrii modyfikowanych nanostruktur, jak również różnicy we właściwościach fizycznych i chemicznych materiału. Ponadto, po raz pierwszy została opracowana metoda laserowego zamykania nanorurek. Ostatni rozdział opisuje wymagania, które musi spełnić materiał, aby możliwy był efektywny rozkład wody. Wytworzone elektrody, które zostały zmodyfikowane metalami przejściowymi i wiązką laserową zostały poddane ewaluacji pod kątem zdolności do wytwarzania tlenu jak i wodoru. Ponadto, bazując na literaturze oraz wynikach eksperymentalnych zaproponowano mechanizm przeniesienia ładunku oparty na teorii złącza p-n, uwzględniający zarówno funkcję lasera jak i różnice wynikające z zastosowania różnych metali przejściowych. Sumarycznie, oddziaływania opisane w rozprawie mogą mieć zastosowanie w projektowaniu coraz wydajniejszych elektrod do rozkładu wody.

Aims and objectives

Due to the rising worldwide demands for clean and affordable devices for hydrogen production, the primary aim of the research undertaken in the following dissertation was to create an electrode material for efficient water splitting. The work described herein tackles the subject by following the three main objectives:

- Preparation of the substrate material consisting of the free-standing titania nanotubes and evaluation of their properties,
- Optimization of the processing parameters of the pulsed nanosecond laser for modification of the titania substrates,
- Introduction of the sputtered transition metals from the 4th period to the surface of the electrodes and their evaluation for water electrolysis.

The secondary goal of the thesis was to fill the gaps of knowledge in fundamental research related to the topics involved in the dissertation. These include: exploring the dependence between anodization parameters and properties of the grown titania nanotubes, investigating pulsed laser interactions with titania nanotubes, and analyzing the mechanism of water splitting on the metal-oxide electrodes.

Chapter one

Anodization and oxide growth

Titanium dioxide or TiO_2 is a common mineral that, despite having multiple polymorphs, is most commonly used in its crystalline phase called anatase, due to its stability in normal conditions. Because of the naturally forming oxygen vacancies in its crystal lattice, the anatase TiO_2 is an intrinsic n-type semiconductor with a bandgap of 3.2 eV in the bulk material [1]. It is mostly known for its good corrosion resistance [2], biocompatibility [3], and photoactivity in UV light [4]. However, one of the most interesting properties of titania is its ability to form hollow cylindrical shapes when created through the oxidation of titanium. Although they were first created nearly four decades ago by Assefpour-Dezfuly et al. [5], the titania nanotubes fascinate scientists to this day, finding applications in, for example, water treatment [6], dye-sensitized solar cells [7], and implants [8]. Although there are few other ways to synthesize titania nanotubes (TiO_2NTs) [5,9], the anodization of the titanium foil remains the most common method nowadays as it allows for relatively simple control over the final geometry of the nanotubes. The process itself relies on the forced current flow between two electrodes through the conducting medium, where the cathode typically consists of platinum and the titanium foil positioned as an anode is being oxidized (Figure 1).

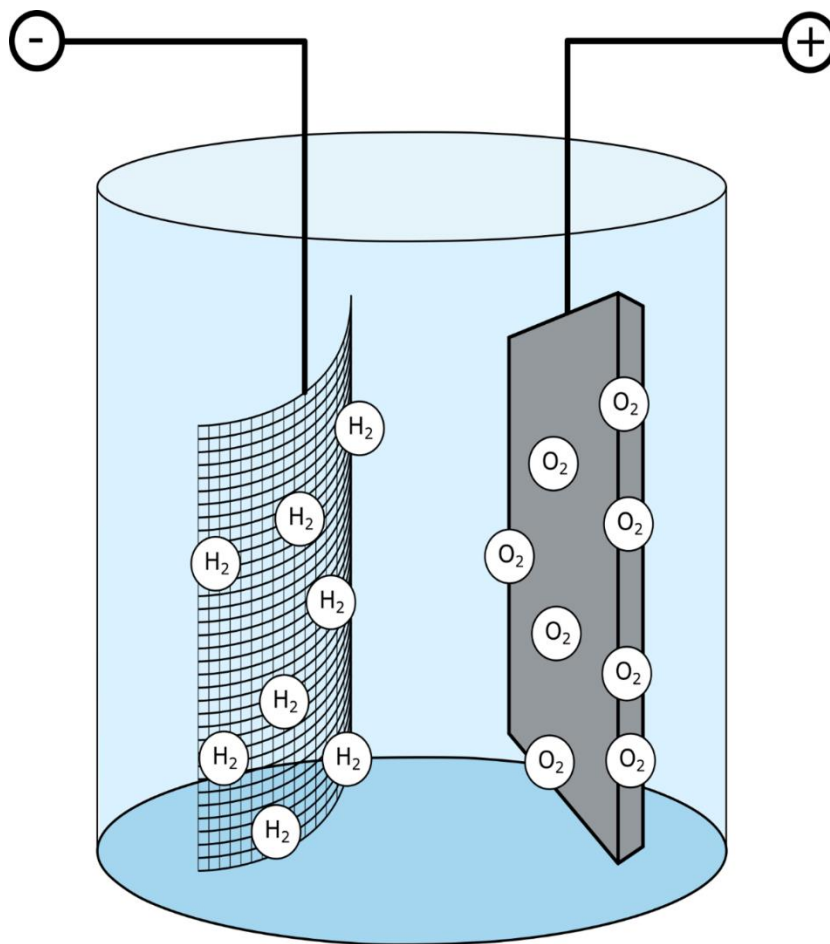


Figure 1: Scheme of a typical two-electrode system used in anodization of titania

The exact mechanism of nanotube formation, however, to this day remains a point of contention among researchers. The most common theory suggests a state of equilibrium between the formation of the oxide layer and its dissolution, where the tubular forms are created through random cracks. Here, the applied electric field facilitates the movement of the $\text{Ti}^{4+}/\text{O}^{2-}$ ions through the oxide, especially in places where the cavities are formed. Later in the process, the field-assisted oxidation within the nanotubes should equalize with their dissolution rate. However, the formation of randomly dispersed crevices does not align with the even distribution of the nanotubes or the formation of spaces between individual nanostructures [10]. Furthermore, the alternative route of the formation of the nanotubes has been supported by recent discoveries [11–14].

In the so-called “bubble mold” model, three stages of growth of the nanotubes can be distinguished (Figure 2). In the first phase, the rapidly decaying anodization current can be attributed to the flow of Ti^{4+} and O^{2-} ions that create the barrier oxide layer [15], thus self-limiting their diffusion rate. The oxide is shown to grow both in the direction of the titanium substrate and the electrolyte, however, the part grown closer to the solution becomes contaminated with fluoride and hydroxide anions. As the process enters stage two, the oxygen evolution between barrier oxide and anion contaminated layer (ACL) gives rise to the proto-bubbles which, when expanding, deform neighboring oxides. This corresponds to the rise of the electronic current and the release of the bubbles breaking through the overlying oxide layer. The electrolyte then fills the pits, creating more anion-contaminated layer at its bottom. In the last stage, consecutive oxide bubbles evolving at the bottom of the cavities still exert pressure when growing, creating a stress-induced plastic flow of the oxide, which forms the walls of the nanotubes.

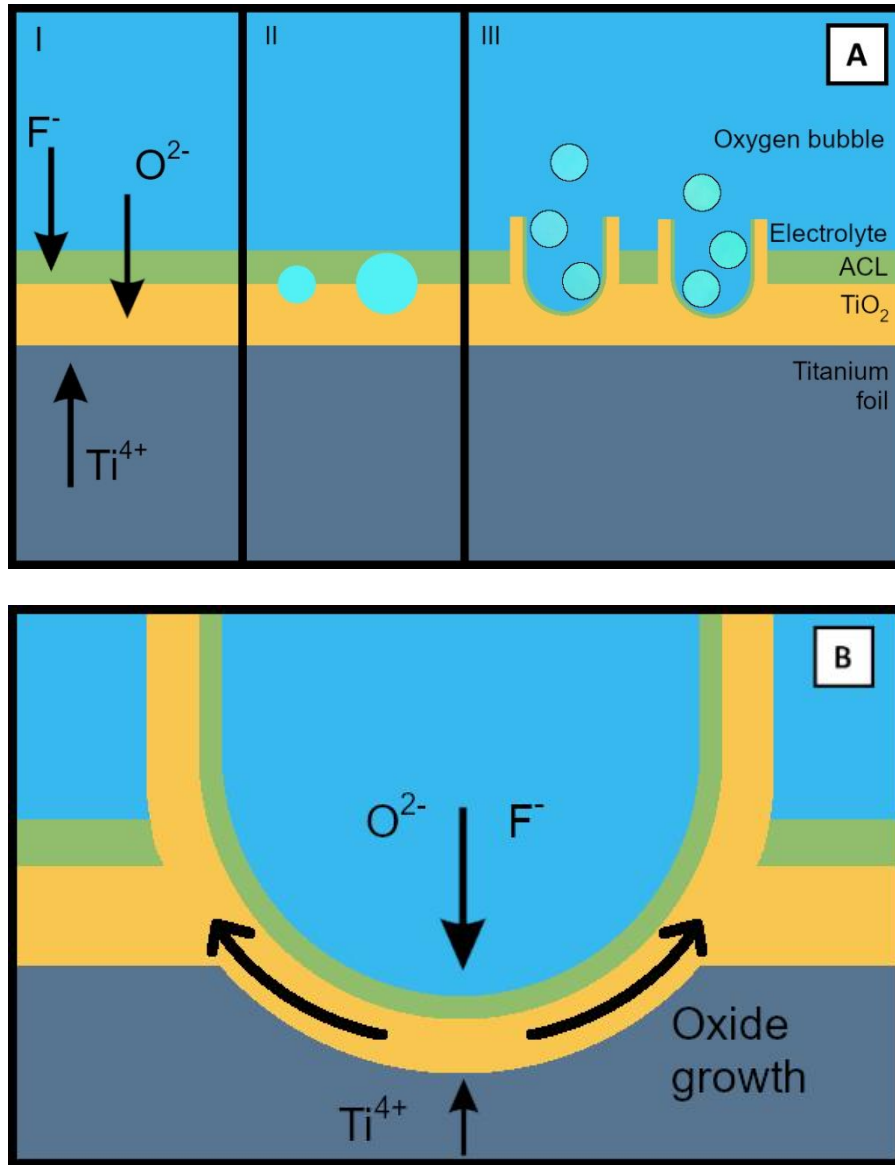


Figure 2: Stages of the titanium dioxide nanotube growth on the anodized titanium sheet (A). Mechanism of the nanotube formation (B).

The balance between ionic and electronic current responsible for oxide growth and oxygen evolution respectively is heavily reliant on the composition of the electrolyte, which is reflected in the different morphologies of the four so-called “generations” of the nanotubes [16,17]. The 1st one relied on the aqueous hydrogen fluoride solution which, due to its aggressive dissolution of the oxide layer and large water content, yielded NTs only up to 500 nm long. The 2nd generation solution utilized inorganic fluoride salts

(such as NH_4F) instead of HF to reduce acidity and slow the breakdown of the nanotubes. Although it allowed the synthesis of the structures up to 5 μm long, they suffered from the same rippled structure as the 1st, which came from the oxygen bubbles forming on the anode during anodization. In the following 3rd generation, the water content in the solution was therefore significantly limited. Instead, organic electrolytes such as ethylene glycol served as a primary medium, with the amount of fluoride ions and water being variables controlling the geometry. Careful adjustment of the electrolyte content and anodization parameters can result in smooth structures as tall as 1 mm [18]. The 4th generation pathways of the nanotube synthesis encase novel, sometimes entirely different ways. This includes waterless anodization, rapid breakdown anodization in fluoride-free solution, and microwave-assisted [9,19,20]. Although some of these methods can be much quicker than the first three generations, they also suffer from a much higher variance of the obtained geometry. Nonetheless, the 4th generation synthesis is used both as a way to create nanotube powders and well-organized membranes (Figure 3). Furthermore, due to the scalability of the anodization process, it can be performed just as easily on a large-scale, regardless of the generation of the electrolyte used [21].

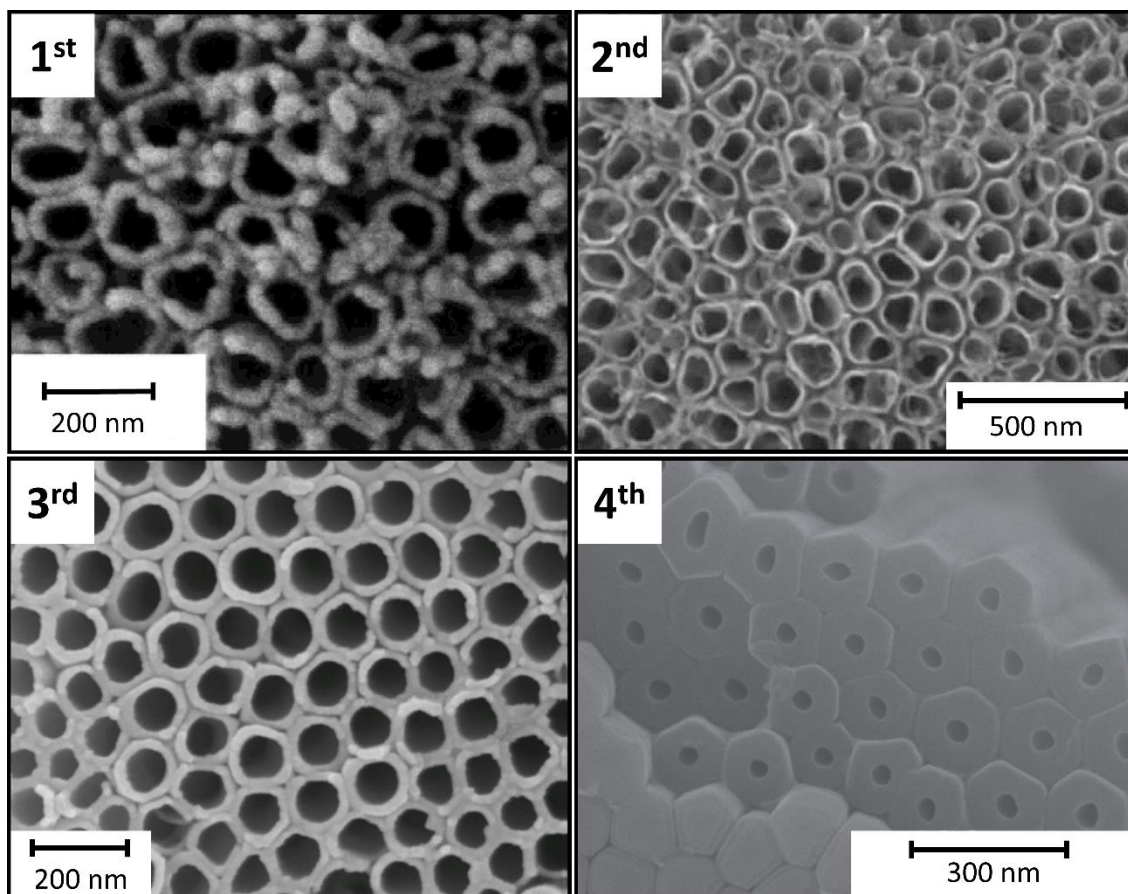


Figure 3: SEM images of the titania nanotubes formed in four generations of electrolytes [20,22–24].

Work one: The geometry of free-standing titania nanotubes as a critical factor controlling their optical and photoelectrochemical performance

Manipulation and fine-tuning of the nanotubes' geometry is an interesting and complex topic. However, as the physical properties of the nanomaterials are heavily dependent on the size of their features, very few works investigated in detail the relation between the two [25]. Those that do, however, are very difficult to interpret because of the differences between electrolytes and anodizing conditions, as the effects of some parameters are intertwined. For example, when comparing the effects of HF vs NH_4F , one should note that the HF solution is aqueous, therefore, in reality, such a comparison is made between NH_4F and HF with H_2O . Furthermore, the water content affects the total length of the nanotubes but, to a varying degree, so does time and ambient pressure [15,26–28]. Therefore, the initial analysis comprised of the determination of the effects of the seven most important parameters to the nanotube growth, as well as their boundaries for feasible growth of nanotubes. The influence of the amount of water, HF, and NH_4F , set potential, time, temperature, pressure, and electrolyte media was therefore evaluated.

The goal of the first work was to prepare the substrate material for further studies. To allow the modification of the outer walls of the nanotubes, diethylene glycol was chosen as an electrolyte media, as its viscosity allows the creation of a distinct spacing between them. The remaining parameters were chosen based on the multi-criteria analysis of the literature data, as well as preliminary experiments. As a result, the electrolyte was composed (by weight percent) of 7% water, 0.5% HF, and 0.3% NH_4F in diethylene glycol, whereas the temperature was set to 40°C , and the synthesis was done at ambient pressure. Because the applied voltage affects the scale of the grown structures (so, their length, diameter, and spacing) for the purpose of this study it was considered a variable.

Therefore, the investigation of the structures grown in the first work was done in the potential range of 20 – 60 V. Moreover, two times of anodization (2 and 5h) were investigated to see whether prolonged anodization has a meaningful impact on the performance of the obtained samples (see Attachment 1).

The investigation of the obtained substrates reveals no significant difference in nanotubes' morphology between investigated anodization times. The anodization voltage, however, greatly affects the geometrical features of the obtained substrates and thus, their physical properties. The NTs synthesized at higher voltages were taller, more separated, and exhibited a lower energy bandgap. Interestingly though, while the changes in the 20 – 40 V range show a linear dependence on potential, they are much smaller past the 40 V mark. This phenomenon can be associated with the effect of quantum confinement, which is especially pronounced for nanostructures with very small geometrical features – the nanotube walls in this case. As the anodization voltage rises, so does the wall thickness and thus its impact is lower. Nevertheless, the sample anodized at 40 V has shown the highest photocurrent density and thus was chosen for further electrochemical studies.



Contents lists available at ScienceDirect

Surface & Coatings Technology

journal homepage: www.elsevier.com/locate/surfcoat

The geometry of free-standing titania nanotubes as a critical factor controlling their optical and photoelectrochemical performance

Jakub Wawrzyniak^a, Katarzyna Grochowska^{a,*}, Jakub Karczewski^b, Piotr Kupracz^a, Jacek Ryl^c, Anna Dołęga^d, Katarzyna Siuzdak^a

^a Centre for Plasma and Laser Engineering, The Szwedzki Institute of Fluid-Flow Machinery, Polish Academy of Sciences, Fiszer 14 St., 80-231 Gdańsk, Poland

^b Faculty of Applied Physics and Mathematics, Gdańsk University of Technology, Narutowicza 11/12 St., 80-233 Gdańsk, Poland

^c Department of Electrochemistry, Corrosion and Materials Engineering, Faculty of Chemistry, Gdańsk University of Technology, Narutowicza 11/12 St., 80-233 Gdańsk, Poland

^d Department of Inorganic Chemistry, Faculty of Chemistry, Gdańsk University of Technology, Narutowicza 11/12 St., 80-233 Gdańsk, Poland

ARTICLE INFO

Keywords:

Spaced titania nanotubes
Photoactivity
Tauc plot
Flat band position
Surface trapped holes

ABSTRACT

Titanium dioxide nanotubes are regarded as one of the most important functional materials and due to their unique electronic properties, chemical stability and photocorrosion resistance, they find applications in, for example, highly efficient photocatalysis or perovskite solar cells. Nevertheless, modification of TiO₂ nanotubes is required to overcome their main drawback, i.e. large energy bandgap (> 3.2 eV) limiting their ability to capture solar light. In this work, we report the changes in optical and photoelectrochemical properties of well-separated TiO₂ nanotubes that are tuned by varying the geometry of the material. The ordered tubular titania is formed via anodization in the presence of fluoride ions in diethylene glycol at elevated temperature. Length, inner diameter, wall thickness, and separation distance are described in function of synthesis parameters such as applied voltage and duration. The morphology and optical properties are characterized by means of scanning electron microscopy and UV-Vis spectroscopy techniques, respectively, while cyclic voltammetry, linear voltammetry and chronoamperometry are used to determine electrochemical/photoelectrochemical activity in different light conditions. The obtained results suggest a link between specific surface area, the width of the band-gap, and photoactivity, each of which could be individually optimised via anodization conditions. Moreover, the behaviour of the Mott-Schottky plot before and after 3 min of irradiation is studied indicating the positive shift of the flat band position and an increase in donor density values for all the obtained materials. The Mott-Schottky analysis was correlated with the linear voltammetry scans suggesting the important role of surface trapped holes. Presented in here results significantly supplement the current state-of-art regarding separated TiO₂ nanotubes that are considered as not fully investigated and unappreciated class of titania materials which due to the exposure of inner and outer wall can be used for further modifications.

1. Introduction

Today, titanium dioxide nanotubes (TiO₂NTs) can be placed among the most researched nanomaterials and substrates used for further modification. So far, the attention has been put on studies regarding environmental protection [1], gas sensing [2,3], photocatalysis [4–6], and solar cells [7–10]. Due to their remarkable corrosion resistance [11], chemical stability, and developed surface area [12], the number of papers dedicated to them grows year by year. TiO₂NTs can be synthesized hydrothermally [13], via atomic layer deposition of titania over the porous alumina template [14], or anodization of the titanium foil under particular conditions [15]. However, the electrochemical

procedure stands out among other routes, because of its simplicity and quite low equipment requirements. To fabricate titania NTs, the arrangement of two electrodes placed opposite of each other and immersion in the electrolyte containing fluoride ions is used while the voltage applied between them stays as a driving force of the whole process. Such a synthesis enables the formation of the nanostructured material directly onto the conducting substrate and thus no further immobilization method is required to reach the form adequate for further characterization, especially for the electrochemical measurements. Particularly distinctive in comparison to other listed preparation routes, is that by adjusting electrolyte composition and temperature as well as process parameters - for example, applied voltage or the

* Corresponding author.

E-mail address: kgrochowska@imp.gda.pl (K. Grochowska).

<https://doi.org/10.1016/j.surfcoat.2020.125628>

Received 29 December 2019; Received in revised form 18 February 2020; Accepted 11 March 2020

Available online 12 March 2020

0257-8972/ © 2020 Elsevier B.V. All rights reserved.

distance between electrodes - various NT geometry can be reached. It should be also strongly emphasized that every geometric dimension of NT can be tuned: length, internal diameter and wall thickness [16,17], that makes such material an ideal candidate for further modification, depending on desired application. It has been already shown that, the distance between tubes [17] can be regulated and even well separated, upright standing NTs can be formed. While closely-packed nanotubes can be obtained via anodization in water/ethylene glycol mixtures [18], employing diethylene glycol or dimethyl sulfoxide as an organic solvent can result in free-standing morphologies [19]. According to Kowalski et al. [20], low electric field conditions arising during initiation of NT growth plays an important role in the formation of individual tubular structures. Comparing to the densely packed nanotubes that can be grown even up to several tens of μm , the length of spaced TiO_2NTs ($s\text{-TiO}_2\text{NTs}$) does not usually exceed few μm and only in some cases over 10 μm is reached [21]. Such layer thickness is mostly limited due to synthesis conditions and the fact that single NT is not supported by neighbouring NTs, which often results in their collapse. It should be also underlined that the internal diameter of spaced TiO_2 could be as wide as 600 nm when very high voltage is applied (120 V). According to Mohammadpour et al. [22], titania NTs with a diameter as wide as the wavelength can show well-defined Fabry-Perot interference fringes. Moreover, particularly broad pores can act as nanodepots ready to host other material which can be useful especially for biological agents, e.g. growth factors, antibiotics genes and even proteins [23]. Although the $s\text{-TiO}_2\text{NTs}$ can be characterized by unique morphological features, the synthesis of free-standing titania substrates have been presented in reports only since 2014 [20] and has been mastered mostly within the Schumki research group [17,24,25]. However, when tracking the publication record for $s\text{-TiO}_2\text{NTs}$, they can still be regarded as a less explored class of titania NTs. Until now, the characterization of laterally spaced titania concerns the comparison of their optical properties and photoactivity to the packed titania NTs or compact layer composed of TiO_2 nanoparticles [19]. Basing on the reflectance spectra recorded for different titania classes, it was indicated that due to the spacing, light is absorbed in much deeper parts of the tubular layer which could be beneficial for the photoconversion efficiency. Other reports only cover elaboration about critical parameters, anodization voltage, water content [25], electrolyte temperature [21], and synthesis duration [17] affecting the final synthesis product. Those systematically performed anodization processes enable identification of the boundary conditions where the spaced TiO_2NTs could be obtained and when exceeding the particular value results in the unordered porous layer. Moreover, the spaced titania offers other very unique feature compared to the packed NTs, namely exposed surface area of outer tube wall available for further modification. The presence of the interconnecting space was cleverly used for deposition of Pt or PdPtAg alloy [26] for hydrogen generation [27], decoration by Fe_2O_3 applied in Li-ion battery [28], or coating with Nb_2O_3 for supercapacitor application [29]. Regarding solar driven water splitting, it was proven that the usage of spaced TiO_2NTs substrate enables more efficient hydrogen production in comparison to the hexagonally packed titania NTs or the porous film. According to Necula et al. [30] it was indicated that lateral spacing impacted the biological applications regarding osteoblast cell adhesion and morphology as well as cytoskeleton organization. Nevertheless, still the studies onto the spaced titania NTs cover only several selected aspects and, to the best of our knowledge the relationship between the morphology and the optical properties as well as the electrochemical behaviour of the irradiated material has not been investigated so far.

Herein, we focus onto the fabrication of the series of titania samples where nanotubes are well separated but still exhibit a high degree of ordering and cylindrical shape. The anodization process was carried out in two time regimes and under different voltages in the range of 20–60 V while keeping other parameters constant. On the basis of the recorded SEM images, the in-depth analysis of morphological changes was carried out. The morphology inspection was compiled with the

optical properties investigated using UV-vis absorbance spectroscopy. We would like to show that following the changes in geometry, both the shape of reflectance spectra and bandgap value are tuned without the introduction of any dopant atoms. In order to indicate that the photo-electrochemical activity follows the morphology of spaced titania nanotubes, linear voltammetry curves were registered under electrode irradiation by the solar simulator. The flat band position as well as donor concentration for each titania NT layer was revealed based on the Mott-Schottky plot. Finally, the electrochemical behaviour of the samples in dark and under irradiation was compared to indicate the most photoactive electrode and to identify factors that significantly determines improved photoresponse.

2. Experimental

2.1. Sample preparation

The free-standing titanium dioxide nanotube arrays were synthesized via electrochemical oxidation in a cylindrical cell in a two-electrode system. Please note that by free-standing, we understand laterally separated nanotubes attached to the Ti substrate. The anode consisted of titanium foil (99.7% pure, 0.127 mm thick, Strem) piece (35×25 mm) and platinum net (20×25 mm) acted as a cathode. Prior to the anodization, the foil was ultrasonically cleaned for 10 min in acetone (p.a. Protolab), ethanol (96%, Chempur) and deionized water (0.08 μS , Hydrolab) respectively, then rinsed with isopropanol (p.a. POCH) and dried in air. The electrolyte consisted of 0.3 wt% NH_4F (p.a. Chempur), 0.5 wt% HF (p.a. Chempur), and 7.0 wt% of deionized water in diethylene glycol (p.a. Chempur). The electrolyte temperature was maintained at 40 °C with the use of thermostat (Julabo F-12). Two sets of samples were fabricated during different anodization times: 2 and 5 h, while within each set the voltages were in the range of 20–60 V. The electrical conditions were controlled by the driver built in-house and supplied by a voltage generator (MPS-600-5 L-2). Both ramp-up and ramp-down voltages were set to 0.1 V/s. After the process, the substrates were rinsed with and submerged in ethanol for c.a. 1 h after which they were dried in the ambient air. In order to obtain the crystalline phase, the titanium foil with TiO_2NTs was then placed in a furnace (Nabertherm) and gradual heating was applied with 2 °C/min rate enabled reaching 450°. The samples were kept for 2 h in elevated temperature whereas the post-calcination cooling was let freely to room temperature.

Scanning Electron Microscope FE-SEM, FEI Quanta FEG 250 with a secondary electron detector was used to obtain images of produced nanotubes. The pictures were taken using acceleration voltage of 10 kV in various places on the surface and in couple cross-sections to confirm uniformity of the material.

The UV-Vis spectra were taken in reflectance mode using PerkinElmer Lambda 35 dual-beam spectrophotometer in the range of 300–1100 nm with scanning speed set to 120 nm/min.

The study of electrochemical properties was done with Autolab PGStat 302 N potentiostat-galvanostat (Metrohm, Autolab) system in a three-electrode system. The synthesized NTs acted as a working electrode (WE), Pt mesh was used as counter electrode and reference electrode consisted of $\text{Ag}/\text{AgCl}/0.1$ M KCl. The electrodes were submerged in deaerated (5 N argon), pH-neutral electrolyte (0.5 M Na_2SO_4 – p.a. POCH). Investigated material was illuminated by 150 W Xenon lamp (Osram XBO 150) through AM 1.5 filter and a high-transmittance quartz window on the side of the electrochemical cell. For studies in visible light only, additional UV filter was used (GG420, Schott).

The electrochemical results were obtained in the range between –1.0 and +1.0 V with the scan rates of 50 mV/s for cyclic voltammetry (CV) and 10 mV/s for linear voltammetry (LV). Additionally, the chronoamperometric (CA) curves were recorded to describe photo-stability. While CV and LV measurements were conducted in dark, additional LV and CA sweeps were done under vis and UV-vis

irradiation to indicate the difference in photoactivity between examined samples. Chronoamperometry curves were recorded under the +0.5 V vs. Ag/AgCl/0.1 M KCl potential when the WE was periodically irradiated using the motorized shutter with 0.2 Hz frequency.

Moreover, for samples anodized for 2 h, the potentiodynamic electrochemical impedance spectroscopy experiments were carried out at a frequency of 1000 Hz. The EIS data were recorded for WE polarized between -0.7 and 1 V. In order to obtain steady-state, before each measurement, the potential was held still for 1 min. Furthermore, the space-charge layer capacitance was calculated according to the following equation [31]:

$$C_{sc} = \frac{-i}{2\pi f Z_{im}} \quad (1)$$

where f stands for the frequency of the AC signal and Z_{im} is the imaginary part of the impedance. Consequently, according to Mott-Schottky theory of the space charge capacitance of semiconductor, donor densities were calculated using the following equation [32]:

$$N_d = \left(\frac{2}{\epsilon_0 \epsilon} \right) \left[\frac{d \left(\frac{1}{C_{sc}^2} \right)}{dE} \right]^{-1} \quad (2)$$

where ϵ_0 stands for permittivity of vacuum ($\epsilon_0 = 8.85 \times 10^{-12} \text{ Fm}^{-1}$), ϵ is dielectric constant of the anatase TiO_2 ($\epsilon = 38$ [33]), e is an electron charge ($e = 1.602 \times 10^{-19} \text{ C}$), and E stands for the potential applied.

3. Morphology, structure and chemical nature

Fig. 1 presents morphological features of titania nanotubes anodized between 20 and 60 V for 2 (Fig. 1A–E) and 5 h (Fig. 1F–J), whereas graphs presented in Fig. 2 highlight the connection between anodization voltage and geometrical features of the NTs. Shown SEM images indicate that fabricated materials exhibit a high degree of ordering independently of the applied voltage conditions. Anodization in the voltage > 60 V, however, leads to the non-uniform nanotube distribution over the Ti plate, as illustrated in Fig. 3. In the case of substrates anodized at 70 V, the bottom parts of the titanium foil are free from any form of nanotubes and only porous oxide is present (Fig. 3A). Moving upwards, groups of nanotubes begin to form (Fig. 3B), and gradually become denser, until they cover most of the surface, aside from some bald patches (Fig. 3C). In the uppermost part of the anodized foil, the nanotubular structure is present (Fig. 3D). The non-uniform distribution immensely limits further applications of the foil anodized at voltages ≥ 70 V, therefore electrochemical process was carried out within 20–60 V. Additionally, although the nanotubes created employing anodization voltages of 50 and 60 V show good uniformity during SEM investigations, there are different regions present that are visible with the naked eye, that will be discussed in Optical properties section.

The average inner diameter of the nanotubes synthesized at 20 V for 2 h was measured to be approximately 65 nm, the distances between nanotubes of c.a. 35 nm, and their height at almost 400 nm. While increasing potential applied during anodization to 60 V, the NTs radius increased over 3 times to c.a. 225 nm, the distances between them exceeded 160 nm ($\times 4.5$), and their length > 6-fold to nearly 2500 nm (Figs. 1, 2). Extending anodization time to 5 h has increased size of most geometrical features by only several percent. The upper wall thickness, however, was lower in every case. This can be expected, as longer anodization times provide fluoride ions within the electrolyte more time to etch the NTs, especially in regimes directly exposed to them, such as upper parts of the nanotubes [34]. Additionally, the length of the nanotubes prepared at 60 V was slightly lower than those anodized when 50 V was applied. Although the relation is not direct, similar reduction of length by prolonging anodization was described by Ozkan et al. [35] and Matsuda et al. [36]. It can be ascribed to the phenomenon in which

the nanotube growth rate at the bottom of the tube becomes slower due to the increased diffusion resistance of both F^- and the reaction products with the increased tube length. This results in dominance of the dissolution rate and decrease of the nanotube length with time.

In comparison, Ozkan et al. [17] created wider, more separated nanotubes of similar length in comparable conditions (voltage, time, temperature), but have also reported seeing smaller NTs growing in-between bigger ones, which were not present in our case. The inter-tubular distances are also similar to those obtained by Kowalski et al. [20], despite him anodizing for longer times. Although the creation of much taller, free-standing nanotubes is possible, the use of a different electrolyte composition is required [37].

To better describe the synthesized nanotubes, a model estimating their real surface has been proposed, similar to those available in literature [12,38]. Assuming, that spaced TiO_2 NTs are hollow cylinders that grow on a triangular lattice (Fig. 4), we can calculate their specific surface area (S_a) by using the following equation:

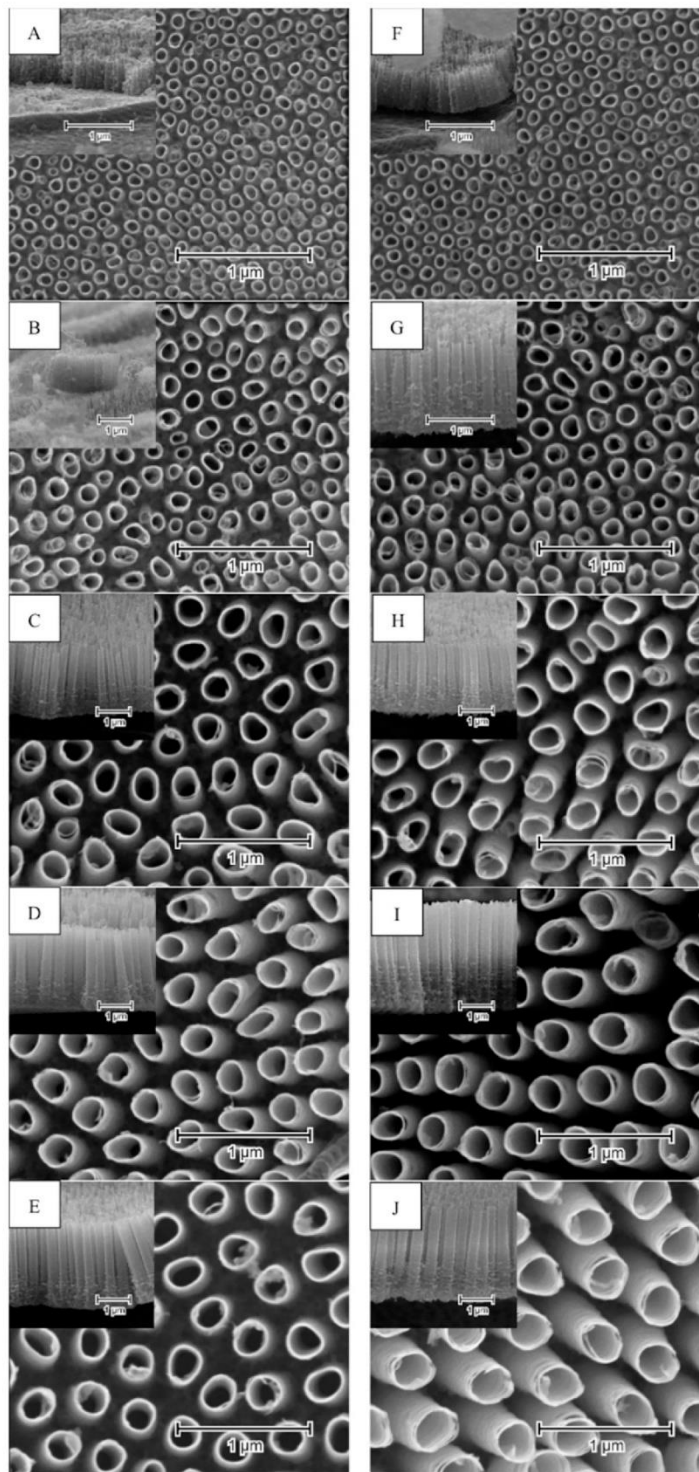
$$S_a = 1 + \frac{4\pi h(r+R)}{\sqrt{3}(2R+s)^2} \quad (3)$$

where s is a spacing between nanotubes, h stands for their height, and r and R are the inner and outer radius, respectively. The S_a values for all discussed samples are shown in Table 1 where the applied unit concerns the geometric surface area in cm^2 . For both anodization times, the available surface area is the smallest when the voltage is set to 20 V, then rapidly rises through 30 and 40 V, reaching maximum at 50 V. For the samples anodized at 60 V, the available surface area is again lower. This is due to the fact, that although the inter-tube distances and inner tube diameters increase with voltage in its whole spectrum, the growth rate of the height of the NTs slows between 50 and 60 V. This parameter is of high importance because developed surface area have enormous impact onto the photo- [39] and catalytic activity [40] of the nanomaterials.

To confirm the crystalline phase of TiO_2 NTs, selected samples (i.e. amorphous and calcined ones prepared at 40 V for 2 and 5 h) were investigated by means of Raman spectroscopy, X-ray diffractometry (XRD) and infrared spectroscopy (FT-IR). As it comes to Raman measurements (Fig. S1 in Supporting Information file), for calcined samples typical anatase peaks can be identified: E(1 g) at 144, E(2 g) at 197, B(1 g) at 395, A(1 g) at 519, and E(3 g) at 635 cm^{-1} , while for amorphous ones broad spectra with no clear peaks can be seen. Obtained results are in agreement with other researchers works [41–44]. Also X-ray diffractograms are typical for this kind of material [45] – see Fig. S2. For amorphous samples only peaks corresponding to Ti acting as a NTs support can be observed, while for calcined materials patterns related to TiO_2 anatase and rutile are clearly seen. Nevertheless, the formation of rutile oxide layer occurs at the Ti/TiO_2 NTs interface and small amount of it is found to be normal [46]. Considering the FT-IR spectra, we observed two very broad bands centred approximately at 760 (shoulder band) and 460 cm^{-1} in the case of the amorphous TiO_2 , which resolved into four narrower bands at ca. 900 cm^{-1} , 780 cm^{-1} , 520 cm^{-1} and 427 cm^{-1} for calcined samples (Fig. S3). The change in the character of the spectra is in agreement with the predicted crystal phase of the material. With increasing disorder, the characteristic IR or Raman bands of the semiconductors are generally shifted to lower wavelengths and substantially broaden. The result may be interpreted as a loss of crystalline selection rules. [47]. The calcination transforms the amorphous material into the ordered crystalline structure of anatase and this alteration resolves the TiO_2 lattice vibrations at 750 cm^{-1} and 517 cm^{-1} , which is clearly observed in Fig. S3. Summertime, performed measurements confirm the anatase phase of prepared materials.

Moreover, for sample anodized at 40 V for 2, the X-ray photoelectron spectroscopy (XPS) investigation was conducted. The high resolution XPS spectra recorded in the binding energy range typical for titanium and oxygen are shown in Fig. S4. In the case of Ti, the XPS spectra was fitted by three doublets composed of $\text{Ti}2p_{1/2}$ and $\text{Ti}2p_{3/2}$

Attachment 1



(caption on next page)

Fig. 1. SEM images presenting topology of the anatase TiO₂NTs anodized for 2 (left column) and 5 h (right column) under 20 (A, F), 30 (B,G), 40 V (C, H), 50 V (D, I) and 60 V (E, J). Insets presented show their respective cross-sections.

signals characteristic for different Ti oxidation states and present in the form of: TiO₂ (458.8 eV), Ti₂O₃ (457.2 eV) and TiO (455.7 eV) [48]. The XPS spectra registered in the binding energy range typical for oxygen was fitted by two signets with maxima located at 530.1 eV and 531.3 eV attributed to the lattice oxygen [49] and oxygen present in the surface hydroxyl groups [50] or some carbon contamination, respectively. Those carbon species originate from the adventitious hydrocarbon from the XPS instrument itself or could be related with some electrolyte residuals [51] since diethylene glycol is the main component of the anodization bath.

4. Optical properties

As previously discussed, the changes to NTs morphology were primarily reliant on the anodization voltage, and only slightly on time. Because of it, only the performance of nanotubes anodized for 2 h will be discussed in here and the next chapters. Nevertheless, for comparison purposes the optical tests of TiO₂NTs obtained for 5 h are given in Fig. S5. To indicate the changes in the optical properties depending on the anodization conditions, the UV-Vis spectra were acquired in the wide wavelength range (see Fig. 5). In the reflectance spectra, one can find two characteristic bands, one in the UV range typical for all titania nanostructures and the second in the visible range. While the first one is attributed to the bandgap energy, the maxima found within the 450–700 nm range can be interpreted as the result of the specific architecture of titania NTs, as some groups report its presence in their UV-Vis spectra [19,52], while others do not [53,54]. Similar shape for spaced TiO₂ was reported by Ozkan et al. [19] and is characterized by improved light absorption due to the light being able to illuminate much deeper, exposed parts in spacing between the tubular layer. This feature of the reflectance band is also related to the back light reflection

from the underlying Ti metal substrate [55]. Despite overall lower amount of absorber present in comparison with typically used aligned nanotubes, the wide absorption band in the visible range can be detected, which can be considered as beneficial for the photoconversion efficiency.

Regarding the influence of the applied voltage, from Fig. 5 A, we can see that reflectance of the samples anodized at lower voltages (namely 20 and 30 V) is significantly higher, than for those anodized at greater voltages. This, in turn, means that their absorbance is lower, limiting the possible number of excitons that could be created. In addition, the maximum of absorption is located at c.a. 550 nm for NTs anodized at 20 V, but shifts as far as to 660 nm for sample anodized at 40 V. For even higher voltages, the maximum moves back to shorter wavelengths, to approximately 590 nm at 60 V. Additionally, if we superimpose normalized solar spectrum onto the absorption spectra and integrate area underneath the curve, we can calculate the amount of total light absorbed, which reaches its maximum for sample anodized at 40 V (Fig. 5 B).

The optical bandgap of titania nanotubes was derived from Tauc plots (Fig. 6A), which were prepared assuming an indirect-allowed type of transition in anatase TiO₂. With an increased anodization voltage, the E_{bg} values drop exponentially at first, reaching plateau for higher voltages (Fig. 6). The measured E_{bg} values were as high as 3.62 eV (when anodized at 20 V) or as low as 3.11 eV (for sample anodized at 60 V), decreasing the gap values between them by over 0.5 eV. Additionally, in samples anodized at 50 and 60 V, an additional absorption band edge was detected (Fig. 6A, inset) [56]. It is most likely connected to the uneven distribution of O²⁻ inside the NTs which leads to the formation of suboxides, e.g. TiO and Ti₂O₃, and high valence oxide (TiO₂) in the case of lower and higher concentration, respectively, as the wall thickness rises with anodization voltage [57]. It is also likely

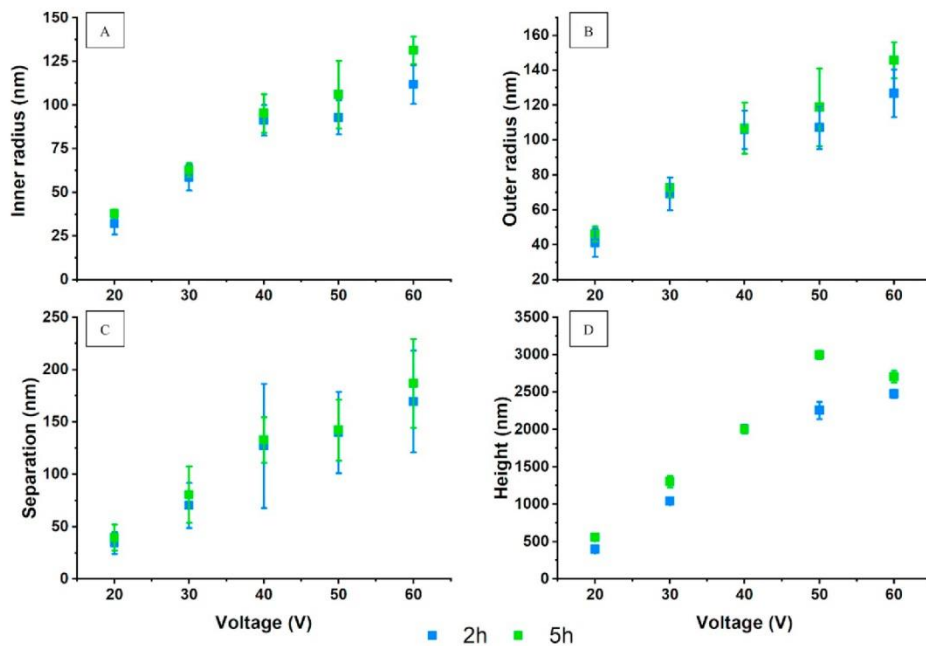


Fig. 2. Graphs presenting inner (A) and outer radii (B), separation (C), and height (D) of the anodized TiO₂NTs as a function of a voltage applied for 2 and 5 h.

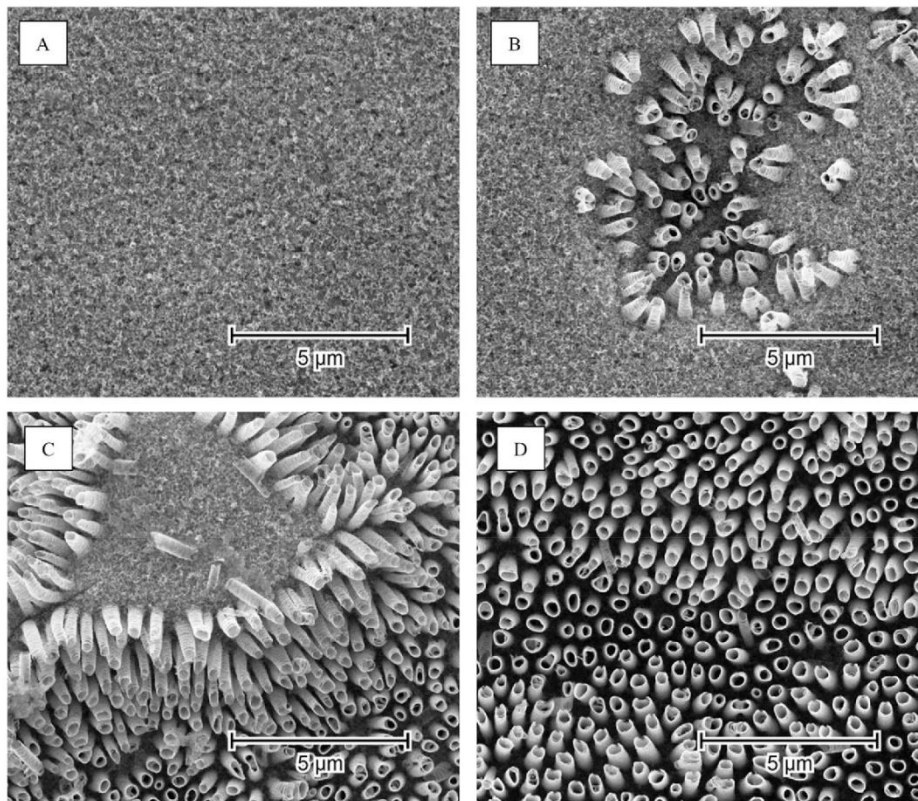


Fig. 3. Different regimes present in substrates anodized at 70 V. Porous oxide layer (A), groups of nanotubes (B), bald patches in nanotube forest (C), nanotubular layer (D).

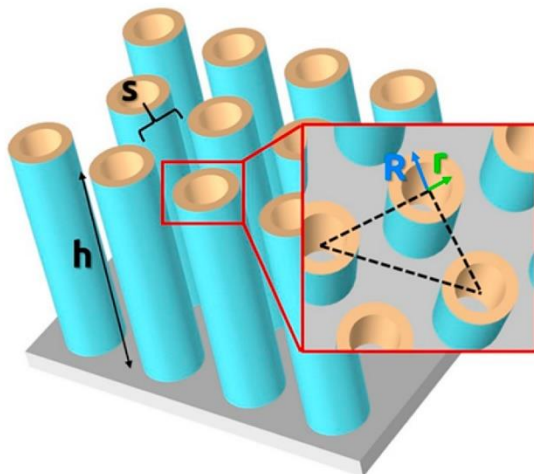


Fig. 4. Schematic representation of the arrangement of TiO_2 NTs.

related to before mentioned unevenness of the material under optical investigation. It is noteworthy that, even though bulk anatase has E_{tbg} equal to 3.2 eV [58,59], the values we measured were different,

depending on NTs geometrical features – see Fig. 6B. This is supported both by theoretical and experimental studies of Al-Haddad et al., where it was proven that the absorption band edge is redshifted with the decrease of distance between NTs and with increased diameter [54]. Moreover, Liu et al. [60] theoretically investigated the impact of the geometrical features of nanotubular structure on their photocatalytic activity. It has been shown that photocatalytic efficiency increases with decreasing of inner diameter and wall thickness until it reaches maximum value and then drop of efficiency can be observed. In the case of the length of NTs, the efficiency grows with the length until saturation. Some groups [19,59], however, have noticed an increase in photocatalytic activity without any change to electron bandgap width of the investigated material. It indicates that E_{tbg} value is only one of the factors responsible for improving the photoactivity of the TiO_2 nanomaterials.

For deeper understanding of optical and electronic properties, photoluminescence (PL) spectra for TiO_2 NTs prepared for 2 h at different voltages in the range from 20 to 60 V (see Fig. S6). The strongest relationship is observed between green and red emissions versus applied anodization voltage. It can be observed that the intensity of green and red band emissions grow with the voltage up to 50 V and then decreases, while there are no distinct differences for the blue one. It should be in here highlighted that PL intensity depends on the excited electrons density and relation between radiative and non-radiative recombination transitions. As was already mentioned in the manuscript, absorption of titania nanotube materials is higher for the ones

Table 1Specific surface area (S_a given in cm^2/cm^2) of the titania nanotubes anodized for 2 and 5 h at voltages between 20 and 60 V.

→ Voltage (V) →	20	30	40	50	60
↓ Anodization Time (h) ↓					
2	10.3 ± 5.8	14.2 ± 2.9	16.4 ± 2.3	17.4 ± 4.8	16.1 ± 2.1
5	12.4 ± 3.1	16.2 ± 4.6	16.0 ± 3.8	21.5 ± 2.9	15.6 ± 3.3

fabricated at higher voltages. Therefore, the growth of PL can be attributed to the increase of excited electrons density. Moreover, green and red bands photoluminescence is stimulated by the recombination of mobile electrons with trapped on oxygen vacancy sites holes and the recombination of trapped on Ti^{3+} electrons with mobile holes respectively, while the blue band emission originates from the recombination of conducting electron and valence hole [61,62]. It can be then concluded from our results that electron recombination on sites related to Ti^{3+} ions, as revealed by XPS analysis and oxygen vacancies is more probable than the one via conduction-valence band transition. Additionally, taking into account data provided in Fig. 2 and Table 1, the increase of green and red photoluminescence is ascribed to the growing number of near-surface defects.

5. Electrochemical activity

In order to study the electrochemical response, cyclic voltammetry measurements were carried out for the whole series of the titania NTs anodized for 2 h. As it can be seen from Fig. 7 A, very similar shape and current density values were recorded for all tested materials within the whole potential range. Analysing the electrochemical behaviour, one may distinguish two regimes: a) above -0.3 V vs. Ag/AgCl/0.1 M KCl where very low capacitive currents are observed and b) from -1.0 to -0.3 V vs. Ag/AgCl/0.1 M KCl, where the developing reduction of the Ti^{III} to Ti^{IV} takes place [63]. This process is attributed to the conduction-band filling accompanied by the proton insertion that could be given as $\text{Ti}^{\text{IV}}\text{O}_2 + \text{e}^- + \text{H}^+ (\text{aq}) \rightarrow \text{Ti}^{\text{III}}\text{O}(\text{OH})$ [64,65]. Here, the H^+ represents a counter ion that is responsible for the compensation of the negative charge when the Ti^{III} donor centres arise at the electrode.

Further measurements covering the collection of EIS data were limited to the range from $+1.0$ V to -0.6 V taking into account poor

faradaic activity in wide potential processing window. The EIS measurements were carried out twice in dark conditions, before and after 3 min irradiation period and observed changes will be discussed later on. In both cases, basing on the value of the imaginary part of the impedance and the relation provided in the experimental section (Eq. (1)), Mott-Schottky plots were prepared. As the run of all the prepared plots for the investigated samples is similar, only the ones for TiO_2NTs fabricated at 40 V are presented in Fig. 7B. The positions of flat band potentials were depicted in Fig. 8A and are in the range from -0.26 V to -0.22 V vs. Ag/AgCl/0.1 M KCl, while the most negative values are found for the samples obtained at the lowest anodization voltage and the most anodically shifted belongs to the sample anodized at 40 V. Those slight changes in the localization of flat band potential within the investigated set of samples could be related to the variation of oxygen vacancies and hydroxyl ions that is strongly related to the material surface area. Those species involve the formation of some Ti suboxides within the tubular structure. According to the functional density calculations [66], the OH^- insertion and generation of oxygen vacancies in the TiO_2 lattice, identified on high resolution XPS spectra, can affect energetic states under the titania conduction band. Apart from the E_{fb} values, the tangent to the Mott-Schottky function guided in the vicinity of its inflexion was used to determine the donor density basing on the relation (Eq. (2)) and the value of particular constants. The trend of the calculated donor densities depends on the applied anodization voltage and is provided in Fig. 8B. In general, the obtained values are typical since they fit the standard range 10^{19} – 10^{20} cm^{-3} [67,68]. The lowest slope and in consequence the highest N_d is determined for sample anodized at only 20 V, whereas the lowest value was found for the material obtained at 40 V. The observed relation between N_d and the anodization voltage approximately overlaps with the change of the specific surface area and greatly depends on the preparation conditions,

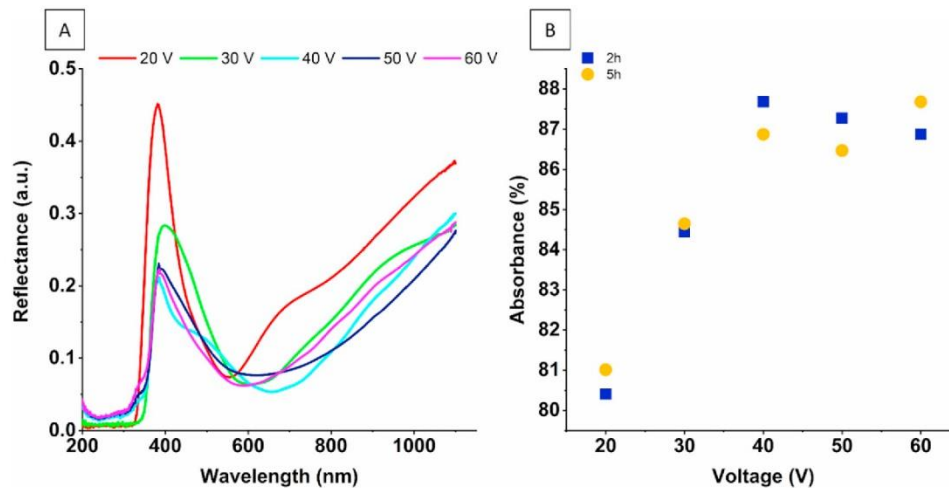


Fig. 5. Reflectance spectra of the titania nanotubes anodized for 2 h at a different voltages (A) and calculated amount of the solar spectra absorbed by each substrate (B) – results for samples anodized for 5 h are given for comparison.

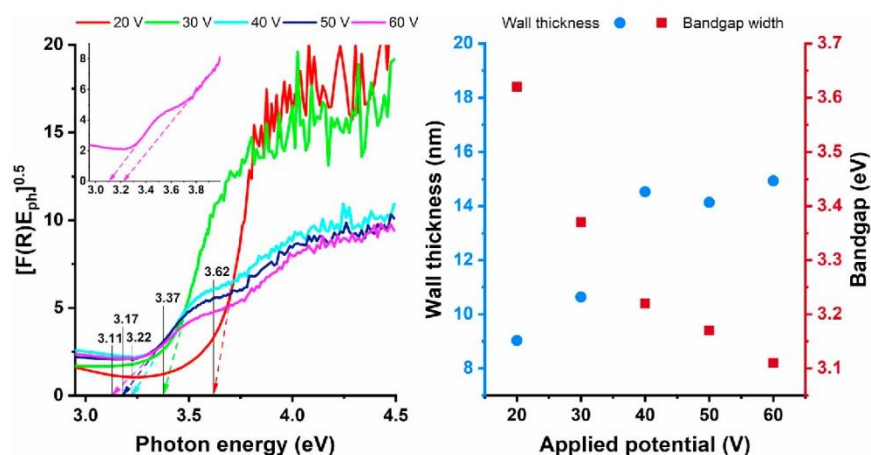


Fig. 6. Calculated Tauc plots of anodized TiO₂NTs with respective E_{bg} values marked (A) and the change in the value of NT walls thickness and E_{bg} depending on the anodization voltage (B).

namely the voltage listed in Table 1. Generally, higher N_d values induce larger upward shift of the Fermi level, resulting in a significant energy band bending at the oxide surface which can help efficient charge separation at the working electrode/electrolyte interface [69]. According to Acevedo et al. [70], these separation centres could be attributed to the presence of different Ti species (Ti²⁺, Ti³⁺ and Ti⁴⁺) or oxygen defects and therefore more disordered material. Following that, higher N_d could positively impact onto the conductivity of the semiconductor and enhances photoactivity. Thus, taking into account only this parameter, one may expect recording of the highest photocurrents for TiO₂NTs obtained at 20 V, since they exhibit the highest N_d . Comparing the relation between values of developed surface area and E_{fb} within the investigated set of samples, a similar trend was reported by Giorgi et al. [71], where higher specific surface area results rather in lower N_d values.

The second round of EIS measurements, preceded by 3 min long illumination, results in the positive shift of the flat band potential and some increase of donor density value for all the investigated TiO₂NTs. Such a behaviour is rarely reported since usually impedance data are collected only once, prior to the exposure of the material to light. Nevertheless, the detailed investigations that have been already carried

out by Chen et al. [72] also indicates such a positive movement of the E_{fb} position of the material after a period of its illumination. As was proposed by Chen et al., this shift is due to the preservation of accumulated holes at the electrode/electrolyte interface and thus, the Nernstian behaviour is maintained. This interesting phenomenon reflects the efficient storage of some of the photoinduced holes in surface states of TiO₂NTs/solution interface despite stopping the irradiation. This surface trapped holes (STH) are characterized by high stability, since the initial position of the E_{fb} was not ideally preserved after a certain illumination period. When the electrode is irradiated, the photooxidation of water molecules takes place, which results in the formation of two types of intermediate species: hydroxyl radicals and peroxide species. Regarding their stability, the hydroxide species are much less stable than peroxide ones, that impacts significantly onto the kinetics of reactions occurring at the electrode/electrolyte interface. Taking into account Chen et al. results, one may conclude that those changes are due to the long-living STHs identified as relatively stable peroxide species. They are usually noted as Ti_s-O-O-Ti_s, Ti_s-O-O-H or Ti_s-H₂O₂, where Ti_s stands for surface titanium. Their undisturbed accumulation suggests that the rate-determining step could be ascribed as follows: Ti_s-O-O-Ti_s + 2 h⁺ + 2H₂O → 2Ti_sO⁻ + O₂ + 4H⁺. According to Chen

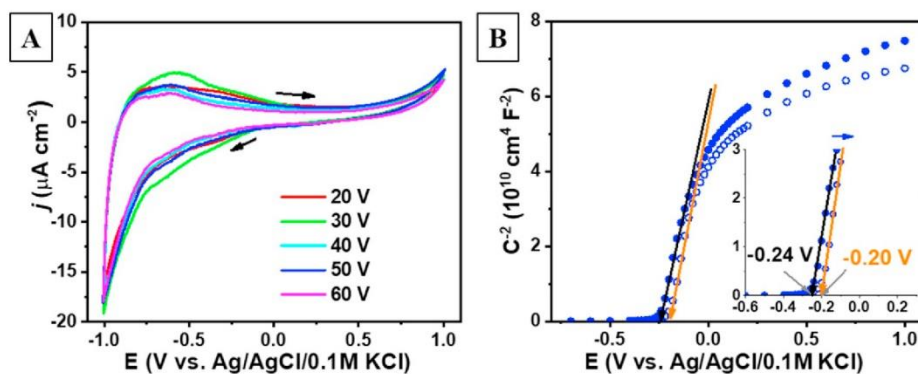


Fig. 7. Cyclic voltammetry curves registered at 50 mV/s scan rate (A) and Mott-Schottky plot prepared from data collected before and after irradiation of the TiO₂NTs anodized at 40 V (B).

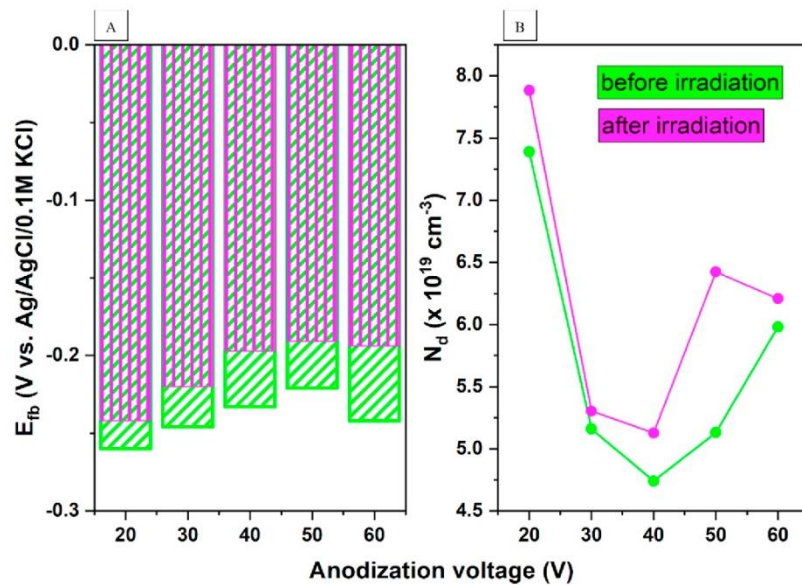


Fig. 8. The change of the calculated values of flat band potential (A), and donor densities before and after working electrode irradiation (B).

et al., the release of accumulated holes, and therefore inhibition of the flat band variation, can be achieved by the introduction of additional species into the electrolyte. Nevertheless, in comparison to the case described by Chen et al., the shift found for our samples is not as significant, but its presence cannot be neglected. Taking into account above discussion and the analysis of geometric factors delivered in the previous section, especially the specific surface area (see Table 1), the difference between the E_{fb} before and after material irradiation (ΔE_{fb}) is more pronounced for samples exhibiting the greatest S_a value (anodized at 40–60 V) since accumulated holes in those cases have more area to occupy.

On the other hand, it should be remembered that the value of developed surface area considered here as a geometric space (topography) that has a direct contact with outer environment is not the same as the space charge layer and the surface states affecting the real situation at the semiconductor-electrolyte interface [73]. Moreover, the detailed analysis of the band bending depends rather on the thickness of the TiO_2 wall while the surface area is not regarded in this case as a key factor. It is in agreement with Pu et al. [74] who indicated that the thickness of the tube walls significantly affects semiconducting properties of the material, namely the potential drop across the tube walls. Depending on the wall thickness (w) the space charge layer (L_{SC}) could be modulated. For the thin walls, when $w/2 < L_{SC}$ the flat band conditions are present within the tube wall and band bending can only occur at the bottom of the tubes. In opposite case, when the wall is thicker ($w/2 > L_{SC}$) the band bending may extend to a few tens of nm throughout the half thickness of the wall in the wide potential range depending on the donor level. Taking above into account and knowing that photogenerated e^-h^+ pairs could be more or less effectively separated, depending on the relation between the width of the depletion layer and the half thickness of the tube wall, the difference in the behaviour of the series of the TiO_2NTs material of various wall thickness is expected. According to the mechanism described by Sang et al. [75] the wider the depletion layer, the farther the photoinduced electrons will be driven, which thus benefits the photoelectrical properties. Comparing the value of wall thickness given in Fig. 6b for particular anodization voltages and the difference in E_{fb} depicted in Fig. 8a, one can

observe that the both trends overlap, namely the wider the thickness the higher changes in E_{fb} value.

Following the changes in the E_{fb} towards the anodic regime, much higher amount of oxygen vacancies could be found in the material [76–78], but still the lowest value is calculated for the material anodized at 40 V. It may indicate the lowest number of different Ti species or surface defects which are recognized to play crucial role in efficient charge separation affecting overall photoconversion efficiency. As has been already mentioned, those defects generally enhance electrical conductivity as well as charge transport in TiO_2 [79].

However, it should be pointed out that it is one set of factors that can be responsible for better or worse photoresponse and the estimated N_d amount when the electrode is kept in darkness does not determine further enhancement in photoresponse [80]. It should be also highlighted, that similarly to other authors, in our calculations we apply the facile assumption that electrode material composed of NTs is flat [81] and therefore the obtained donor density does not provide accurate information for the highly porous TiO_2 nanostructures. Comparing the values listed in Table 1 with the donor concentration values, one may observe that the lowest N_d was estimated for the material exhibiting one of the highest developed area. According to many reports [81–84], Mott-Schottky analysis is regarded rather as a surface analysing technique, which could rather indicate the electrical conductivity trends reflecting the composition of the tubes at the surface than at the NTs/substrate interface. Thus, concerning well-separated nanotubes with a particularly wide inner diameter and both inner and outer walls exposed to the electrolyte species, the simplified approach towards N_d determination should be carefully analysed.

In order to verify the effect of the developed surface area, optical properties, the position of flat band potential, and finally donor density onto the material photoactivity, the linear voltammetry curves (see Fig. 9) were registered under three various conditions: in dark and under electrode exposition to vis and UV-vis irradiation. When the material was kept in the dark, as was in the case of cyclic voltammetry curves, the recorded current is very low and almost no difference between tested samples was observed. The same measuring protocol was applied during the working electrode irradiation with the visible light

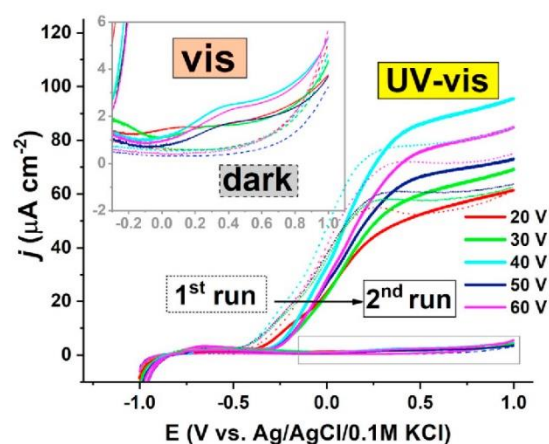


Fig. 9. Linear voltammetry curves recorded for the set of TiO_2NTs samples in 0.5 M Na_2SO_4 with 10 mV/s scan rate in different conditions: in dark and under electrode irradiation by visible and UV-vis light. 1st run is presented as solid lines, while 2nd one as dotted.

and the slight increase of current is noticed above +0.1 V vs. Ag/AgCl/0.1 M KCl (see inset of Fig. 9). Such a small photoresponse is justified by the wide bandgap energy of titania that corresponds to the UV light. Thus, even though the titania materials exhibit strong absorption within the visible range of 400–700 nm it does not contribute to the significant photocurrent increase. Nevertheless, among others, the sample fabricated at 40 V exhibits the highest enhancement. The confirmation of such increase, as well as photostability, was revealed by 3 min long chronoamperometry curves recorded upon chopped vis/dark irradiation given in Fig. 10A.

Further electrochemical measurements were performed when the material was exposed to the full solar spectrum. The registered LV and adequate CA graphs are shown in Figs. 9 and 10B, respectively. According to the information provided in the experimental section, the LV scans were carried out twice, before and after 3 min long exposition of

the TiO_2NTs electrodes to the solar radiation. As can be observed in Fig. 9, the shapes of both runs of LV curves are very similar but do not overlap. Nevertheless, the material that exhibits the highest photo-conversion efficiency expressed here as the highest photocurrent, is again the one fabricated via anodization at the 40 V.

As it is known the photoelectrocatalytic performance is a several-step process and the overall enhancement depends on many different factors, namely strong light absorption, efficient charge separation and their low recombination efficiency. The first phenomenon that occurs when the light interacts with the material is their absorption, then formation of an exciton and its dissociation into opposite charges and finally charge percolation, electrons to the contact Ti substrate and holes at the electrode/electrolyte interface where they take part in oxidation process (in our case it is water molecule). Following that, the outstanding properties of this sample could be ascribed to the synergistic effect related with the value of E_{fb} , morphology features - especially highly developed surface area (16.4 cm^2 per 1 cm^2 of the flat surface), the most positive flatband energy and the presence of the surface trapped holes. Especially, the higher population of oxygen vacancies and mobile holes for the materials obtained above 40 V, as confirmed by the photoluminescence data, can effectively contribute to the management of photogenerated charges.

When it comes to the anodic shift and some changes in the shape of the LV curve above +0.2 V vs. Ag/AgCl/0.1 M KCl, the explanation of such behaviour has been already discussed above. As was reported by Cheng et al. [72] the photoinduced flat band potential shift can occur despite the dark conditions were once again provided due to the presence of the holes trapped at the electrode/electrolyte surface. Analysing the difference between LV recorded during the first and the second run, one may conclude that these STH can play crucial role leading to another favourable pathway for indirect charge transfer and a new undesirable recombination pathway [85,86]. Similar behaviour of LV curves was simulated by Bertoluzzi et al. and following his results the first run is attributed to the direct transfer of holes from the valence band while the second run can be interpreted as a competition of the direct hole transfer with the indirect charge transfer from the surface states. In this case, the photo-anodic currents grow up when those surface states assist in hampering the recombination processes, namely when the population of trapped electrons decreases. Therefore, it is of great interest to distinctly detect the surface states present on the

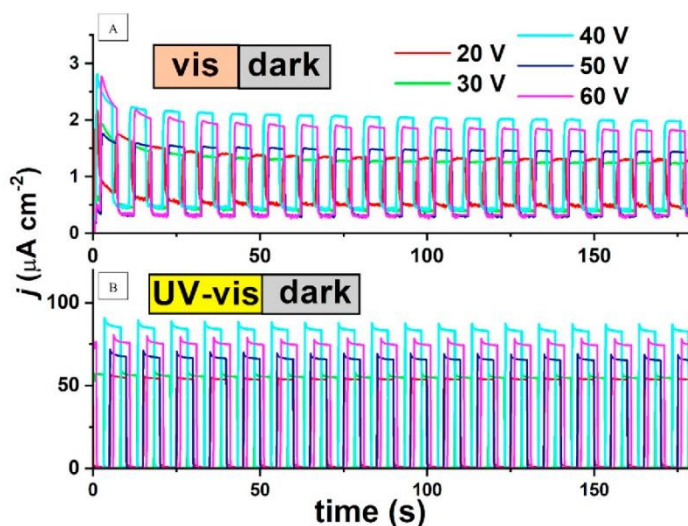


Fig. 10. Chronoamperometry curves recorded for the set of titania NTs samples at +0.5 V vs. Ag/AgCl/0.1 M KCl under intermitted vis and UV-vis illumination.

photoelectrodes and to deeply understand the key role they play in still explored class of free-standing TiO₂NTs, that provide both inner and outer tube walls to form the electrode/electrolyte interface.

Regarding the current stability when the samples are alternately illuminated by the whole solar spectrum, for none of the materials any obvious current diminution is observed. Nevertheless, as in the case with visible light, the highest photoresponse was observed for the material fabricated at 40 V, while the lowest currents were recorded when the anodization was carried out at 20 and 30 V. This trend is in line with the run of the potentiodynamic LV curves. Concluding, the difference in the materials photoactivity is mostly caused by the amount of the developed surface area and the bandgap energy, while surface trapped holes, as identified by analysis of optical properties and electrochemical activity, can support the charge transfer during photooxidation processes that occur at the interface of electrode/electrolyte species.

6. Conclusions

In the present manuscript, we investigated the influence of the two selected anodization parameters, namely duration and the value of the applied voltage onto the geometry, optical properties as well as electrochemical activity and photostability of the fabricated samples. Due to the applied optimization approach of the Ti electrochemical oxidation, the process resulted in the formation of highly ordered but well separated TiO₂ nanotubes. Such tubular arrangement differs from the typically used aligned TiO₂ since both inner and outer wall surface is easily available. As a consequence, the penetration of light and electrolyte species to the deeper parts of the TiO₂NTs layer is facilitated. According to the detailed analysis of the changes of TiO₂NTs morphology forced by the electric field present during anodization, we showed that relation between the applied voltage in the range of 20–60 V and the inner and outer radius of TiO₂NTs as well and separation distance is almost linear. What is of particular interest, the elongation of the anodization time from 2 to 5 h, does not impact significantly onto the tube length. Moreover, taking into account proposed simplified relationship including the values of the geometrical parameters, specific surface area was estimated. Following that, the highest developed area of tubular layer covering particular geometric surface was obtained when 50 V was applied during anodization. However, optical characterization covering the analysis of both the shape of the reflectance spectra and bandgap energy values, indicates that even with a slightly wider bandgap comparing to above mentioned sample, the titania fabricated at 40 V has the best overall light absorption. Finally, the series of samples obtained via 2 h-long electrochemical oxidation were subjected to the electrochemical testing. The recorded cyclic voltammetry scans for investigated titania NTs almost overlap while Mott-Schottky analysis points out some differences in flatband positions and the donor concentrations. Once again for TiO₂NTs fabricated at 40 V, the local maxima or minima was obtained regarding the highest (the most anodic) E_{fb} and the lowest N_d , respectively. The most anodic shifted E_{fb} was ascribed to the presence of the oxygen vacancies or other Ti species playing very important role in photoelectrochemical activity. Indeed, such properties found in the dark conditions affect the recorded photocurrents both in vis and UV-vis radiation. Within the series of samples, TiO₂NTs formed at 40 V generated the highest current in both light conditions. In our work we also showed the significant impact of the surface holes traps onto the overall photo-performance revealed as a shift in flat band potential as well as the shape and current density values observed on the linear voltammetry scans registered before and after short exposition of working electrode to the full solar spectrum. Summarizing, we widen the knowledge about the unique properties of spaced TiO₂ nanotubes and we believe that their application will gain as much attention as aligned titania.

CRediT authorship contribution statement

Jakub Wawrzyniak: Investigation, Validation, Writing - original draft. **Katarzyna Grochowska:** Conceptualization, Visualization, Resources, Writing - original draft, Writing - review & editing. **Jakub Karczewski:** Investigation. **Piotr Kupracz:** Investigation. **Jacek Ryl:** Investigation. **Anna Dolega:** Investigation. **Katarzyna Siuzdak:** Conceptualization, Writing - original draft, Writing - review & editing, Resources, Supervision, Project administration.

Declaration of competing interest

The authors declare that they have no known competing financial interests or personal relationships that could have appeared to influence the work reported in this paper.

Acknowledgements

This work received financial support from the Polish National Science Centre: Grant No. 2017/26/E/ST5/00416.

Appendix A. Supplementary data

Supplementary data to this article can be found online at <https://doi.org/10.1016/j.surfcoat.2020.125628>.

References

- [1] L. Li, Z. Liu, Q. Zhang, C. Meng, T. Zhang, J. Zhai, Underwater superoleophobic porous membrane based on hierarchical TiO₂ nanotubes: multifunctional integration of oil-water separation, flow-through photocatalysis and self-cleaning, *J. Mater. Chem. A* 3 (2015) 1279–1286, <https://doi.org/10.1039/C4TA04699D>.
- [2] B. Karunakaran, P. Uthirakumar, S.J. Chung, S. Velumani, E.-K. Suh, TiO₂ thin film gas sensor for monitoring ammonia, *Mater. Charact.* 58 (2007) 680–684, <https://doi.org/10.1016/j.matchar.2006.11.007>.
- [3] H.-M. Lin, C.-H. Keng, C.-Y. Tung, Gas-sensing properties of nanocrystalline TiO₂, *Nanostructured Mater* 9 (1997) 747–750, [https://doi.org/10.1016/S0965-9773\(97\)00161-X](https://doi.org/10.1016/S0965-9773(97)00161-X).
- [4] R. Daghrir, P. Drogui, D. Robert, Modified TiO₂ for environmental photocatalytic applications: a review, *Ind. Eng. Chem. Res.* 52 (2013) 3581–3599, <https://doi.org/10.1021/ie303468t>.
- [5] G.L. Chiarello, M.H. Aguirre, E. Selli, Hydrogen production by photocatalytic steam reforming of methanol on noble metal-modified TiO₂, *J. Catal.* 273 (2010) 182–190, <https://doi.org/10.1016/j.jcat.2010.05.012>.
- [6] X. Kang, S. Chen, Photocatalytic reduction of methylene blue by TiO₂ nanotube arrays: effects of TiO₂ crystalline phase, *J. Mater. Sci.* 45 (2010) 2696–2702, <https://doi.org/10.1007/s10853-010-4254-5>.
- [7] K.H. Ko, Y.C. Lee, Y.J. Jung, Enhanced efficiency of dye-sensitized TiO₂ solar cells (DSSC) by doping of metal ions, *J. Colloid Interface Sci.* 283 (2005) 482–487, <https://doi.org/10.1016/j.jcis.2004.09.009>.
- [8] Y. Lee, J. Chae, M. Kang, Comparison of the photovoltaic efficiency on DSSC for nanometer sized TiO₂ using a conventional sol-gel and solvothermal methods, *J. Ind. Eng. Chem.* 16 (2010) 609–614, <https://doi.org/10.1016/j.jiec.2010.03.008>.
- [9] A. Hegazy, N. Kinadjan, B. Sadeghimakki, S. Sivorthaman, N.K. Allam, E. Prouzet, TiO₂ nanoparticles optimized for photoanodes tested in large area dye-sensitized solar cells (DSSC), *Sol. Energy Mater. Sol. Cells* 153 (2016) 108–116, <https://doi.org/10.1016/j.solmat.2016.04.004>.
- [10] M. Shakeel Ahmad, A.K. Pandey, N. Abd Rahim, Advancements in the development of TiO₂ photoanodes and its fabrication methods for dye sensitized solar cell (DSSC) applications. A review, *Renew. Sust. Energ. Rev.* 77 (2017) 89–108, <https://doi.org/10.1016/j.rser.2017.03.129>.
- [11] W. Yu, J. Qiu, L. Xu, F. Zhang, Corrosion behaviors of TiO₂ nanotube layers on titanium in Hank's solution, *Biomed. Mater.* 4 (2009) 065012, <https://doi.org/10.1088/1748-6041/4/6/065012>.
- [12] P. Pu, H. Cachet, E. Ngaboyamahina, E.M.M. Sutter, Relation between morphology and conductivity in TiO₂ nanotube arrays: an electrochemical impedance spectroscopic investigation, *J. Solid State Electrochem.* 17 (2013) 817–828, <https://doi.org/10.1007/s10008-012-1931-0>.
- [13] C.-C. Tsai, H. Teng, Structural features of nanotubes synthesized from NaOH treatment on TiO₂ with different post-treatments, *Chem. Mater.* 18 (2006) 367–373, <https://doi.org/10.1021/cm051852t>.
- [14] T.R.B. Foong, Y. Shen, X. Hu, A. Sellinger, Template-directed liquid ALD growth of TiO₂ nanotube arrays: properties and potential in photovoltaic devices, *Adv. Funct. Mater.* 20 (2010) 1390–1396, <https://doi.org/10.1002/adfm.200902063>.
- [15] P. Roy, S. Berger, P. Schmuki, TiO₂ nanotubes: synthesis and applications, *Angew. Chem. Int. Ed.* 50 (2011) 2904–2939, <https://doi.org/10.1002/anie.201001374>.
- [16] Z. Jedy-soltanabadi, N. Pishkar, M. Ghoranneviss, Enhanced physical properties of

- the anodic TiO₂ nanotubes via proper anodization time, *J. Theor. Appl. Phys.* 12 (2018) 135–139, <https://doi.org/10.1007/s40094-018-0290-3>.
- [17] S. Ozkan, A. Mazare, P. Schmuki, Critical parameters and factors in the formation of spaced TiO₂ nanotubes by self-organizing anodization, *Electrochim. Acta* 268 (2018) 435–447, <https://doi.org/10.1016/j.electacta.2018.02.120>.
- [18] J. Kim, B. Kim, C. Oh, J. Ryu, H. Kim, E. Park, K. No, S. Hong, Effects of NH₄F and distilled water on structure of pores in TiO₂ nanotube arrays, *Sci. Rep.* 8 (2018) 12487, <https://doi.org/10.1038/s41598-018-30668-3>.
- [19] S. Ozkan, N.T. Nguyen, A. Mazare, P. Schmuki, Optimized spacing between TiO₂ nanotubes for enhanced light harvesting and charge transfer, *ChemElectroChem* 5 (2018) 3183–3190, <https://doi.org/10.1002/celec.201801136>.
- [20] D. Kowalski, J. Mallet, J. Michel, M. Molinari, Low electric field strength self-organization of anodic TiO₂ nanotubes in diethylene glycol electrolyte, *J. Mater. Chem. A* 3 (2015) 6655–6661, <https://doi.org/10.1039/C4TA06714B>.
- [21] S. Ozkan, N.T. Nguyen, A. Mazare, R. Hahn, I. Cerri, P. Schmuki, Fast growth of TiO₂ nanotube arrays with controlled tube spacing based on a self-ordering process at two different scales, *Electrochem. Commun.* 77 (2017) 98–102, <https://doi.org/10.1016/j.elecom.2017.03.007>.
- [22] A. Mohammadpour, K. Shankar, Anodic TiO₂ nanotube arrays with optical wavelength-sized apertures, *J. Mater. Chem.* 20 (2010) 8474, <https://doi.org/10.1039/c0jm02198a>.
- [23] K. S. Oh, C. J. S. Ji, Biomaterials and biotechnology schemes utilizing TiO₂ nanotube arrays, in: R. Pignatello (Ed.), *Biomater. Sci. Eng. InTech*, 2011, <https://doi.org/10.5772/23320>.
- [24] N.T. Nguyen, S. Ozkan, I. Hwang, A. Mazare, P. Schmuki, TiO₂ nanotubes with laterally spaced ordering enable optimized hierarchical structures with significantly enhanced photocatalytic H₂ generation, *Nanoscale* 8 (2016) 16868–16873, <https://doi.org/10.1039/C6NR06329B>.
- [25] S. Ozkan, N.T. Nguyen, A. Mazare, I. Cerri, P. Schmuki, Controlled spacing of self-organized anodic TiO₂ nanotubes, *Electrochem. Commun.* 69 (2016) 76–79, <https://doi.org/10.1016/j.elecom.2016.06.004>.
- [26] N.T. Nguyen, S. Ozkan, S. Hejazi, N. Denisov, O. Tomanec, R. Zboril, P. Schmuki, Providing significantly enhanced photocatalytic H₂ generation using porous PtPdAg alloy nanoparticles on spaced TiO₂ nanotubes, *Int. J. Hydrog. Energy* 44 (2019) 22962–22971, <https://doi.org/10.1016/j.ijhydene.2019.06.200>.
- [27] S. Ozkan, J. Yoo, N.T. Nguyen, S. Mohajernia, R. Zazpe, J. Prikril, J.M. Macak, P. Schmuki, Spaced TiO₂ nanotubes enable optimized Pt atomic layer deposition for efficient photocatalytic H₂ generation, *ChemistryOpen* 7 (2018) 797–802, <https://doi.org/10.1002/open.201800172>.
- [28] S. Ozkan, G. Cha, A. Mazare, P. Schmuki, TiO₂ nanotubes with different spacing, Fe₂O₃ decoration and their evaluation for Li-ion battery application, *Nanotechnology* 29 (2018) 195402, <https://doi.org/10.1088/1361-6528/aab062>.
- [29] S. Ozkan, N.T. Nguyen, I. Hwang, A. Mazare, P. Schmuki, Highly conducting spaced TiO₂ nanotubes enable defined conformal coating with nanocrystalline Nb₂O₅ and high performance supercapacitor applications, *Small* 13 (2017) 1603821, <https://doi.org/10.1002/sml.201603821>.
- [30] M.G. Necula, A. Mazare, R.N. Ion, S. Ozkan, J. Park, P. Schmuki, A. Gimpean, Lateral spacing of TiO₂ nanotubes modulates osteoblast behavior, *Materials* 12 (2019) 2956, <https://doi.org/10.3390/ma12182956>.
- [31] R. Beranek, (photo)electrochemical methods for the determination of the band edge positions of TiO₂-based nanomaterials, *Adv. Phys. Chem.* 2011 (2011) 1–20, <https://doi.org/10.1155/2011/786759>.
- [32] H. Tsuchiya, J.M. Macak, A. Gheiov, A.S. Räder, L. Taveira, P. Schmuki, Characterization of electronic properties of TiO₂ nanotube films, *Corros. Sci.* 49 (2007) 203–210, <https://doi.org/10.1016/j.corsci.2006.05.009>.
- [33] B.H. Park, L.S. Li, B.J. Gibbons, J.Y. Huang, Q.X. Jia, Photovoltaic response and dielectric properties of epitaxial anatase-TiO₂ films grown on conductive La_{0.5} Sr_{0.5} CoO₃ electrodes, *Appl. Phys. Lett.* 79 (2001) 2797–2799, <https://doi.org/10.1063/1.1412822>.
- [34] D. Regonini, C.R. Bowen, A. Jaroenworarluck, R. Stevens, A review of growth mechanism, structure and crystallinity of anodized TiO₂ nanotubes, *Mater. Sci. Eng. R. Rep.* 74 (2013) 377–406, <https://doi.org/10.1016/j.mser.2013.10.001>.
- [35] S. Ozkan, N.T. Nguyen, A. Mazare, I. Cerri, P. Schmuki, Controlled spacing of self-organized anodic TiO₂ nanotubes, *Electrochem. Commun.* 69 (2016) 76–79, <https://doi.org/10.1016/j.elecom.2016.06.004>.
- [36] A. Matsuda, S. Sreekantam, W. Krengvirat, Well-aligned TiO₂ nanotube arrays for energy-related applications under solar irradiation, *J. Asian Ceram. Soc.* 1 (2013) 203–219, <https://doi.org/10.1016/j.jascer.2013.07.001>.
- [37] N.T. Nguyen, S. Ozkan, I. Hwang, X. Zhou, P. Schmuki, Spaced TiO₂ nanotube arrays allow for a high performance hierarchical supercapacitor structure, *J. Mater. Chem. A* 5 (2017) 1895–1901, <https://doi.org/10.1039/C6TA01079H>.
- [38] S. Farsinezhad, P.R. Waghmare, B.D. Wiltshire, H. Sharma, S. Amiri, S.K. Mitra, K. Shankar, Amphiphobic surfaces from functionalized TiO₂ nanotube arrays, *RSC Adv.* 4 (2014) 33587–33598, <https://doi.org/10.1039/C4RA06402J>.
- [39] Brian O'Regan, Jacques Moser, Marc Anderson, Michael Graetzel, Vectorial electron injection into transparent semiconductor membranes and electric field effects on the dynamics of light-induced charge separation, *J. Phys. Chem.* 94 (1990) 8720–8726, <https://doi.org/10.1021/j100387a017>.
- [40] M. Adachi, Y. Murata, M. Harada, S. Yoshikawa, Formation of titania nanotubes with high photo-catalytic activity, *Chem. Lett.* 29 (2000) 942–943, <https://doi.org/10.1246/cl.2000.942>.
- [41] X. Chen, S.S. Mao, Titanium dioxide nanomaterials: synthesis, properties, modifications, and applications, *Chem. Rev.* 107 (2007) 2891–2959, <https://doi.org/10.1021/cr0500535>.
- [42] A. Lamberti, A. Chiodoni, N. Shahzad, S. Bianco, M. Quaglio, C.F. Pirri, Ultrafast room-temperature crystallization of TiO₂ nanotubes exploiting water-vapor treatment, *Sci. Rep.* 5 (2015) 7808, <https://doi.org/10.1038/srep07808>.
- [43] Q. Zhang, L. Ma, M. Shao, J. Huang, M. Ding, X. Deng, X. Wei, X. Xu, Anodic oxidation synthesis of one-dimensional TiO₂ nanostructures for photocatalytic and field emission properties, *J. Nanomater.* 2014 (2014) 1–14, <https://doi.org/10.1155/2014/831752>.
- [44] V. Likodimos, T. Stergiopoulos, P. Falaras, J. Kunze, P. Schmuki, Phase composition, size, orientation, and antenna effects of self-assembled anodized titania nanotube arrays: a polarized micro-Raman investigation, *J. Phys. Chem. C* 112 (2008) 12687–12696, <https://doi.org/10.1021/jp8027462>.
- [45] S. Meriam Suhaimey, C. Lai, H. Tajuddin, E. Samsudin, M. Johan, Impact of TiO₂ nanotubes' morphology on the photocatalytic degradation of simazine pollutant, *Materials* 11 (2018) 2066, <https://doi.org/10.3390/ma11112066>.
- [46] S. Das, R. Zazpe, J. Prikril, P. Knotek, M. Krbal, H. Sopha, V. Podzemna, J.M. Macak, Influence of annealing temperatures on the properties of low aspect-ratio TiO₂ nanotube layers, *Electrochim. Acta* 213 (2016) 452–459, <https://doi.org/10.1016/j.electacta.2016.07.135>.
- [47] P.F. McMillan, Amorphous materials: vibrational spectroscopy, *Encyclopedia of Materials: Science and Technology*, Elsevier, 2001, pp. 251–256, <https://doi.org/10.1016/B0-08-043152-6/00054-1>.
- [48] M. Hannula, H. Ali-Löyty, K. Lahtonen, E. Sarlin, J. Saari, M. Valden, Improved stability of atomic layer deposited amorphous TiO₂ photoelectrode coatings by thermally induced oxygen defects, *Chem. Mater.* 30 (2018) 1199–1208, <https://doi.org/10.1021/acs.chemmater.7b02938>.
- [49] X. Zhou, B. Jin, S. Zhang, H. Wang, H. Yu, F. Peng, Preparation of boron and phosphor co-doped TiO₂ nanotube arrays and their photoelectrochemical property, *Electrochem. Commun.* 19 (2012) 127–130, <https://doi.org/10.1016/j.elecom.2012.03.020>.
- [50] H. Li, J. Xing, Z. Xia, J. Chen, Preparation of extremely smooth and boron-fluorine co-doped TiO₂ nanotube arrays with enhanced photoelectrochemical and photocatalytic performance, *Electrochim. Acta* 139 (2014) 331–336, <https://doi.org/10.1016/j.electacta.2014.06.172>.
- [51] Q. Li, J.K. Shang, Self-organized nitrogen and fluorine co-doped titanium oxide nanotube arrays with enhanced visible light photocatalytic performance, *Environ. Sci. Technol.* 43 (2009) 8923–8929, <https://doi.org/10.1021/es902214s>.
- [52] S. Li, S. Lin, J. Liao, N. Pan, D. Li, J. Li, Nitrogen-doped TiO₂ nanotube arrays with enhanced photoelectrochemical property, *Int. J. Photoenergy*. 2012 (2012) 1–7, <https://doi.org/10.1155/2012/794207>.
- [53] L.C. Sim, K.W. Ng, S. Ibrahim, P. Saravanan, Preparation of improved p-n junction NiO/TiO₂ nanotubes for solar-energy-driven light photocatalysis, *Int. J. Photoenergy*. 2013 (2013) 1–10, <https://doi.org/10.1155/2013/659013>.
- [54] A. Al-Haddad, Z. Wang, R. Xu, H. Qi, R. Vellacheri, U. Kaiser, Y. Lei, Dimensional dependence of the optical absorption band edge of TiO₂ nanotube arrays beyond the quantum effect, *J. Phys. Chem. C* 119 (2015) 16331–16337, <https://doi.org/10.1021/acs.jpcc.5b02665>.
- [55] S. So, A. Kriesch, U. Peschel, P. Schmuki, Conical-shaped titania nanotubes for optimized light management in DSSCs reach back-side illumination efficiencies > 8%, *J. Mater. Chem. A* 3 (2015) 12603–12608, <https://doi.org/10.1039/C5TA02834E>.
- [56] M.B. Sarkar, A. Mondal, B. Choudhuri, B.K. Mahajan, S. Chakrabarty, C. Nangbam, Enlarged broad band photodetection using indium doped TiO₂ alloy thin film, *J. Alloys Compd.* 615 (2014) 440–445, <https://doi.org/10.1016/j.jallcom.2014.06.184>.
- [57] X. Wang, J. Zhao, X. Wang, J. Zhou, Causes for the formation of titania nanotubes during anodization, *IEEE Trans. Nanotechnol.* 14 (2015) 113–117, <https://doi.org/10.1109/TNANO.2014.2370041>.
- [58] W.-J. Yin, S. Chen, J.-H. Yang, X.-G. Gong, Y. Yan, S.-H. Wei, Effective band gap narrowing of anatase TiO₂ by strain along a soft crystal direction, *Appl. Phys. Lett.* 96 (2010) 221901, <https://doi.org/10.1063/1.3430005>.
- [59] S. Liang, J. He, Z. Sun, Q. Liu, Y. Jiang, H. Cheng, B. He, Z. Xie, S. Wei, Improving photoelectrochemical water splitting activity of TiO₂ nanotube arrays by tuning geometrical parameters, *J. Phys. Chem. C* 116 (2012) 9049–9053, <https://doi.org/10.1021/jp300552s>.
- [60] B. Liu, K. Nakata, S. Liu, M. Sakai, T. Ochiai, T. Murakami, K. Takagi, A. Fujishima, Theoretical kinetic analysis of heterogeneous photocatalysis by TiO₂ nanotube arrays: the effects of nanotube geometry on photocatalytic activity, *J. Phys. Chem. C* 116 (2012) 7471–7479, <https://doi.org/10.1021/jp300481a>.
- [61] D.K. Pallotti, L. Passoni, P. Maddalena, F. Di Fonzo, S. Lettieri, Photoluminescence mechanisms in anatase and rutile TiO₂, *J. Phys. Chem. C* 121 (2017) 9011–9021, <https://doi.org/10.1021/acs.jpcc.7b00321>.
- [62] K.Y. Jung, S.B. Park, M. Anpo, Photoluminescence and photoactivity of titania particles prepared by the sol-gel technique: effect of calcination temperature, *J. Photochem. Photobiol. A* 170 (2005) 247–252, <https://doi.org/10.1016/j.jphotochem.2004.09.003>.
- [63] H. Yu, J. Ma, Y. Zhang, X. Zhang, W. Shi, Cyclic voltammetry studies of TiO₂ nanotube arrays electrode: conductivity and reactivity in the presence of H⁺ and aqueous redox systems, *Electrochim. Acta* 56 (2011) 6498–6502, <https://doi.org/10.1016/j.electacta.2011.05.004>.
- [64] F. Fabregat-Santiago, I. Mora-Seró, G. Garcia-Belmonte, J. Bisquert, Cyclic voltammetry studies of nanoporous semiconductors. Capacitive and reactive properties of nanocrystalline TiO₂ electrodes in aqueous electrolyte, *J. Phys. Chem. B* 107 (2003) 758–768, <https://doi.org/10.1021/jp0265182>.
- [65] H. Pelouchova, P. Janda, J. Weber, L. Kavan, Charge transfer reductive doping of single crystal TiO₂ anatase, *J. Electroanal. Chem.* 566 (2004) 73–83, <https://doi.org/10.1016/j.jelechem.2003.11.013>.
- [66] C. Di Valentin, G. Pacchioni, A. Selloni, Reduced and n-type doped TiO₂ nature of Ti³⁺ species, *J. Phys. Chem. C* 113 (2009) 20543–20552, <https://doi.org/10.1021/>

- jp9061797.
- [67] F.Y. Oliva, L.B. Avallé, E. Santos, O.R. Cámara, Photoelectrochemical characterization of nanocrystalline TiO₂ films on titanium substrates, *J. Photochem. Photobiol. Chem.* 146 (2002) 175–188, [https://doi.org/10.1016/S1010-6030\(01\)00614-1](https://doi.org/10.1016/S1010-6030(01)00614-1).
 - [68] M. Dolata, P. Kedzierzawski, J. Augustynski, Comparative impedance spectroscopy study of rutile and anatase TiO₂ film electrodes, *Electrochim. Acta* 41 (1996) 1287–1293, [https://doi.org/10.1016/0013-4686\(95\)00449-1](https://doi.org/10.1016/0013-4686(95)00449-1).
 - [69] J. Zheng, H. Zhou, Y. Zou, R. Wang, Y. Lyu, S.P. Jiang, S. Wang, Efficiency and stability of narrow-gap semiconductor-based photoelectrodes, *Energy Environ. Sci.* 12 (2019) 2345–2374, <https://doi.org/10.1039/C9EE00524B>.
 - [70] P. Acevedo-Peña, J. Vazquez-Arenas, R. Cabrera-Sierra, L. Lartundo-Rojas, I. González, Ti anodization in alkaline electrolyte: the relationship between transport of defects, film hydration and composition, *J. Electrochem. Soc.* 160 (2013) C277–C284, <https://doi.org/10.1149/2.063306jes>.
 - [71] L. Giorgi, T. Dikonimos, R. Giorgi, F. Buonocore, G. Faggio, G. Messina, N. Lisi, Electrochemical synthesis of self-organized TiO₂ crystalline nanotubes without annealing, *Nanotechnology* 29 (2018) 095604, <https://doi.org/10.1088/1361-6528/aaa448>.
 - [72] X. Cheng, D.-S. Kong, Z. Wang, Y.-Y. Feng, W.-J. Li, Inhibiting effect of carbonate on the photoinduced flatband potential shifts during water photooxidation at TiO₂/solution interface, *J. Solid State Electrochem.* 21 (2017) 1467–1475, <https://doi.org/10.1007/s10008-016-3500-4>.
 - [73] H. Ge, H. Tian, Y. Zhou, S. Wu, D. Liu, X. Fu, X.-M. Song, X. Shi, X. Wang, N. Li, Influence of surface states on the evaluation of the flat band potential of TiO₂, *ACS Appl. Mater. Interfaces* 6 (2014) 2401–2406, <https://doi.org/10.1021/am404743a>.
 - [74] P. Pu, H. Cachet, E. Ngaboyamahina, E.M.M. Sutter, Relation between morphology and conductivity in TiO₂ nanotube arrays: an electrochemical impedance spectroscopic investigation, *J. Solid State Electrochem.* 17 (2013) 817–828, <https://doi.org/10.1007/s10008-012-1931-0>.
 - [75] L. Sang, H. Tan, X. Zhang, Y. Wu, C. Ma, C. Burda, Effect of quantum dot deposition on the interfacial flatband potential, depletion layer in TiO₂ nanotube electrodes, and resulting H₂ generation rates, *J. Phys. Chem. C* 116 (2012) 18633–18640, <https://doi.org/10.1021/jp305388c>.
 - [76] A.I. Savva, K.A. Smith, M. Lawson, S.R. Croft, A.E. Weltner, C.D. Jones, H. Bull, P.J. Simmonds, L. Li, H. Xiong, Defect generation in TiO₂ nanotube anodes via heat treatment in various atmospheres for lithium-ion batteries, *Phys. Chem. Chem. Phys.* 20 (2018) 22537–22546, <https://doi.org/10.1039/C8CP04368J>.
 - [77] T. Su, Y. Yang, Y. Na, R. Fan, L. Li, L. Wei, B. Yang, W. Cao, An insight into the role of oxygen vacancy in hydrogenated TiO₂ nanocrystals in the performance of dye-sensitized solar cells, *ACS Appl. Mater. Interfaces* 7 (2015) 3754–3763, <https://doi.org/10.1021/am5085447>.
 - [78] V.K. Mahajan, M. Misra, K.S. Raja, S.K. Mohapatra, Self-organized TiO₂ nanotubular arrays for photoelectrochemical hydrogen generation: effect of crystallization and defect structures, *J. Phys. Appl. Phys.* 41 (2008) 125307, <https://doi.org/10.1088/0022-3727/41/12/125307>.
 - [79] Q. Kang, J. Cao, Y. Zhang, L. Liu, H. Xu, J. Ye, Reduced TiO₂ nanotube arrays for photoelectrochemical water splitting, *J. Mater. Chem. A* 1 (2013) 5766, <https://doi.org/10.1039/c3ta10689f>.
 - [80] M.N. Shaddad, D. Cardenas-Morcoso, M. García-Tecedor, F. Fabregat-Santiago, J. Bisquert, A.M. Al-Mayouf, S. Gimenez, TiO₂ nanotubes for solar water splitting: vacuum annealing and Zr doping enhance water oxidation kinetics, *ACS Omega* 4 (2019) 16095–16102, <https://doi.org/10.1021/acsomega.9b02297>.
 - [81] I. Cesar, K. Sivula, A. Kay, R. Zboril, M. Grätzel, Influence of feature size, film thickness, and silicon doping on the performance of nanostructured hematite photoanodes for solar water splitting, *J. Phys. Chem. C* 113 (2009) 772–782, <https://doi.org/10.1021/jp809060p>.
 - [82] F. La Mantia, H. Habazaki, M. Santamaria, F. Di Quarto, A critical assessment of the Mott-Schottky analysis for the characterisation of passive film-electrolyte junctions, *Russ. J. Electrochem.* 46 (2010) 1306–1322, <https://doi.org/10.1134/S102319351011011X>.
 - [83] G. Cooper, Mott-Schottky plots and flatband potentials for single crystal rutile electrodes, *J. Electrochem. Soc.* 129 (1982) 1973, <https://doi.org/10.1149/1.2124334>.
 - [84] F. Cardon, W.P. Gomes, On the determination of the flat-band potential of a semiconductor in contact with a metal or an electrolyte from the Mott-Schottky plot, *J. Phys. Appl. Phys.* 11 (1978) L63–L67, <https://doi.org/10.1088/0022-3727/11/4/003>.
 - [85] L. Bertoluzzi, P. Lopez-Varo, J.A. Jiménez Tejada, J. Bisquert, Charge transfer processes at the semiconductor/electrolyte interface for solar fuel production: insight from impedance spectroscopy, *J. Mater. Chem. A* 4 (2016) 2873–2879, <https://doi.org/10.1039/C5TA03210E>.
 - [86] J. Bisquert, Theory of the impedance of charge transfer via surface states in dye-sensitized solar cells, *J. Electroanal. Chem.* 646 (2010) 43–51, <https://doi.org/10.1016/j.jelechem.2010.01.007>.

Chapter two

Laser interactions with matter

When propagating light encounters an interface between two media, it can be either reflected or can continue its propagation through the new media. Depending on the permittivity of the medium, it can also be absorbed through the interactions with the matter it passes. The primary factors determining light interactions with the material are: wavelength, fluence, and the time of interaction. The wavelength determines if and how the light is absorbed, as the response of the different compounds varies, depending on their surface and molecular composition. On the other hand, fluence and time of irradiation along with the thermal conductivity determine the magnitude of the light-induced interactions [29].

In principle, valence electrons interact with incident photons absorbing them. Depending on the amount of energy transferred, the electron can either move to the excited state, get launched further into the crystal lattice as a hot electron, or be ejected from the surface in a photoelectric effect. Naturally, the added energy creates a non-equilibrium state, therefore after some time excited electron recombines creating a photon (radiative recombination) or dissipating into heat via phonons (non-radiative recombination) [30]. Typically, the relaxation in semiconductors occurs between the 10^{-12} and 10^{-10} s of the excitement [31,32], so depending on the laser type and pulse duration, the excited carriers may or may not be able to thermalize obtained energy. Within the constraints of this work, only the nanosecond pulsed laser radiation (10^{-9} s) is considered, which allows repeated excitation and thermalization of the surface electrons during a single pulse. Therefore, the thermal equilibrium between electrons and phonons can be assumed and only the thermal

effects of the laser radiation are taken into the account [29,32]. These include heating, melting, and ablation from the surface. Because of the highly localized heating provided by the nanosecond laser radiation, they are commonly used in, for example, cutting, welding, and surface treatment [32,33].

Work two: Formation of the hollow nanopillar arrays through the laser-induced transformation of TiO₂ nanotubes

Although pulsed lasers are commonly used on titania, it is usually done to ablate, melt, or structure titania layers and powders [34–37]. The effects of laser irradiation on the titania nanotubes were, however, investigated only briefly in the attempts to crystallize amorphous TiO₂ and boost their photoactivity. Although partial crystallization was achieved through the use of pulsed lasers, the continuous heat sources provided a much more reliable phase transformation, while preserving the original tubular morphology [38,39]. The investigation into the effects of laser treatment on the photoelectrochemical performance of the densely packed, crystalline titania nanotubes revealed that it can have beneficial effects on the photocurrent densities under simulated solar radiation [40,41]. Interestingly though, the effects were exactly opposite in the case of spaced NTs, chosen as a substrate for modification (Figure 4).

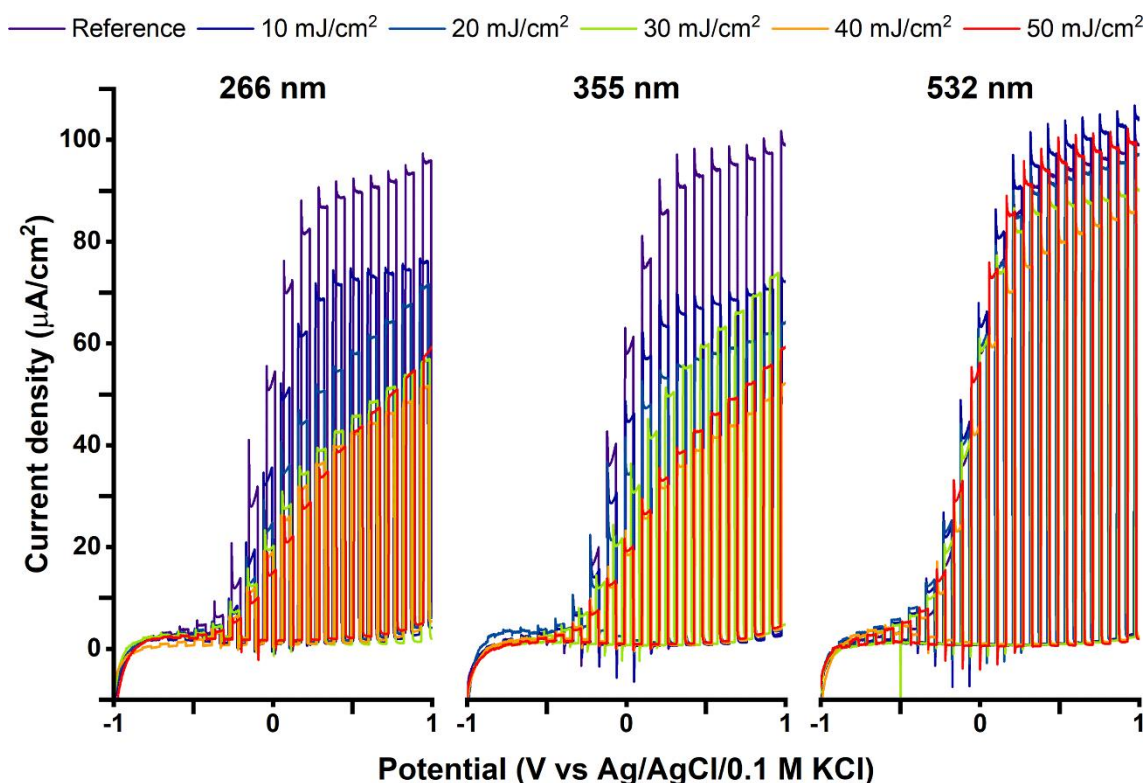


Figure 4: Linear voltamperograms of the spaced titania nanotubes treated with three different wavelengths of the pulsed laser in the 0 – 50 mJ/cm² fluence range. The investigation was done with chopped AM 1.5 illumination in 0.5 M Na₂SO₄.

The investigation of the effects of different laser wavelengths on the geometry and properties of the nanotubes conducted in a work two revealed significant differences between the wavelengths and energies used (see Attachment 2). Most notably, within the investigated fluence range (0 – 50 mJ/cm²) irradiation with photons of energy lower than the materials bandgap did not affect its physical properties. After the modification with the wavelengths from the UV range (266, 355 nm), however, the substrates displayed a varying degree of melting and some alteration of their physical properties. The UV-vis spectra reveal the presence of the interference fringes created by the reflection of the light from the sealed caps [42] and significantly lower UV absorption which suggests the possible creation of oxygen vacancies [6]. The profile of the deconvoluted photoluminescence spectra revealed a slight shift of emission from

blue to green light, which hints at the increased presence of trapped holes (so, the oxygen vacancies in the case of TiO_2) [43].

However, the most interesting finding of the work reveals that the use of 355 nm wavelength at the fluence of 30 mJ/cm^2 , results in an elegant encapsulation of the nanotubes without their excessive melting or merging with neighboring structures. The structure itself is especially intriguing, as the tight seal over the nanotube completely isolates its interior. The unique geometry of the nanopillars allows the possibility of embedding different compounds inside them before encapsulation. This could lead to the creation of interesting titania-based nanocapsules or photonic structures.



OPEN

Formation of the hollow nanopillar arrays through the laser-induced transformation of TiO₂ nanotubes

Jakub Wawrzyniak^{1✉}, Jakub Karczewski², Piotr Kupracz³, Katarzyna Grochowska¹, Emerson Coy³, Adam Mazikowski⁴, Jacek Ryl⁵ & Katarzyna Siuzdak¹

In the following article, we present a simple, two-step method of creating spaced, hollow nanopillars, from the titania nanotube arrays via pulsed laser-treatment. Due to the high ordering of the structure, the prepared material exhibits photonic properties, which has been shown to increase the overall photoefficiency. The optical and morphological changes in the titania nanotubes after pulsed laser-treatment with 532, 355, and 266 nm wavelengths in the 10–50 mJ/cm² fluence range are studied. The investigation reveals, that by using appropriate wavelength and energy, the number of surface defects, geometrical features, or both can be tailored.

Due to rising worldwide energy demand and increasing awareness about the dangers of using fossil fuels, more and more attention is being paid to renewable sources of power. The titanium dioxide nanotubes (TiO₂NTs) have been excessively studied for years since their first synthesis by Assefpour-Dezfuly et al.¹ due to their excellent photocorrosion resistance², non-toxicity, and outstanding optical properties³. Moreover, the TiO₂NTs exhibit very high surface area and have easily tuneable nanotube length⁴, spacing^{5,6}, and pore size^{7–9}, all influencing properties of the nanotube array. Because of that, they have found immense success in research involving gas sensors¹⁰, filtering systems¹¹, solar cells¹², and photocatalysis^{13,14}.

However, one of the biggest drawbacks of TiO₂NTs is their wide bandgap of 3.2 eV limiting their absorption to the UV range, which represents only a small part of the solar spectrum. To successfully employ titania nanotubes in solar-driven applications, various methods of widening absorption band have been discussed in the literature. Modifications with non-metals or organics primarily focus on employing narrow bandgap materials which help in exciton generation over a broader light spectrum^{15,16}. On the other hand, doping with noble metals, which strongly interact with light in the visible spectrum through plasmonic resonance, allows the injection of hot-electrons into nanotube arrays improving their overall photoactivity^{17,18}.

Interestingly though, structural and morphological changes have also been shown to be a key factor in band-gap engineering¹⁹. The synthesis of TiO₂NTs with the high surface-to-volume ratio results in improved radiation harvesting. Simultaneously, optimization of the length of the TiO₂NTs is crucial to avoid excessive recombination of generated charge carriers²⁰.

It should be highlighted that those methods do not rely on the incorporation of foreign atoms into the structure of titania, but rather modify existing one to broaden the absorbance spectra. It is done through so-called self-doping and relies heavily on the creation of structural defects such as oxygen vacancies and employs various methods, e.g. microwave or laser irradiation^{21–24}. Likewise, the additional absorbance bands can be created or widened by adjusting TiO₂NTs spatial distribution, similarly to how it is done in photonic structures⁵.

Recently, the use of titania nanotubes as photonic crystal (PC) arrays gains increased traction in literature^{18,25–27}. Due to the high refractive index of TiO₂ structures, and regular spatial distribution of the nanotubes, the TiO₂NTs are clear candidates for use as photonic materials. Coupled with the scattering of incident light on top of the tubular layer, the total material absorption could be greatly improved while retaining their charge percolation capabilities^{28–30}.

¹Centre of Plasma and Laser Engineering, Institute of Fluid-Flow Machinery, Polish Academy of Sciences, Fiszerka 14 st., 80-231 Gdańsk, Poland. ²Department of Solid-State Physics, Gdańsk University of Technology, Gabriela Narutowicza 11/12 st., 80-233 Gdańsk, Poland. ³NanoBioMedical Centre, Adam Mickiewicz University, Wszechnicy Piastowskiej 3 st., 61-614 Poznań, Poland. ⁴Department of Metrology and Optoelectronics, Gdańsk University of Technology, Gabriela Narutowicza 11/12 st., 80-233 Gdańsk, Poland. ⁵Department of Electrochemistry, Corrosion and Materials Engineering, Gdańsk University of Technology, Gabriela Narutowicza 11/12 st., 80-233 Gdańsk, Poland. ✉email: jwawrzyniak@imp.gda.pl

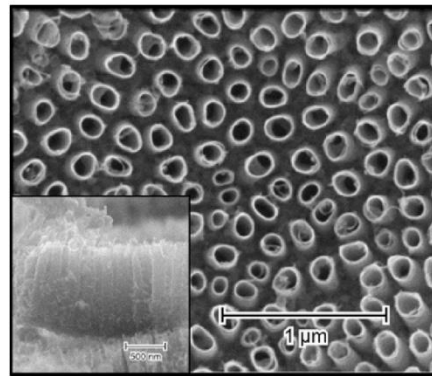


Figure 1. SEM image of the anodized TiO₂NTs with their cross-section shown in the inset.

In our work, we present a blueprint for the creation of an array of empty, evenly spaced, self-standing TiO₂ nanopillars. The proposed smart laser treatment of an open tube TiO₂NTs results in their closing and formation of the tight cap over the hollow tube. Although they exhibit photonic properties by themselves, they can also serve as a base for further modifications, allowing encapsulation of different materials inside, potentially serving as a shell in novel core-shell type of photonic nanostructures.

Results and discussion

Morphology. As-anodized TiO₂NTs have an inner radius of about 60 nm, the wall thickness of 12 nm, they are evenly distributed with the average distance between them of 70 nm, and have 1 μm in length (Fig. 1). The calcination process does not affect their morphology in any way, and they retain all their geometrical features. The effects of laser irradiation of different wavelengths within a fluence range of 10–50 mJ/cm² are presented in Fig. 2. The first column shows the effects of modification with 4th harmonics generator crystal ($\lambda = 266$ nm), representing photon energy (~ 4.6 eV) well above the bandgap of the material ($E_{\text{bg}} = 3.3$ eV). In the case of the lowest fluence used, no meaningful changes to TiO₂NTs morphology can be observed (Fig. 2A). However, as the pulse energy rises, some nanotube tops begin to melt, forming connected platforms made of two or three closest nanotubes, resulting in non-uniform surface morphologies. Although the degree of their melting in the upper region varies clearly, the height of the TiO₂NTs modified with $\lambda = 266$ nm changes only slightly with the energy used. While TiO₂NTs irradiated with 20 mJ/cm² are about 750 nm in length, those treated with 50 mJ/cm² are only about 150 nm shorter.

Considering laser-modifications with 3rd harmonics and photon energy (3.5 eV) close to the bandgap of the material, the degree of changes seems to be much more uniform across energies used (Fig. 2F–J). In the case of the lowest fluence applied, the nanotubes tops melt slightly inwards, forming half-open cylinders. Regarding fluences of 20 and 30 mJ/cm², the upper parts of the nanotubes are fully closed and the vast majority of the nanotubes are self-standing, not merging with neighboring ones. Using higher energies results in gradually more interconnections between TiO₂NTs. The nanotubes have shortened to about 840 nm after irradiation with 10 mJ/cm², and were approximately 65 nm shorter each time the fluence was increased, down to 575 nm at 50 mJ/cm².

Modification with photon energies (2.3 eV) much lower than the electron bandgap did not result in any changes in overall nanotubes length within the investigated range of fluences. There were, however, visible distortions in the nanotube openings when fluence 50 mJ/cm² was reached.

The TEM images confirm the empty core of the nanotubes (Fig. 3A) and show a tight cap in their upper region. Notice, that the beam has enough energy to cross the cap and reveal the internal section of the tubes. The images indicate, that the melted cap is approximately 170 nm thick, and there is still nearly 700 nm of the empty nanotube core underneath (Fig. 3D). Moreover, the evidence of the anatase crystalline phase have been found, as the Fast-Fourier Transform of the close-ups of the cap (Fig. 3B,E) reveal $d_{(101)} = 0.35$, $d_{(103)} = 0.24$, and $d_{(105)} = 0.17$ nm peaks (Fig. 3C,F). This shows that the majority of the anatase phase is undisturbed by laser modification.

To our knowledge, such structures have not been yet reported in the literature. Although few works regarding laser-modification of TiO₂NTs are available^{22,23,31,32}, all of the investigators have focused on the densely packed nanotube arrays, where melting of neighboring nanotubes caused their individual features to disappear. Irradiation of differently spaced nanotubes³³ with $\lambda = 355$ nm and 30 mJ/cm², however, is a reliable method of TiO₂NT encapsulation (Fig. 4).

Optical properties. *Reflectance spectra.* The reflectance spectra for investigated samples are shown in Fig. 5. In the case of modification with $\lambda = 266$ and 355 nm, the interference fringes can be seen. They form due to interference of the light-waves reflected from the closed, upper parts of the TiO₂NTs and those propagating through the TiO₂NT film, reflected at the bottom. Chiarello et al.³⁴ have proposed an equation that allows calcu-

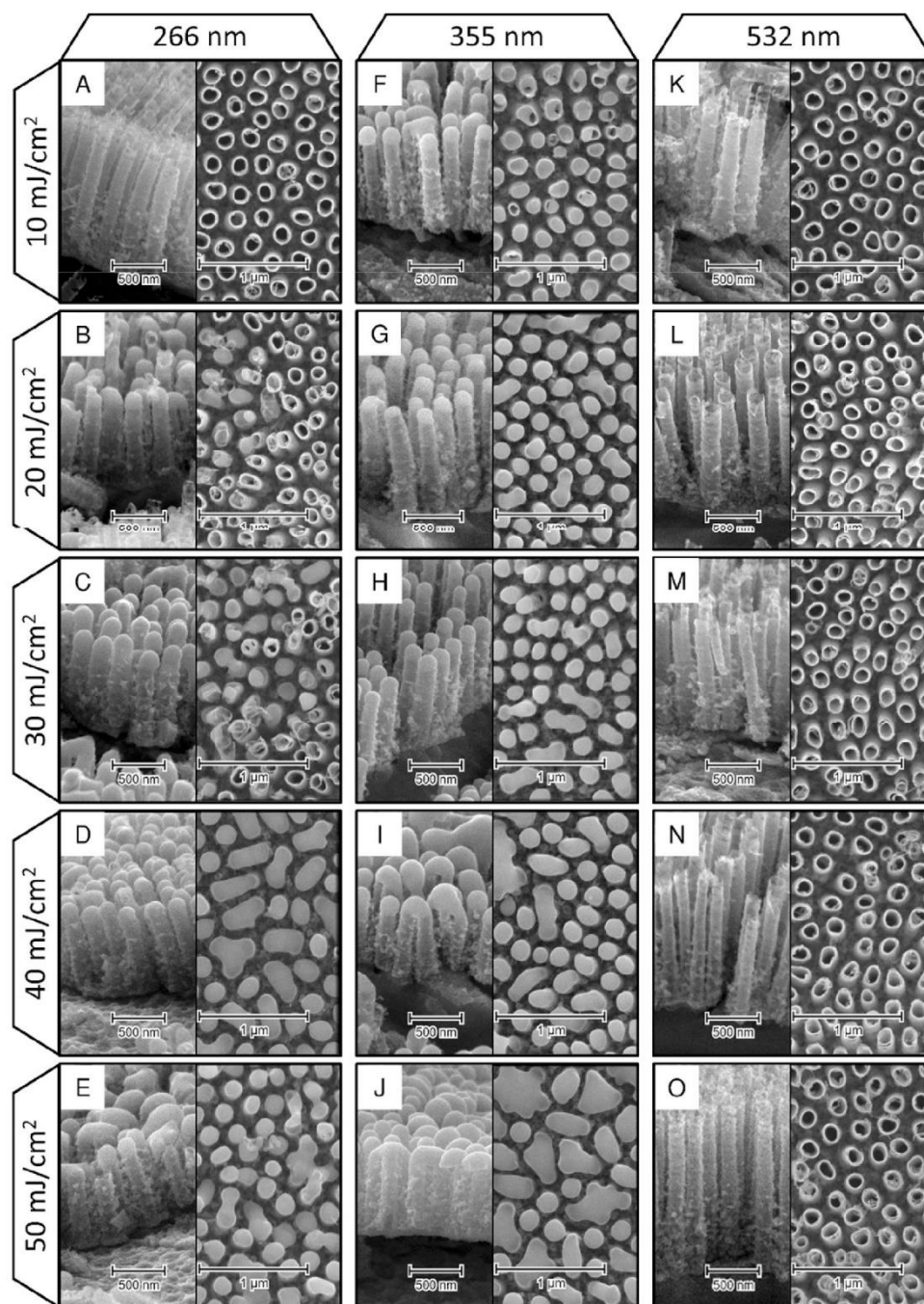


Figure 2. SEM images of the laser-modified TiO_2NTs . The columns show different wavelengths used (266, 355, and 532 respectively) while rows represent fluence used (10–50 mJ/cm^2).

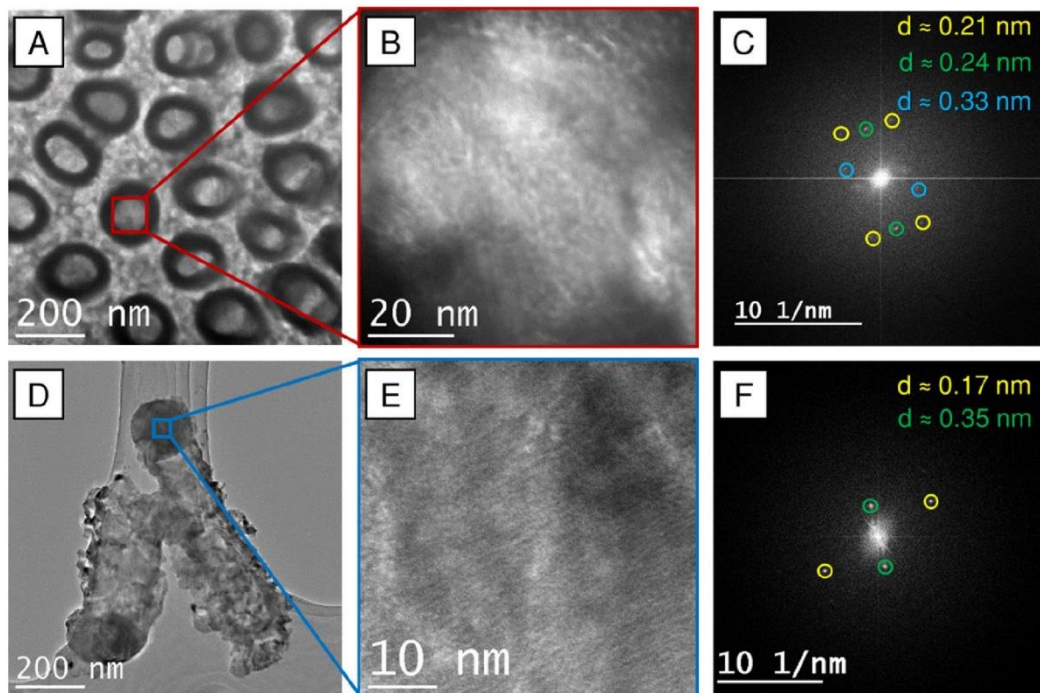


Figure 3. TEM images of the nanotubes irradiated with 30 mJ/cm² with the $\lambda = 355$ nm. (A) shows the top view of the TiO₂NTs. (B) Close-up of the internal section of the TiO₂NTs. (C) The FFT image of (B). (D) Shows a removed TiO₂NT, laying down on the Cu grid allowing for visualization of the cap. (E) Shows a close up of the cap and (F) the FFT image of Panel E).

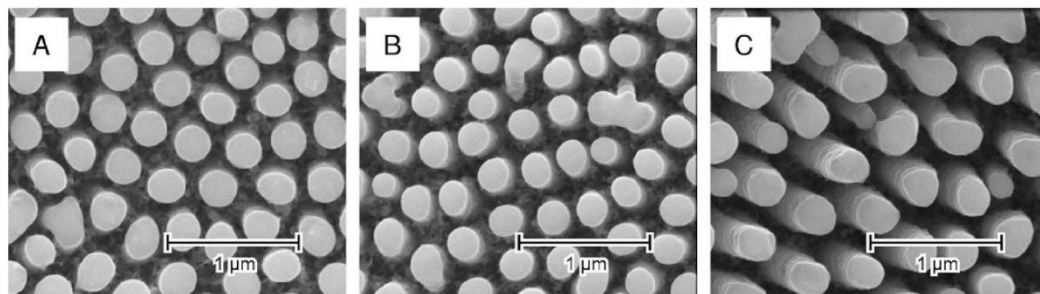


Figure 4. SEM images of the TiO₂NTs anodized at 40 (A), 50 (B), and 60 V (C) post laser-treatment ($\lambda = 355$ nm, 30 mJ/cm²).

lation of the TiO₂NT length, using two consecutive fringe positions. Regarding the irradiation at a normal angle of incidence, it can be simplified to:

$$d = \frac{\lambda_1 \lambda_2}{2n(\lambda_2 - \lambda_1)}$$

where d is the thickness of the layer, n is the refractive index of the anatase (approximately 2.2 between 450 and 600 nm), and λ_1 and λ_2 are the positions of the respective fringes. The equation correlates well into experimental data regarding both geometric and optical features, explaining the periodic nature of the spectrum. Moreover, the presence of the fringes or lack thereof can be explained by the amount of the material present in the upper nanotube region, i.e. in the cap (Figs. 2, 5). The exception, in this case, would be modification with $\lambda = 355$ nm

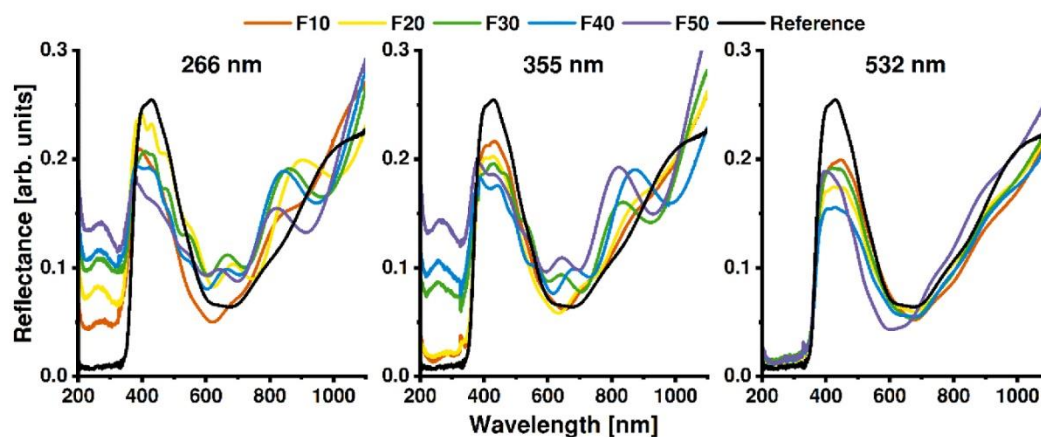


Figure 5. Reflectance spectra of the reference and TiO₂NTs modified with three different laser wavelengths within the fluence range of 10–50 mJ/cm².

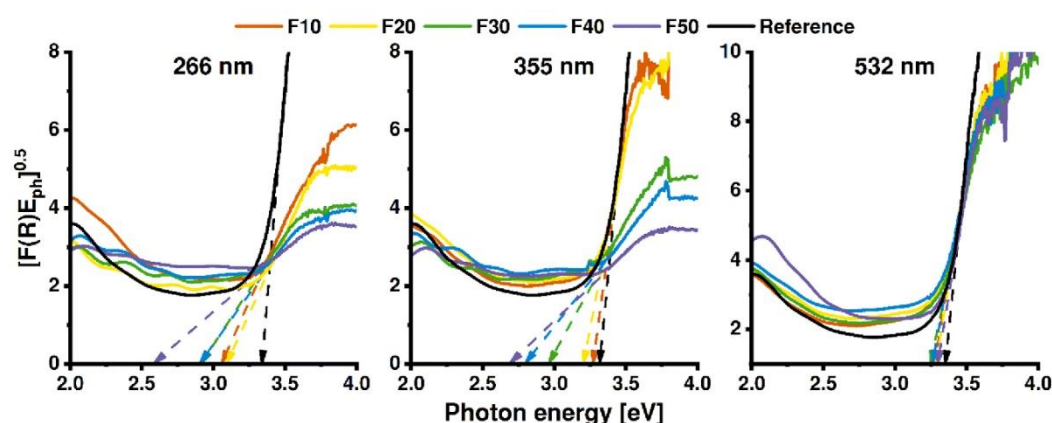


Figure 6. Calculated Tauc plots with dashed lines indicating bandgap values.

with 10 and 20 mJ/cm², where although capping of the TiO₂NTs is present, the periodic nature of the spectra is not distinguished. It may be explained by the very thin capping layer and a negligible amount of light reflecting from the cap. Interestingly, whereas Chiarello et al.³⁴ observed fringes for spectra recorded for TiO₂NT layers as thick as 2 μm, we could not define them for the reference material with half the thickness. In this case, the defined spacing between the TiO₂NTs could be the determining factor responsible for the shape of the reflectance spectra. Interestingly, the changes in the UV region of the reflectance spectra are, except fringes, unrelated to the degree of morphological changes in the TiO₂NTs (see Fig. 2). An increase in the UV reflectance is present in samples irradiated with 266 and 355 nm lasers. Although in the case of irradiation with 4th harmonics the absorbance drops rapidly, slowing in the upper energy regime, a significant increase in 3rd harmonics is present only when fluence over 30 mJ/cm² is used. As the light absorption in this region is mainly attributed to the electron transitions from O²⁻ orbital to the Ti⁴⁺³⁵, an increased presence of oxygen vacancies can result in the rise of radiative recombination seen as the increment in the reflectance spectra.

Figure 6 shows Tauc plots of the laser-modified TiO₂NTs accompanied with the untreated sample. The bandgap of the reference sample equals approximately 3.3 eV, slightly higher than for bulk anatase, due to the so-called electron-confinement effect, often present in nanomaterials^{36–38}. The E_{bg} shifts towards lower values with increased fluence for both irradiation with 266 and 355 nm, whereas it drops only slightly when the wavelength of 532 nm is applied during the modification. The narrowing of the E_{bg} values is likely related to the creation of additional localized states within the bandgap allowing lower-energy photons to be absorbed³⁹.

Photoluminescence. Taking into account resolved photoluminescence (PL) spectra reported by other authors, obtained data points were fitted into distinctive emission bands (Fig. 7) using parameters listed in Table 1^{40–44}.

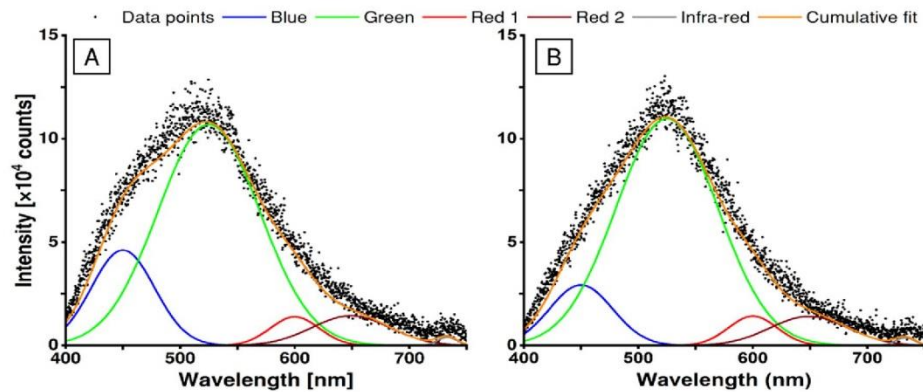


Figure 7. Deconvoluted photoluminescence spectra for unmodified sample (A) and the sample modified by 355 nm laser with 30 mJ/cm² (B).

Colour	Blue	Green	Red 1	Red 2	Infra-red
Peak position [nm]	450	525	600	649	733
FWHM [nm]	65	105	50	80	20

Table 1. Fitting parameters used to perform deconvolution of photoluminescence spectra.

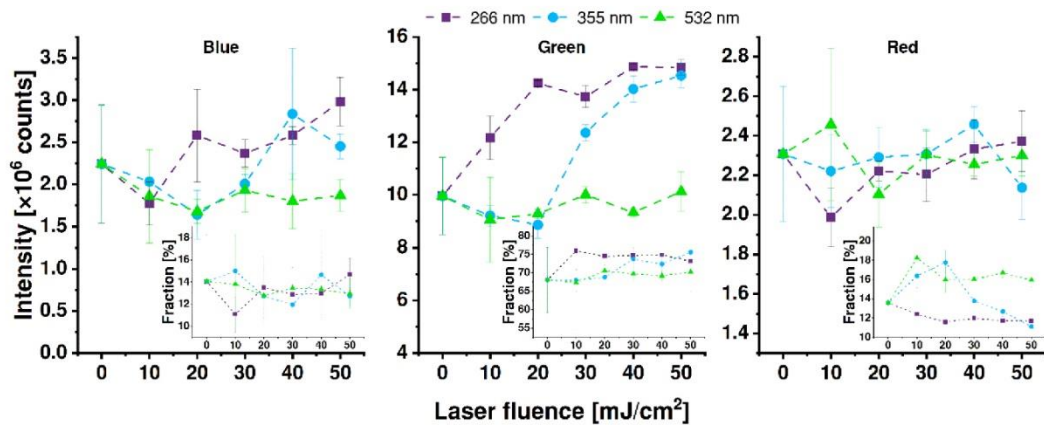


Figure 8. Intensities of the blue, green, and red photoluminescence of the samples as a function of laser fluence used for modification. Insets show the contribution to the total emission.

Analysis of the photoluminescence results, in general, shows that laser annealing of the TiO₂NTs changes their overall emissivity spectrum. The strongest influence of laser treatment can be observed for the green light emission (Fig. 8) after irradiation of titania with 266 and 355 nm lasers. Although in the case of 4th harmonics the enhancement of emissivity is evident even when the low fluence is used, it quickly saturates at 20 mJ/cm² and a further increase in laser energy does not affect the total green emission. Changes induced by 3rd harmonics are, on the other hand, minimal for fluences up to 20 mJ/cm², but rise and saturate at higher investigated energies. Moreover, a slight increase in the total blue emissivity was observed in the case of modification via both 3rd and 4th harmonics in their respective processing thresholds. However, none of the applied laser wavelengths modulates the red-emission sector and the usage of 2nd harmonics does not noticeably affect the emission spectrum.

In TiO₂NTs, the blue photoluminescence band is related to electron–hole recombination between conduction and valence bands, green is the effect of recombination of mobile electrons with trapped holes, and red arises due to the recombination of electrons trapped on Ti³⁺ ions with valence band^{44,45}. Thus, the increment of the green PL

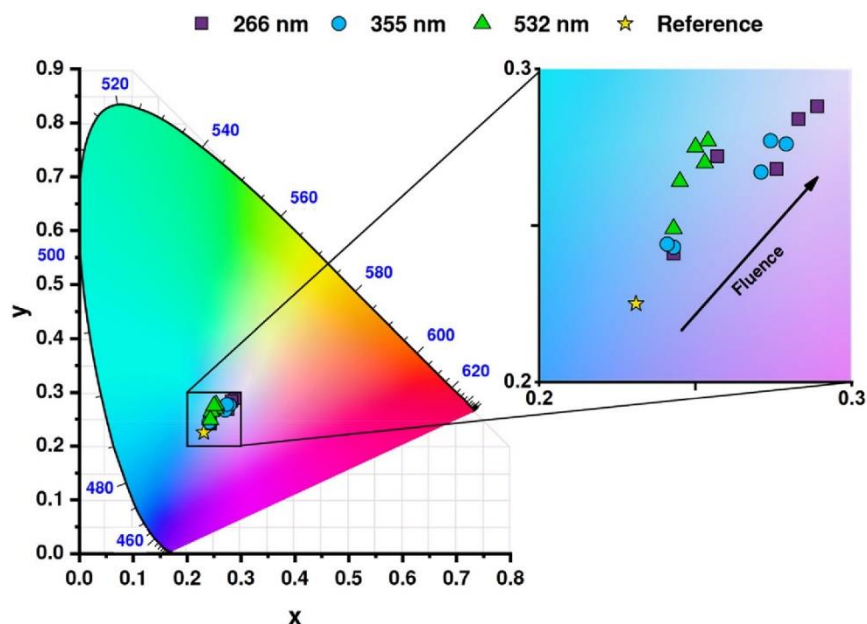


Figure 9. CIE xy chromaticity diagram marked with positions of investigated samples. The inset presents a close-up of the color spectrum and the arrow indicates an increase in fluence.

after the treatment with $\lambda = 266$ and 355 nm may be explained by the growing number of trapped holes related to the increasing number of oxygen vacancies regarding as the tuning factor of the electronic properties of the TiO_2 nanostructures⁴⁶. The laser-induced increase of the number of oxygen vacancies was further confirmed by the high-resolution X-ray photoelectron spectra recorded within binding energy of $\text{Ti}2p$ (see Figure S1 with appropriate analysis provided in ESI file)^{47,48}.

Colorimetry. Apart from the typical analysis of the reflectance spectra, we performed colorimetric analysis and the results were summarized as particular points on a CIE 1931 chromaticity diagram (see Fig. 9). The colorimetric investigation lines up with previously observed effects verified via reflectance measurements. In the series representing the shortest wavelength used for titania treatment, the sample color changes rapidly towards the center of the map (white) and reaching almost the same coordinates at the high-end of measured fluence range. Modification with 355 nm laser pulses affects color only slightly for fluences of 10 and 20 mJ/cm^2 , but the skip on the CIE chart for 30 mJ/cm^2 is very definitive. Interestingly, the color is changing as well for samples modified with 2nd harmonics. Although no apparent huge shift could be observed via the naked eye, the change from the reference sample towards green color is present and saturates for fluences above 30 mJ/cm^2 . Similar behavior was found for chromium coatings after their exposure to the energetic photons from various laser sources. It confirms that laser modification could be regarded as not fully used, but a powerful tool for optical tuning of thin films⁴⁹. Therefore, without the introduction of any metal or non-metal atoms to the titania structure, optimized laser treatment provides intriguing light-matter interaction behaviors.

Conclusion

Summarizing, in the frames of this work a unique approach of obtaining free-standing, nanotube-based, hollow titania nanopillars has been shown. In the first step, self-standing titania nanotubes were fabricated via an optimized anodization process, followed by calcination which ensured crystallization. Next, three different wavelengths of a pulsed laser, namely 266, 355 and 532 nm, were used to tailor the upper part of the TiO_2NTs . Analysis of the SEM/TEM images confirms that the treatment with 355 nm led to the formation of crystalline caps over each hollow pillar, while the photon energies at 266 and 532 nm were either too high or too low resulting in overmelting of the nanotubes or simply preservation of their original geometry. Optical measurements reveal that materials exposed to laser radiation exhibit the nature of photonic crystal. Moreover, the increased number of oxygen vacancies with increased fluence for 266 and 355 nm wavelengths was confirmed by the photoluminescence spectra fitting approach, while colorimetric analysis indicates the possibility of color switching depending on the applied processing parameters. Obtained results strongly suggest that laser interaction with TiO_2 nanotubes can lead not only to change of their geometrical features but also opens up the possibility of

tuning their optical behavior with preserving the crystalline phase and the hollow interior. To the best of our knowledge, such an approach has been shown for the very first time. Additionally, due to the chemical stability of the titania, we believe that prepared material can be adapted for many purposes, especially as a platform for encapsulation of other materials.

Experimental section

Sample preparation. Titanium foil (99.7% pure, 0.127 mm thick, Strem) was cut into 35 × 25 mm pieces and degreased ultrasonically for 10 min in acetone (p.a. Protolab), ethanol (96%, Chempur) and deionized (DI) water (0.08 µS, Hydrolab) respectively. After drying in air, it was used as a working electrode in the electrochemical oxidation process to create free-standing TiO₂NTs, whereas platinum net (25 × 25 mm) was used as a counter electrode. The electrolyte in which both electrodes were submerged consisted of NH₄F (0.3 wt%, p.a. Chempur), HF (0.5 wt%, p.a. Chempur), and of deionized water (7.0 wt%) in diethylene glycol (p.a. Chempur). Anodization was performed at 30 V, with ramp-up and ramp-down voltages set to 0.1 V/s and controlled by in-house built hardware which was supplied by a constant voltage generator (MPS-600-5L-2). The process was performed at a constant temperature of 40 °C, controlled by a thermostat (Julabo F-12) for 2 h. After anodization, the foil was rinsed and submerged in ethanol for ca. 1 h and dried in air subsequently.

To obtain a crystalline anatase phase, the nanotubes underwent thermal treatment in the furnace (Nabertherm) at 450 °C for 2 h. While the heating rate was set to 2 °C/min, the cooling down to room temperature was performed freely overnight. A sample prepared in such a way was treated as a reference for laser-modified material.

Nd:YAG pulsed laser (6 ns, Quantel) equipped with 2nd, 3rd, and 4th harmonics generator crystals ($\lambda = 266, 355, \text{ and } 532 \text{ nm}$) was used to modify the surface of TiO₂NTs structure. The laser repetition rate was set to 2 Hz and its fluence to 10–50 mJ/cm². The beam was homogenized and focused on the surface, creating 2.4 × 2.4 mm spot. The sample was placed on the motorized, computer-controlled stage (SmarAct) enabling precise movement and thus allowing modification on any part of the surface.

Characterization. Scanning Electron Microscope (SEM) images were taken with FE-SEM, FEI Quanta FEG 250 which was equipped with a secondary electron detector. The pictures were taken at the surface and at the cross-section in multiple places to confirm sample uniformity. During the measurements, a constant acceleration voltage of 10 kV was applied.

Transmission Electron Microscopy (TEM) investigation was done using JEOL ARM 200F, working at 80 kV. Data collected was used to confirm the crystallinity and detailed morphology of the formed nanopillars.

The UV–Vis study was done in the reflectance mode using the PerkinElmer dual-beam spectrophotometer in the range of 300–1100 nm with a scanning speed set to 120 nm/min.

Photoluminescence (PL) spectra were taken using SHAMROCK-SR-3031-A Spectrograph (Andor Technology) at room temperature. It was equipped with 450 mW LED as the excitation light source ($\lambda = 365 \text{ nm}$) and ICCD camera as a detector. FGUV-11 (Thorlabs) and GG 400 (Shott AG) optical filters were used to eliminate unwanted light modes during measurements of the PL spectra. A total of 200 scans in the range of 370–800 nm were done and their average was used for further investigation. The X-ray photoelectron spectroscopy (XPS) studies were carried out using Axis Supra spectrometer equipped with monochromatic AlK α source with 250 µm spot diameter, and 20 eV pass energy, calibrated for adventitious carbon C1s (284.5 eV).

The colorimetric investigation was done using the Konica Minolta CS-2000 spectroradiometer, which allows for the determination of colorimetric coordinates with accuracy and repeatability of ± 0.002 according to CIE xy standard. A halogen bulb (3100 K) was used as a light source, illuminating the sample at 45°, while the measurements were taken perpendicular to the surface from a measuring field of a 1.75 mm in diameter. To become independent of the source spectral characteristics, the Konica Minolta SC-A5 white standard was used for the determination of colorimetric coordinates.

Received: 18 June 2020; Accepted: 9 November 2020

Published online: 19 November 2020

References

1. Assefpour-Dezfuly, M., Vlachos, C. & Andrews, E. H. Oxide morphology and adhesive bonding on titanium surfaces. *J. Mater. Sci.* **19**, 3626–3639 (1984).
2. Mahajan, V., Mohapatra, S. & Misra, M. Stability of TiO₂ nanotube arrays in photoelectrochemical studies. *Int. J. Hydrog. Energy* **33**, 5369–5374 (2008).
3. Shi, J. *et al.* Photoluminescence characteristics of TiO₂ and their relationship to the photoassisted reaction of water/methanol mixture. *J. Phys. Chem. C* **111**, 693–699 (2007).
4. Paulose, M. *et al.* TiO₂ nanotube arrays of 1000 µm length by anodization of titanium foil: Phenol red diffusion. *J. Phys. Chem. C* **111**, 14992–14997 (2007).
5. Ozkan, S., Nguyen, N. T., Mazare, A. & Schmuki, P. Optimized spacing between TiO₂ nanotubes for enhanced light harvesting and charge transfer. *ChemElectroChem* **5**, 3183–3190 (2018).
6. Ozkan, S., Mazare, A. & Schmuki, P. Critical parameters and factors in the formation of spaced TiO₂ nanotubes by self-organizing anodization. *Electrochim. Acta* **268**, 435–447 (2018).
7. Kim, J. *et al.* Effects of NH₄F and distilled water on structure of pores in TiO₂ nanotube arrays. *Sci. Rep.* **8**, 12487 (2018).
8. Bauer, S., Kleber, S. & Schmuki, P. TiO₂ nanotubes: Tailoring the geometry in H₃PO₄/HF electrolytes. *Electrochem. Commun.* **8**, 1321–1325 (2006).
9. Macak, J. M., Hildebrand, H., Marten-Jahns, U. & Schmuki, P. Mechanistic aspects and growth of large diameter self-organized TiO₂ nanotubes. *J. Electroanal. Chem.* **621**, 254–266 (2008).

10. Karunakaran, B., Uthirakumar, P., Chung, S. J., Velumani, S. & Suh, E.-K. TiO₂ thin film gas sensor for monitoring ammonia. *Mater. Charact.* **58**, 680–684 (2007).
11. Li, L. *et al.* Underwater superoleophobic porous membrane based on hierarchical TiO₂ nanotubes: Multifunctional integration of oil–water separation, flow-through photocatalysis and self-cleaning. *J. Mater. Chem. A* **3**, 1279–1286 (2015).
12. Wang, X., Sun, L., Zhang, S. & Wang, X. Ultralong, small-diameter TiO₂ nanotubes achieved by an optimized two-step anodization for efficient dye-sensitized solar cells. *ACS Appl. Mater. Interfaces* **6**, 1361–1365 (2014).
13. Kang, X. & Chen, S. Photocatalytic reduction of methylene blue by TiO₂ nanotube arrays: effects of TiO₂ crystalline phase. *J. Mater. Sci.* **45**, 2696–2702 (2010).
14. Macak, J. M., Zlamal, M., Krysa, J. & Schmuki, P. Self-organized TiO₂ nanotube layers as highly efficient photocatalysts. *Small* **3**, 300–304 (2007).
15. Daghrir, R., Drogui, P. & Robert, D. Modified TiO₂ for environmental photocatalytic applications: A review. *Ind. Eng. Chem. Res.* **52**, 3581–3599 (2013).
16. Piskunov, S. *et al.* C-, N-, S-, and Fe-doped TiO₂ and SrTiO₃ nanotubes for visible-light-driven photocatalytic water splitting: Prediction from first principles. *J. Phys. Chem. C* **119**, 18686–18696 (2015).
17. Chiarello, G. L., Aguirre, M. H. & Selli, E. Hydrogen production by photocatalytic steam reforming of methanol on noble metal-modified TiO₂. *J. Catal.* **273**, 182–190 (2010).
18. Hyam, R. S. *et al.* Plasmonic–photonic interference coupling in submicrometer amorphous TiO₂–Ag nanoarchitectures. *Langmuir* **33**, 12398–12403 (2017).
19. Qu, R. *et al.* Morphology-induced TiO₂ bandgap change for super rapid treatment of dye wastewater under visible light. *Adv. Mater. Technol.* **2**, 1700125 (2017).
20. Ghicov, A. *et al.* TiO₂ nanotubes in dye-sensitized solar cells: Critical factors for the conversion efficiency. *Chem. Asian J.* **4**, 520–525 (2009).
21. Zhang, Z. *et al.* Microwave-assisted self-doping of TiO₂ photonic crystals for efficient photoelectrochemical water splitting. *ACS Appl. Mater. Interfaces* **6**, 691–696 (2014).
22. Xu, Y., Melia, M. A., Tsui, L., Fitz-Gerald, J. M. & Zangari, G. Laser-induced surface modification at anatase TiO₂ nanotube array photoanodes for photoelectrochemical water oxidation. *J. Phys. Chem. C* **121**, 17121–17128 (2017).
23. Hsu, M.-Y., Van Thang, N., Wang, C. & Leu, J. Structural and morphological transformations of TiO₂ nanotube arrays induced by excimer laser treatment. *Thin Solid Films* **520**, 3593–3599 (2012).
24. Sopha, H. *et al.* Laser-induced crystallization of anodic TiO₂ nanotube layers. *RSC Adv.* **10**, 22137–22145 (2020).
25. Guo, M. *et al.* Coupling plasmonic nanoparticles with TiO₂ nanotube photonic crystals for enhanced dye-sensitized solar cells performance. *Electrochim. Acta* **263**, 373–381 (2018).
26. Kim, W.-T. & Choi, W.-Y. Fabrication of TiO₂ photonic crystal by anodic oxidation and their optical sensing properties. *Sens. Actuators A* **260**, 178–184 (2017).
27. Lu, Y., Yu, H., Chen, S., Quan, X. & Zhao, H. Integrating plasmonic nanoparticles with TiO₂ photonic crystal for enhancement of visible-light-driven photocatalysis. *Environ. Sci. Technol.* **46**, 1724–1730 (2012).
28. Lin, J., Liu, X., Zhu, S. & Chen, X. TiO₂ nanotube structures for the enhancement of photon utilization in sensitized solar cells. *Nanotechnol. Rev.* **4**, 2 (2015).
29. Waqas, M. *et al.* Multi-shelled TiO₂/Fe₂O₃ heterostructured hollow microspheres for enhanced solar water oxidation. *Nano Res.* **10**, 3920–3928 (2017).
30. Qi, J. *et al.* Multi-shelled CeO₂ hollow microspheres as superior photocatalysts for water oxidation. *Nanoscale* **6**, 4072–4077 (2014).
31. Haryński, Ł., Grochowska, K., Karczewski, J., Ryl, J. & Siuzdak, K. Scalable route toward superior photoresponse of UV-laser-treated TiO₂ nanotubes. *ACS Appl. Mater. Interfaces* **12**, 3225–3235 (2020).
32. Wawrzyniak, J. *et al.* Laser-assisted modification of titanium dioxide nanotubes in a tilted mode as surface modification and patterning strategy. *Appl. Surf. Sci.* **508**, 145143 (2020).
33. Wawrzyniak, J. *et al.* The geometry of free-standing titania nanotubes as a critical factor controlling their optical and photoelectrochemical performance. *Surf. Coat. Technol.* **389**, 125628 (2020).
34. Chiarello, G. L., Zuliani, A., Ceresoli, D., Martinazzo, R. & Selli, E. Exploiting the photonic crystal properties of TiO₂ nanotube arrays to enhance photocatalytic hydrogen production. *ACS Catal.* **6**, 1345–1353 (2016).
35. Pasikhani, J. V., Gilani, N. & Pirbazari, A. E. Improvement the wastewater purification by TiO₂ nanotube arrays: The effect of etching-step on the photo-generated charge carriers and photocatalytic activity of anodic TiO₂ nanotubes. *Solid State Sci.* **84**, 57–74 (2018).
36. Peng, H. & Li, J. Quantum confinement and electronic properties of rutile TiO₂ nanowires. *J. Phys. Chem. C* **112**, 20241–20245 (2008).
37. Xue, X. *et al.* Raman investigation of nanosized TiO₂: Effect of crystallite size and quantum confinement. *J. Phys. Chem. C* **116**, 8792–8797 (2012).
38. Cummings, F. R., Le Roux, L. J., Mathe, M. K. & Knoesen, D. Structure induced optical properties of anodized TiO₂ nanotubes. *Mater. Chem. Phys.* **124**, 234–242 (2010).
39. Bharti, B., Kumar, S., Lee, H.-N. & Kumar, R. Formation of oxygen vacancies and Ti³⁺ state in TiO₂ thin film and enhanced optical properties by air plasma treatment. *Sci. Rep.* **6**, 32355 (2016).
40. Mathew, S. *et al.* UV-visible photoluminescence of TiO₂ nanoparticles prepared by hydrothermal method. *J. Fluoresc.* **22**, 1563–1569 (2012).
41. Stevanovic, A., Büttner, M., Zhang, Z. & Yates, J. T. Photoluminescence of TiO₂: Effect of UV light and adsorbed molecules on surface band structure. *J. Am. Chem. Soc.* **134**, 324–332 (2012).
42. Mercado, C., Seeley, Z., Bandyopadhyay, A., Bose, S. & McHale, J. L. Photoluminescence of dense nanocrystalline titanium dioxide thin films: Effect of doping and thickness and relation to gas sensing. *ACS Appl. Mater. Interfaces* **3**, 2281–2288 (2011).
43. Abazović, N. D. *et al.* Photoluminescence of anatase and rutile TiO₂ particles. *J. Phys. Chem. B* **110**, 25366–25370 (2006).
44. Pallotti, D. K., Passoni, L., Maddalena, P., Di Fonzo, F. & Lettieri, S. Photoluminescence mechanisms in anatase and rutile TiO₂. *J. Phys. Chem. C* **121**, 9011–9021 (2017).
45. Jung, K. Y., Park, S. B. & Anpo, M. Photoluminescence and photoactivity of titania particles prepared by the sol–gel technique: Effect of calcination temperature. *J. Photochem. Photobiol. A* **170**, 247–252 (2005).
46. Sarkar, A. & Khan, G. G. The formation and detection techniques of oxygen vacancies in titanium oxide-based nanostructures. *Nanoscale* **11**, 3414–3444 (2019).
47. Siuzdak, K. *et al.* Thin layer of ordered boron-doped TiO₂ nanotubes fabricated in a novel type of electrolyte and characterized by remarkably improved photoactivity. *Appl. Surf. Sci.* **357**, 942–950 (2015).
48. Rogala, M. *et al.* Self-reduction of the native TiO₂ (110) surface during cooling after thermal annealing—in-operando investigations. *Sci. Rep.* **9**, 12563 (2019).
49. Kotsedi, L. *et al.* Chromium oxide formation on nanosecond and femtosecond laser irradiated thin chromium films. *Opt. Mater.* **95**, 109206 (2019).

Acknowledgments

This work received financial support from the Polish National Science Centre: Grant No. 2017/26/E/ST5/00416. E.C. acknowledges the partial support provided by the project H2020-MSCA-RISE-2017 (project number: 778157) on the TEM studies of this manuscript.

Author contributions

J.K.—SEM investigation, P.K.—Photoluminescence investigation, E.C.—TEM investigation, A.M.—colorimetric investigation, J.R.—XPS investigation, J.W.—Uv-vis investigation, preparation of the manuscript text and figures, K.G.—research supervision, K.S.—funding acquisition, research supervision.

Competing interests

The authors declare no competing interests.

Additional information

Supplementary information is available for this paper at <https://doi.org/10.1038/s41598-020-77309-2>.

Correspondence and requests for materials should be addressed to J.W.

Reprints and permissions information is available at www.nature.com/reprints.

Publisher's note Springer Nature remains neutral with regard to jurisdictional claims in published maps and institutional affiliations.



Open Access This article is licensed under a Creative Commons Attribution 4.0 International License, which permits use, sharing, adaptation, distribution and reproduction in any medium or format, as long as you give appropriate credit to the original author(s) and the source, provide a link to the Creative Commons licence, and indicate if changes were made. The images or other third party material in this article are included in the article's Creative Commons licence, unless indicated otherwise in a credit line to the material. If material is not included in the article's Creative Commons licence and your intended use is not permitted by statutory regulation or exceeds the permitted use, you will need to obtain permission directly from the copyright holder. To view a copy of this licence, visit <http://creativecommons.org/licenses/by/4.0/>.

© The Author(s) 2020

Chapter three

Electrochemical water-splitting

Production, storage, and utilization of energy are undoubtedly one of our civilization's greatest challenges, as most aspects of everyday life depend on one of its forms. As society develops, it requires more electricity to illuminate homes, fuel to drive cars, and gas to cook food. Unfortunately, however, most of the energy sources we utilize come from non-renewable fossil fuels, which use emits the equivalent of around 50 billion tons of CO₂ annually [44]. As a result of the continually increasing emission of greenhouse gases, we now face progressing destabilization of the natural environment, in the form of natural disasters, acidification of oceans, and weather anomalies. Therefore, much effort has been made to find and develop more efficient ways of harvesting energy from alternative sources. One of the most promising renewable energy sources is the Sun, which by itself could provide more than enough energy to sustain the steady growth of our civilization. However, aside from the cheap production of electricity, the means of its efficient storage are needed. One of the commonly discussed candidates is hydrogen, which when obtained through water electrolysis, is as emission-free as the electricity made to create it.

In principle, electrolysis requires two electrodes with the potential difference of 1.23 V submerged in water. In reality, though, many more requirements must be met to be able to split water efficiently [45]. First, the conductivity of pure water is too low for the reaction to occur. Secondly, the materials of both cathode and the anode need to be chosen carefully to allow for efficient charge transfer [46]. Thirdly, the theoretical minimum

potential assumes ideal process efficiency and no losses, which is unattainable in real-world conditions.

Typically, the first obstacle is bypassed by carrying out electrolysis in water-based electrolytes. Because the electrolyte should not compete with the splitting of water, the half-reaction of cations ought to have a lower standard electrode potential than the reduction of H^+ , while the anions should have it higher than the oxidation of OH^- . The compounds such as Na_2SO_4 or $NaOH$ are therefore the most widely used due to their low cost and good performance. To overcome the second issue, the materials with the right electron structure need to be selected. If the potential of the valence band of the anode is higher than the oxidizing potential of water, it will oxidize instead of water. Similarly, if the lowest level of the conducting band of the cathode is below the reduction potential of hydrogen, it will reduce itself. For this reason, the alloys of the platinum group metal species, such as ruthenium or iridium oxides (RuO_2 / IrO_2) are used as anodes, whereas platinum or carbon are the primary materials for cathodes. Although they currently serve as a benchmark for efficient water splitting, their cost adds to the overall price of produced gases. The final obstacle in designing efficient electrodes for water electrolysis ties to the search for new, cheaper, and more feasible electrode materials. The theoretical minimum potential of 1.23 V does not include losses on the activation energy, diffusion, resistance, adsorption, bubble detachment, and more. Therefore, in search of novel, cheap and efficient electrodes, the overpotential values often dictate the feasibility of the obtained structures.

Work three: Spectacular Oxygen Evolution Reaction Enhancement through Laser Processing of the Nickel-Decorated Titania Nanotubes

Due to their vast availability, the non-noble transition metal oxides pose an interesting alternative to the platinum-group metal species. Many novel works are dedicated to the Mo, Fe, Co, and Ni-containing compounds and their respective oxides and sulfides, producing electrodes with promising properties towards bifunctional water-splitting electrodes [47–55]. Because the developed surface plays a crucial role in the electrolysis, the deposition of one of those transition metals on the electrode comprised of titania nanotubes could lead to significant improvements in the rate at which the oxygen is generated. Furthermore, as the structural defects are known to improve the catalytic performance of both titania and transition metal oxides, laser irradiation can be employed to facilitate their generation [56–58].

Work three provides detailed physicochemical characteristics of the nickel-coated anatase titania nanotubes after irradiation with a pulsed UV laser (Attachment 3). The structural analysis reveals that even at elevated fluences the tight sealing of the nanotubes is present, and the absorption spectra suggest the creation of the oxygen vacancies when fluence exceeds 20 mJ/cm^2 [6]. The voltamperometric curves recorded in alkaline media show negligibly higher current densities towards oxygen production after nickel deposition as compared to the uncoated titania nanotubes. After the irradiation with laser, however, the performance of the electrode raises to values 240-times higher than the unmodified material, and up to 280-times higher under simulated solar irradiation. The XPS investigation revealed that the synthesized electrode contains mostly hydroxide forms of nickel. Crucially, the prepared electrodes remain stable. After the 12-hour galvanostatic load at 10 mA/cm^2 , the potential shifted by less than 2 %. Interestingly, the overall increase of the rate at which the oxygen is generated happens despite the laser-

induced reduction of the active surface – after irradiation, the inner tube walls are sealed off from the electrolyte. Nonetheless, the boost in the electrochemical performance is unquestionable. It suggests that different mechanisms outweigh the negative effects of the limited surface, such as the oxyhydroxides forming from the nickel species on the surface of the electrodes [46].

Spectacular Oxygen Evolution Reaction Enhancement through Laser Processing of the Nickel-Decorated Titania Nanotubes

Jakub Wawrzyniak,* Jakub Karczewski, Emerson Coy, Igor Iatsunskyi, Jacek Ryl, Maria Gazda, Katarzyna Grochowska, and Katarzyna Siuzdak

The selective, laser-induced modification of the nickel-decorated titania nanotubes provides remarkable enhancement toward oxygen evolution reaction. Particularly, the irradiation of the laterally spaced crystalline TiO_2 nanotubes, results in the formation of the tight closure over irradiated end, preserving their hollow interior. The shape of the absorbance spectra is modulated along with applied energy, and the new absorption band appears at 500 nm, where the local minimum can be found for bare nanotubes. The high-resolution X-ray photoelectron spectra indicate the presence of both metallic and hydroxide forms of nickel species. The electrode material treated with 355 nm pulses at 50 mJ cm^{-2} shows significantly improved current densities in the anodic regime, reaching nearly 300 mA cm^{-2} while exposed to solar radiation, whereas the untreated sample barely comes to 1.5 mA cm^{-2} in the same conditions. The tailored titania photoanode also exhibits two orders of magnitude higher donor concentration in comparison to the primary substrate as verified by Mott–Schottky analysis. The electrochemical analysis confirms the key role of laser annealing in enhancing the effectiveness of light-driven water splitting.

Growing concerns for a natural environment drive innovation toward novel, clean energy sources, and storage devices.^[1,2] Among them, cheap but efficient water-splitting devices are being developed, and great hopes are being put into light-enabled catalysts. The titania-based electrode materials are especially looked at, because of their abundance, flexibility, and high stability within a wide pH range.^[3] Moreover, there are plentiful forms in which titania can be synthesized, which makes it a perfect target for further modifications. Apart from decoration with foreign species, doping, and formation of non-stoichiometric titania,^[4–9] many works rely upon the manipulation of titania architecture to improve its light-harvesting capabilities.^[10,11] The ordered titania nanotubes (TiO_2NTs) are of particular interest, due to the straight charge percolation path, high surface area, and adjustable geometrical


features. The optimized electrochemical oxidation of the titanium sheet provides control over the length,^[12] diameter,^[13,14] and spacing^[15,16] of the nanotubes, which allows their tailoring toward specific applications. Adjustments of the surface morphology do not stop with an anodization process, though. With the additional post-processing such as flame annealing,^[17] atomic layer deposition,^[18] or plasma treatment,^[19] crystallinity, and photoelectrochemical response can be freely adjusted as well. Considering efficient water splitting, catalysts containing abundant transition metals are recently being explored,^[20] but often require laborious techniques and generate a lot of harmful waste. Regardless of the treatment procedure, the electrochemical performance of the modified substrate does not exceed a several-fold increase in comparison to the original material.^[21,22] In this paper, spectacular oxygen evolution reaction (OER) and photoresponse improvements of the nickel-decorated titania nanotubes are reported. Incorporation of the 355 nm pulsed laser irradiation, as well as the use of titanium and nickel in their pure metallic forms, minimizes the generation of chemical waste. Moreover, the proposed processing technique can be applied onto a platform of any dimension, as each step of the synthesis is highly scalable.^[23,24]

Scanning electron microscopy (SEM) images of laterally spaced TiO_2 nanotubes before and after modifications as well

J. Wawrzyniak, Dr. K. Grochowska, Prof. K. Siuzdak
Centre for Plasma and Laser Engineering
The Szevalska Institute of Fluid-Flow Machinery
Polish Academy of Sciences
Fiszera 14 st., Gdańsk 80-231, Poland
E-mail: jwawrzyniak@imp.gda.pl

Dr. J. Karczewski, Prof. M. Gazda
Department of Solid-State Physics
Gdańsk University of Technology
Gabriela Narutowicza 11/12 st., Gdańsk 80-233, Poland
Prof. E. Coy, Prof. I. Iatsunskyi
NanoBioMedical Centre
Adam Mickiewicz University
Wszelchnicy Piastowkiej 3 st., Poznań 61-614, Poland

Prof. J. Ryl
Department of Electrochemistry
Corrosion and Materials Engineering
Gdańsk University of Technology
Gabriela Narutowicza 11/12 st., Gdańsk 80-233, Poland
Prof. J. Ryl
Advanced Materials Center
Gdańsk University of Technology
Gabriela Narutowicza 11/12 st., Gdańsk 80-233, Poland

 The ORCID identification number(s) for the author(s) of this article can be found under <https://doi.org/10.1002/admi.202001420>.

DOI: 10.1002/admi.202001420

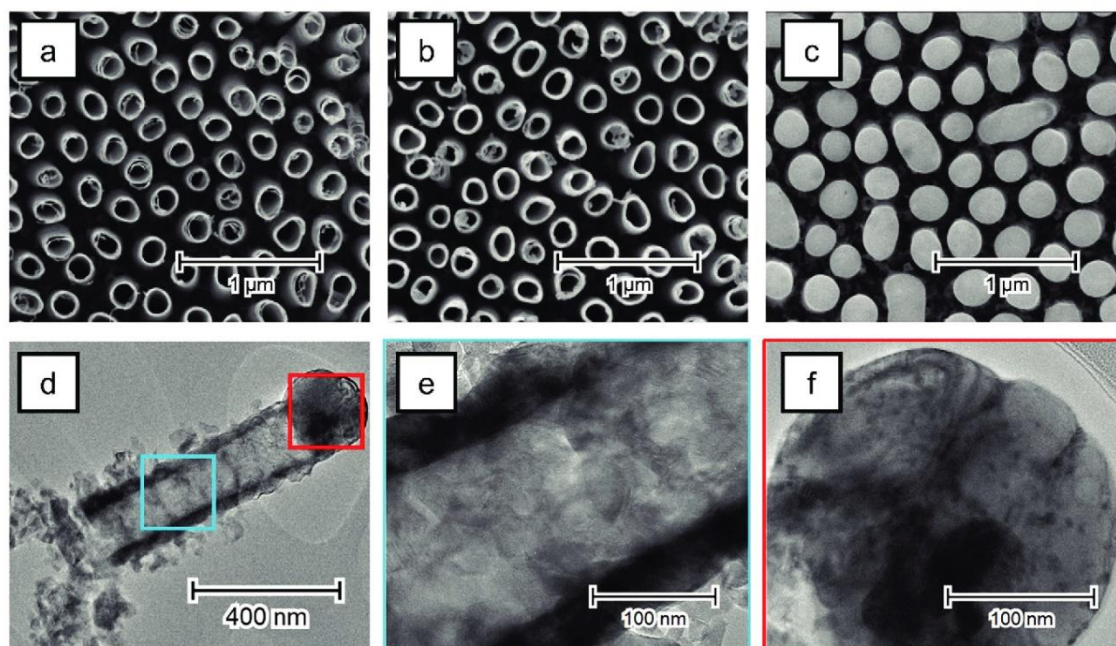


Figure 1. a) SEM images of the as-anodized titania nanotubes, b) the NTs after sputtering with 5 nm nickel, and c) after laser-treatment with 50 mJ cm⁻². d) TEM image of a single nanotube, e) close-up of its core, and its f) cap.

as TEM pictures of the single closed nanotube are shown in **Figure 1**. The as-prepared nanotubes can be characterized by the outer diameter of 188 ± 31 nm, an inner diameter of 142 ± 35 nm, the distance between their centers of 300 ± 70 nm, and length of 1.5 ± 0.1 μ m. Although the deposition of 5 nm thick Ni layer does not affect overall geometry, it is visible as the rim over the NT openings. Mild laser irradiation (10 mJ cm⁻²) leads to the slight deformation of the top nanotube regime not noticeably affecting their length. For 20 mJ cm⁻², the length of the NTs drops to 1.1 ± 0.2 μ m, but the selective closing of NTs is more pronounced. Laser treatment with 30 mJ cm⁻² results in complete sealing of the nanotubes, while further increase in laser energy causes the coupling of the neighboring nanotubes through bridge-like structures (Figure S1, Supporting Information). Nevertheless, throughout the modification process, the interior of the nanotubes remains intact. The energy dispersive X-ray spectroscopy (EDX) and selected area electron diffraction (SAED) investigation of the sealed cap revealed mostly anatase phase with metallic nickel and NiO concentrated within the melted region (Figure S2, Supporting Information). To confirm the presence of the crystalline phase of TiO₂ and Ni/NiO species, XRD patterns were recorded in θ - θ geometry and grazing incidence (Figure S3, Supporting Information). Pristine TiO₂ nanotubes reveal reflections at 25.3°, 37.2°, 38.1°, 48°, and 55.03° which corresponds with anatase, while at 35.2°, 38.5°, 40.2°, 53.1°, 63°, 70.7°, 76.4°, and 82.3° (weak) with Ti.^[25,26] Additional, very faint signal at 27.5°, 37.1°, and 54.2° can be ascribed to residual quantities of rutile phase, as the formation of the rutile oxide layer is initiated at the Ti/TiO₂NTs interface.^[27] The

grazing-incidence XRD reveals more intense rutile peaks at higher angles, indicating its majority share in lower parts of the NTs. High-resolution XPS spectra show signals typical for Ti⁴⁺ and oxygen attributed to the lattice Ti-O and surface Ti-OH,^[28] whereas C1s signal can be assigned to adventitious carbon as typical contamination originating from the instrument and organic residues from the anodization bath (Figure S4, Supporting Information).^[29] Moreover fitting the peaks at 852.6 eV (spin-energy separation of 19.4 eV) and 855.8 eV (spin-energy separation 177 eV) confirms the presence of metallic and hydroxide Ni(OH)₂ forms of nickel respectively.^[30–32] While Ni 2p_{3/2} peak location and geometry confirms the dominant contribution from Ni(OH)₂, the surface contribution of NiOOH or even NiO cannot be completely neglected (**Figure 2a**). Furthermore, the optical properties of the NTs were analyzed based on the UV-vis measurements (Figure 2b). The pristine TiO₂ nanotubes show typical, strong UV absorption, while the deposition of nickel results in an increase of absorbance in the visible range, as well as the formation of the interference fringes.^[28,33] Moreover, the red-shifted band edge is observed, likely due to the decrease of the energy gap between Ti (d) and O (p) orbitals.^[34] Mild irradiation leads to a further increase of absorption in the visible range, while higher reflection in UV is observed, resulting in a similar level of absorbance over the whole spectrum. At higher investigated fluences, more visible than UV light is being absorbed. It can be explained by the formation of the caps over the NTs which may partly reflect incident radiation, or by the elevated number of oxygen vacancies created by the laser.^[35] From the reflectance spectra, the

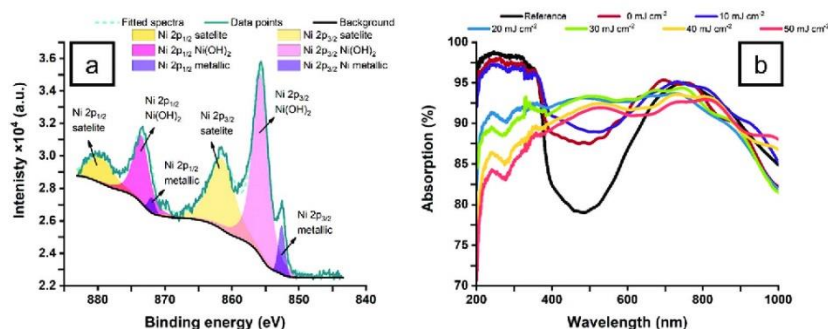


Figure 2. a) Deconvoluted XPS spectra of Ni. b) UV-vis absorbance spectra of reference and laser-modified samples.

Kubelka-Munk plots were calculated (Figure S5, Supporting Information), and the energy bandgap (E_{bg}) values were estimated for reference, nickel sputtered sample, and specimen irradiated with 10 mJ cm⁻². The E_{bg} of pristine titania NTs equals 3.09 eV, less than reported for bulk anatase (3.20 eV),^[36] due to optimization of the spacing and geometrical features of the nanotubes.^[37] As expected, the E_{bg} values drop to 3.00 eV for Ni-decorated sample, and further to 2.88 eV after irradiating with 10 mJ cm⁻². A similar trend was observed previously for laser-treated Cu-TiO₂ NTs,^[38] which indicates synergistic effects of metal/metal oxide and laser processing in E_{bg} reduction. In the case of higher laser fluences, it was impossible to derive optical bandgap values, due to the leveled character of absorbance spectra over the measured range.

Figure 3a shows linear voltammograms measured in the dark and under AM 1.5 illumination. At the highest investigated potential (2.6 V vs RHE), the current density of the reference sample can be seen at 1 mA cm⁻², while the magnetron-sputtered sample exhibits currents 60% higher. The laser-modified specimens, however, dwarfs the reference sample as their current densities exhibit values 14 to 240 times greater in the dark, and up to 280 times higher under applied AM 1.5 radiation. The enhancements of the current densities scale along the laser fluence applied during modification, although the factor of improvement is much greater. In the dark, modification with 10 mJ cm⁻² boosts performance by only about 14 times, whereas applying 20 mJ cm⁻² accounts for 145 times higher currents. In the case of the highest investigated fluence

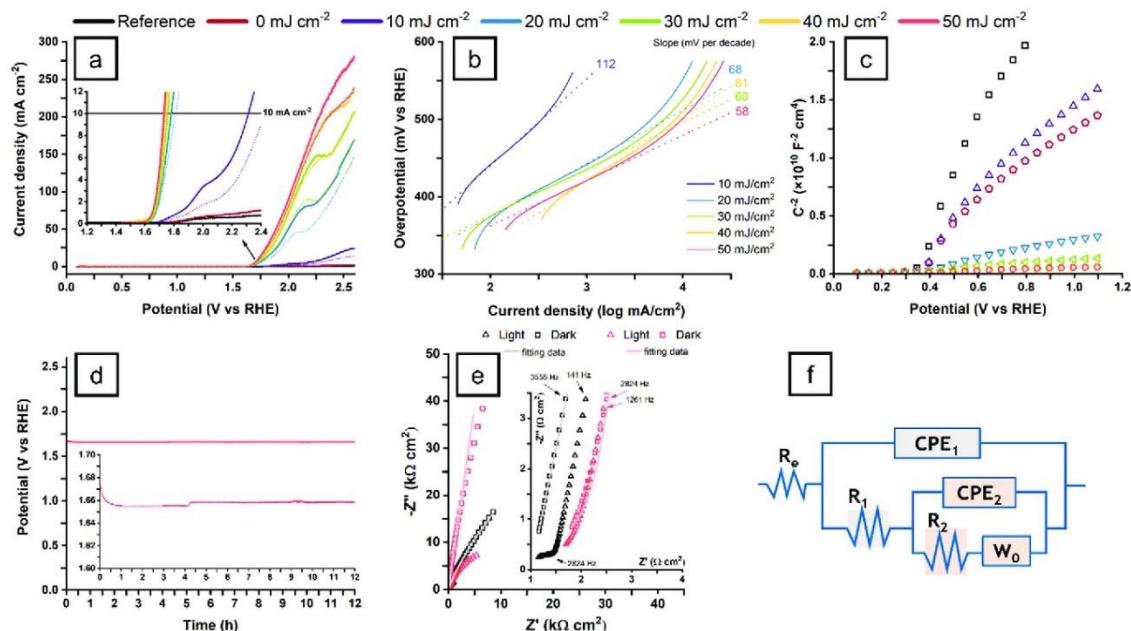


Figure 3. Chemical analysis of the reference and laser-modified samples. a) Linear voltammogram, b) Tafel plot, c) Mott-Schottky plot, d) galvanostatic load at 10 mA cm⁻², e) Nyquist representation of the impedance spectra for best and reference sample, and f) electric equivalent circuit used for fitting.

(50 mJ cm⁻²), the current density of 240 mA cm⁻² was measured. Additional investigation under solar spectrum shows, that the obtained material exhibits photoactive properties, as the current densities rose by up to 50% for sample modified with 10 mJ cm⁻² and by ≈17% for those treated with higher energy laser pulses. The linear voltammetric sweeps also reveal oxidation from NiO to NiOOH at 1.45 V (Figure S6, Supporting Information).^[39] and passivation of surface species or defects at ≈2 V.^[40] The overpotential η for oxygen evolution reaction is shown for 10 mA cm⁻²,^[41] and shifts toward lower values when higher the laser fluence is applied—this trend is further reinforced under the exposure to solar light. Interestingly, the biggest difference is observed between Ni-decorated but untreated sample, which never passes the desired current, the one modified with 10 mJ cm⁻², which reaches 10 mA cm⁻² at η = 1.07 V, and the sample irradiated with 20 mJ cm⁻² laser pulses, which crosses it at η = 0.57 V. Further increases in lasing energy, however, accounts only for an additional decrease of 150 mV, down to η = 420 mV. For the samples reaching 10 mA cm⁻² the Tafel slopes have been calculated and shown in Figure 3b. It can be seen, that the initially steep slope of the sample irradiated with 10 mJ cm⁻² flattens above 20 mJ cm⁻². The graph shows that the sample irradiated with 50 mJ cm⁻² has the mildest slope, indicating the fastest OER kinetics. The density of charge carriers (N_d) was calculated from the Mott-Schottky diagram (Figure 3c),^[42,43] and two orders of magnitude difference is observed between the reference (6.69×10^{19} cm⁻³) and the best performing laser-treated sample (4.09×10^{21} cm⁻³). The flat-band potential was lowered from 0.34 V in the bare substrate to 0.28 V for the most active modified titania. Although the same amount of nickel is present in every case (aside from reference), the results vary drastically. It evidences, that the laser-irradiation plays a crucial role in the reordering of the atoms in the modified region and creating surface states that improve OER kinetics, despite the overall loss of the surface area as shown by the SEM investigation (Figure 1). Moreover, the material is very stable under galvanostatic load (10 mA cm⁻²), as less than 1% change in the potential was observed during a 12 h long load (Figure 3d). Overall, the obtained overpotential values and current densities situate the presented material among the best electrodes for oxygen production (Table S8, Supporting Information). Figure 3e presents the Nyquist impedance plots of the highest-performing and reference samples, whereas plots of the remaining specimen are presented in Figure S7 (Supporting Information). The obtained spectra have been fitted using an electric equivalent circuit (EQC) formerly proposed by Bedar and Klahr^[44,45] with χ^2 of the order of 10^{-3} – 10^{-5} . It contains three resistors (R), two constant phase elements (CPE), and an open Warburg diffusion (W_o), which values are shown in Table S9 (Supporting Information). Due to the inherently irregular NTs surface, the CPE is characterized by the $Z = Q^{-1}(i\omega)^{-n}$ where frequency dispersion n is taken into account.^[46] While the low R_e stands for the electrolyte resistance, the R_1 CPE₁ and R_2 CPE₂ represent double-layer capacitance of porous bulk in the high, and surface states in the low-frequency range. The comparison between reference and laser-annealed materials reveals lower R_1 and CPE₁ due to increased donor concentration (Figure 3b) and lower available surface area resulting from laser-induced sealing (Figure 1c). The increased CPE₂ indicates

a higher double-layer capacitance of defect states located on the material/electrolyte interface which are crucial for OER.^[44] The finite-length ion diffusion with a reflective boundary can be described via W_o , where

$$Z_{W_o}(\omega) = \frac{W_{or}}{\sqrt{j\omega}} (1 - j) \coth(W_{oc} \sqrt{j\omega}) \quad (1)$$

The W_{or} is a Warburg coefficient, and $W_{oc} = d/D^{0.5}$ where d is a length of Nernstian diffusion, and D is a diffusion coefficient of the electroactive species. The lower W_o relates to the charge transport within the NT walls to the blocking electrode. In both cases, the light-induced excitons contribute to the lowering of the electrode resistance.

Utilization of the precise laser processing of the nickel-coated nanotubes allows for a quick formation of closed, self-standing nanopillars with greatly enhanced photocatalytic properties. Due to the synergistic effect of nickel decoration and laser irradiation, the UV-vis spectra exhibits an additional absorbance band between 400 and 600 nm and the donor concentration increases by two orders of magnitude. The series of modified titania samples were electrochemically tested toward OER in the dark and under simulated solar irradiance allowing to track the influence of both Ni and laser within 10–50 mJ cm⁻² range. Most notably, the modification at 50 mJ cm⁻² enables generation of nearly 300 mA cm⁻² at ≈2.6 V versus RHE, which stands in stark contrast with nanotubes that were not irradiated and barely reached 1.5 mA cm⁻² in the same conditions. Moreover, the exceptional stability of the sample was observed, as the galvanostatic evaluation reveals over 99% potential retention after a 12 h working period. To the best of our knowledge, this is the first time such an approach was used to develop highly efficient, yet very stable photoanode material for OER in alkaline media.

Experimental Section

Material Synthesis: The titania nanotubes were created via electrochemical anodization in the two-electrode system. The degreased titanium foil acting as an anode was immersed in diethylene glycol-based electrolyte, containing 0.3 wt% NH₄F, 0.5 wt% HF, and 7 wt% deionized water. The process was conducted at 40 V under a controlled temperature of 40 °C for 2 h. After anodization, the foil was rinsed with ethanol and dried in air. To obtain the reference, anatase TiO₂, the samples were calcined in a furnace at 450 °C for 2 h. The samples were then decorated with 5 nm of nickel via magnetron sputtering using Ni target (99.99%) and placed onto the motorized table in the vacuum chamber (5×10^{-5} bar). They underwent laser treatment with Nd:YAG pulsed laser equipped with 3rd harmonics generator and beam homogenizer within 0–50 mJ cm⁻² fluence range.

Characterization: SEM images were taken with FE-SEM FEI Quanta FEG 250 while TEM investigation was done using JEOL ARM 200F. XRD patterns were recorded by Bruker D2Phaser diffractometer with Cu K α radiation over 20°–90° range, while the grazing incidence XRD patterns were obtained via Philips X'Pert MPD diffractometer with Cu K α radiation over 20°–40° range and incidence angle between 1° and 4°. The XPS spectra were obtained from sample treated with 50 mJ cm⁻² via Escalab250Xi calibrated for adventitious C1s (284.6 eV),^[47] using Al K α anode. Optical reflectance spectra were obtained by the PerkinElmer dual-beam spectrophotometer at a scanning speed of 120 nm min⁻¹. The electrochemical properties were studied in deaerated 0.5 M NaOH

with Autolab PGStat 302 N in a three-electrode system, where the prepared sample acted as a working electrode, while platinum mesh and Ag/AgCl/0.1 M KCl were used as a counter- and reference electrodes respectively. The potential values were recalculated toward RHE using following relation: $E_{\text{RHE}} = E_{\text{Ag/AgCl/0.1 M KCl}} + E^0_{\text{Ag/AgCl/0.1 M KCl}} + 0.059 \text{ pH}$ where $E^0_{\text{Ag/AgCl/0.1 M KCl}} = 0.288 \text{ V}$ and $\text{pH} = 13.69$ for 0.5 M NaOH solution. Cyclic voltammetry sweeps (0.1–2.6 V vs RHE, 50 mV s⁻¹) in the dark and under the illumination of a solar simulator (Oriel LS0500, AM 1.5) preceded linear voltammetry scans (0.1–2.6 V vs RHE, 10 mV s⁻¹) to reach the chemical equilibrium of the working electrode. The impedance measurements were performed at the open circuit potential (OCP) in 20 000–0.1 Hz range at 20 points per decade, whereas the Mott–Schottky analysis was carried out based on the data from potentiodynamic electrochemical impedance spectroscopy carried out between –0.1 and 1.9 V versus RHE at 1 kHz, at the 10 mV amplitude. The spectra were fitted with EIS Analyzer^[48] using Powell algorithm. All of the chemicals used are considered pure for analysis. For a more detailed description of the NT synthesis, please refer to the previous work.^[37]

Supporting Information

Supporting Information is available from the Wiley Online Library or from the author.

Acknowledgements

This work received financial support from the Polish National Science Centre: Grant No. 2017/26/E/ST5/00416. E.C. and I.I. acknowledge the partial financial support under the grant (UMO-2019/35/B/ST5/00248).

Conflict of Interest

The authors declare no conflict of interest.

Keywords

laser treatment, nickel, titania nanotubes, water splitting

Received: August 13, 2020

Revised: October 29, 2020

Published online:

- [1] M. M. Tavakoli, G. Azzellino, M. Hempel, A. Lu, F. J. Martin-Martinez, J. Zhao, J. Yeo, T. Palacios, M. J. Buehler, *Adv. Funct. Mater.* **2020**, *30*, 2001924.
- [2] M. Dehghanimadvar, R. Shirmohammadi, M. Sadeghzadeh, A. Aslani, R. Ghasempour, *Int. J. Energy Res.* **2020**, *44*, 8233.
- [3] V. Mahajan, S. Mohapatra, M. Misra, *Int. J. Hydrogen Energy* **2008**, *33*, 5369.
- [4] C. Xu, Y. Song, L. Lu, C. Cheng, D. Liu, X. Fang, X. Chen, X. Zhu, D. Li, *Nanoscale Res. Lett.* **2013**, *8*, 391.
- [5] M. Nasirian, Y. P. Lin, C. F. Bustillo-Lecompte, M. Mehrvar, *Int. J. Environ. Sci. Technol.* **2018**, *15*, 2009.
- [6] R. P. Vitiello, J. M. Macak, A. Ghicov, H. Tsuchiya, L. F. P. Dick, P. Schmuki, *Electrochem. Commun.* **2006**, *8*, 544.
- [7] L. Sun, J. Li, C. L. Wang, S. F. Li, H. B. Chen, C. J. Lin, *Sol. Energy Mater. Sol. Cells* **2009**, *93*, 1875.
- [8] M. N. Shaddad, D. Cardenas-Morcoso, M. García-Tecedor, F. Fabregat-Santiago, J. Bisquert, A. M. Al-Mayouf, S. Gimenez, *ACS Omega* **2019**, *4*, 16095.
- [9] A. Kertmen, E. Barbé, M. Szkoda, K. Siuzdak, V. Babačić, P. Torruella, I. Iatsunskyi, M. Kotkowiak, K. Rytel, S. Estradé, F. Peiró, S. Jurga, Y. Li, E. Coy, *Adv. Mater. Interfaces* **2018**, *6*, 1801286.
- [10] R. Qu, N. Liu, Y. Chen, W. Zhang, G. Zhu, Q. Zhang, L. Feng, *Adv. Mater. Technol.* **2017**, *2*, 1700125.
- [11] X. Wang, Z. Li, J. Shi, Y. Yu, *Chem. Rev.* **2014**, *114*, 9346.
- [12] M. Paulose, H. E. Prakasham, O. K. Varghese, L. Peng, K. C. Popat, G. K. Mor, T. A. Desai, C. A. Grimes, *J. Phys. Chem. C* **2007**, *111*, 14992.
- [13] X. Wang, L. Sun, S. Zhang, X. Wang, *ACS Appl. Mater. Interfaces* **2014**, *6*, 1361.
- [14] A. Mohammadpour, K. Shankar, *J. Mater. Chem.* **2010**, *20*, 8474.
- [15] F. Riboni, N. T. Nguyen, S. So, P. Schmuki, *Nanoscale Horiz.* **2016**, *1*, 445.
- [16] N. T. Nguyen, S. Ozkan, I. Hwang, A. Mazare, P. Schmuki, *Nanoscale* **2016**, *8*, 16868.
- [17] A. Mazare, I. Paramasivam, F. Schmidt-Stein, K. Lee, I. Demetrescu, P. Schmuki, *Electrochim. Acta* **2012**, *66*, 12.
- [18] F. Dvorak, R. Zazpe, M. Krbal, H. Sopha, J. Prikryl, S. Ng, L. Hromadko, F. Bures, J. M. Macak, *Appl. Mater. Today* **2019**, *14*, 1.
- [19] T. Zhang, S. Cui, B. Yu, Z. Liu, D. Wang, *Chem. Commun.* **2015**, *51*, 16940.
- [20] F. Lyu, Q. Wang, S. M. Choi, Y. Yin, *Small* **2019**, *15*, 1804201.
- [21] C. E. Finke, S. T. Omelchenko, J. T. Jasper, M. F. Lichterman, C. G. Read, N. S. Lewis, M. R. Hoffmann, *Energy Environ. Sci.* **2019**, *12*, 358.
- [22] Y. Hu, T. Ding, K. Zhang, B. Li, B. Zhu, K. Tang, *ChemNanoMat* **2018**, *4*, 1133.
- [23] C. Xiang, L. Sun, Y. Wang, G. Wang, X. Zhao, S. Zhang, *J. Phys. Chem. C* **2017**, *121*, 15448.
- [24] L. Assaud, S. Bochmann, S. Christiansen, J. Bachmann, *Rev. Sci. Instrum.* **2015**, *86*, 073902.
- [25] S. Meriam Suhaimy, C. Lai, H. Tajuddin, E. Samsudin, M. Johan, *Materials* **2018**, *11*, 2066.
- [26] D. Gu, Y. Wang, Z. Li, Y. Liu, B. Wang, H. Wu, *RSC Adv.* **2016**, *6*, 63711.
- [27] S. Das, R. Zazpe, J. Prikryl, P. Knotek, M. Krbal, H. Sopha, V. Podzemna, J. M. Macak, *Electrochim. Acta* **2016**, *213*, 452.
- [28] Ł. Haryński, K. Grochowska, J. Karczewski, J. Ryl, K. Siuzdak, *ACS Appl. Mater. Interfaces* **2020**, *12*, 3225.
- [29] K. Siuzdak, M. Szkoda, A. Lisowska-Oleksiak, K. Grochowska, J. Karczewski, J. Ryl, *Appl. Surf. Sci.* **2015**, *357*, 942.
- [30] H. W. Nesbitt, D. Legrand, G. M. Bancroft, *Phys. Chem. Miner.* **2000**, *27*, 357.
- [31] Z. Zhang, Y. Jiang, X. Zheng, X. Sun, Y. Guo, *New J. Chem.* **2018**, *42*, 11285.
- [32] A. P. Grosvenor, M. C. Biesinger, R. St. C. Smart, N. S. McIntyre, *Surf. Sci.* **2006**, *600*, 1771.
- [33] G. L. Chiarello, A. Zuliani, D. Ceresoli, R. Martinazzo, E. Selli, *ACS Catal.* **2016**, *6*, 1345.
- [34] Z. Wu, Y. Wang, L. Sun, Y. Mao, M. Wang, C. Lin, *J. Mater. Chem. A* **2014**, *2*, 8223.
- [35] J. V. Pasikhani, N. Gilani, A. E. Pirbazari, *Solid State Sci.* **2018**, *84*, 57.
- [36] C. Dette, M. A. Pérez-Osorio, C. S. Kley, P. Punke, C. E. Patrick, P. Jacobson, F. Giustino, S. J. Jung, K. Kern, *Nano Lett.* **2014**, *14*, 6533.
- [37] J. Wawrzyniak, K. Grochowska, J. Karczewski, P. Kupracz, J. Ryl, A. Dołęga, K. Siuzdak, *Surf. Coat. Technol.* **2020**, *389*, 125628.
- [38] K. Grochowska, Z. Molenda, J. Karczewski, J. Bachmann, K. Darowicki, J. Ryl, K. Siuzdak, *Int. J. Hydrogen Energy* **2020**, *46*, 19192.
- [39] M. Yang, L. Huo, L. Pei, K. Pan, Y. Gan, *Electrochim. Acta* **2014**, *125*, 288.
- [40] A. Mazare, M. Dilea, D. Ionita, I. Demetrescu, *Surf. Interface Anal.* **2014**, *46*, 186.

- [41] Y. Yin, X. Zhang, C. Sun, *Prog. Nat. Sci.: Mater. Int.* **2018**, 28, 430.
- [42] R. Beranek, *Adv. Phys. Chem.* **2011**, 2011, 1.
- [43] H. Tsuchiya, J. M. Macak, A. Ghicov, A. S. Räder, L. Taveira, P. Schmuki, *Corros. Sci.* **2007**, 49, 203.
- [44] A. R. C. Bredar, A. L. Chown, A. R. Burton, B. H. Farnum, *ACS Appl. Energy Mater.* **2020**, 3, 66.
- [45] B. Klahr, S. Gimenez, F. Fabregat-Santiago, T. Hamann, J. Bisquert, *J. Am. Chem. Soc.* **2012**, 134, 4294.
- [46] G. J. Brug, A. L. G. van den Eeden, M. Sluyters-Rehbach, J. H. Sluyters, *J. Electroanal. Chem. Interfacial Electrochem.* **1984**, 176, 275.
- [47] P. Swift, *Surf. Interface Anal.* **1982**, 4, 47.
- [48] G. A. Ragoisha, A. S. Bondarenko, *Electrochim. Acta* **2005**, 50, 1553.

Work four: Nanostructure of the laser-modified transition metal nanocomposites for water splitting

The final work of the presented cycle of publications encompasses the investigation of more transition metal species from the 4th period of the periodic table of elements, namely iron, cobalt, nickel, and copper. It further expands the description of the mechanism of the enhanced evolution of hydrogen and oxygen gases (HER and OER) on the laser-treated electrodes in an extended fluence range (Attachment 4).

In the work four, the previously optimized nanotubes [59] were sputtered with 5 nm layers of Fe, Co, Ni, and Cu. They were then irradiated with a 355 nm pulsed laser with fluences up to 100 mJ/cm², which led to the partial melting of their uppermost part and fusion with sputtered metals without creating visible nanoparticles. The linear voltamperograms obtained by polarizing electrodes in the cathodic domain reveal that the performance of all of the electrodes worsened post-laser treatment. Polarization towards oxygen evolution reaction, however, shows fluence-dependent improvements in the obtained current densities for cobalt- and nickel-coated electrodes. Interestingly, the same electrodes recorded the highest increase in the density of charge carriers after reaching a steady state in the electrolyte. The XPS study done after each modification step (sputtering, laser-treatment, electrochemical analysis) has shown that in the process of creating the electrodes, the sputtered nickel and cobalt layers transform into metal oxides and, after submerging in the electrolytes, metal hydroxides. This was not the case for iron and copper metal species, as they did not change their oxidation state significantly during the process. Based on the data in the literature [60–64], the nickel and cobalt oxides are p-type semiconductors, whereas titanium, iron, and copper are of the n-type. The results, therefore, indicate the formation of the p-n type of junction between the titania substrate and metal hydroxide on top of the electrode. Because the metal layer

on top is very thin (5 nm), we can assume that it is fully depleted. Therefore, due to the potential forming within the junction, all of the electrons taken from the adsorbed oxyhydroxides are automatically forced into the titania underlayer, increasing the effectiveness of the oxygen evolution reaction [65]. The same mechanism works against efficient hydrogen generation, as the potential within the depleted p-n junction works against the applied external potential. Based on the presented mechanism of charge transfer, novel electrode junctions can be engineered to lower the overpotentials required for effective water-splitting.

Nanostructure of the laser-modified transition metal nanocomposites for water splitting

Jakub Wawrzyniak¹ , Jakub Karczewski² , Emerson Coy³ ,
Jacek Ryl² , Katarzyna Grochowska¹  and Katarzyna Siuzdak¹ 

¹ The Szewalski Institute of Fluid-Flow Machinery, Polish Academy of Sciences, Fiszerza 14, 80-231 Gdansk, Poland

² Faculty of Applied Physics and Mathematics, Institute of Nanotechnology and Materials Engineering, Gdansk University of Technology, Narutowicza 11/12, 80-233 Gdansk, Poland

³ NanoBioMedical Centre, Adam Mickiewicz University, Wszechnicy Piastowskiej 3, 61-614 Poznan, Poland

E-mail: jwawrzyniak@imp.gda.pl

Received 22 October 2021, revised 13 January 2022

Accepted for publication 2 February 2022

Published 21 February 2022



Abstract

Although hydrogen is considered by many to be the green fuel of the future, nowadays it is primarily produced through steam reforming, which is a process far from ecological. Therefore, emphasis is being put on the development of electrodes capable of the efficient production of hydrogen and oxygen from water. To make the green alternative possible, the solution should be cost-efficient and well processable, generating less waste which is a huge challenge. In this work, the laser-based modification technique of the titania nanotubes containing sputtered transition metal species (Fe, Co, Ni, and Cu) was employed. The characteristics of the electrodes are provided both for the hydrogen and oxygen evolution reactions, where the influence of the laser treatment has been found to have the opposite effect. The structural and chemical analysis of the substrate material provides insight into pathways towards more efficient, low-temperature water splitting. Laser-assisted integration of transition metal with the tubular nanostructure results in the match-like structure where the metal species are accumulated at the head. The electrochemical data indicates a significant decrease in material resistance that leads to an overpotential of only +0.69 V at 10 mA cm⁻² for nickel-modified material.

Supplementary material for this article is available [online](#)

Keywords: laser, titanium dioxide, nanotubes, anodization, water splitting, oxygen evolution

(Some figures may appear in colour only in the online journal)

1. Introduction

The progressing climate change driven by the overuse of fossil deposits compels us to find cleaner, more efficient fuels of the future. Hydrogen is often considered to be one of the

best alternatives, due to its incredible energy density, potentially unlimited availability, and, as it burns back to the water, sustainability. Unfortunately, it is rarely created through eco-friendly means, as much cheaper, though dirtier techniques are available. One of the factors contributing to the high price of hydrogen created through electrocatalysis of water is the price of electrode materials, such as platinum group metal species. Similarly, even though high surface area materials are known to perform better catalytically, the techniques used to create them often leave a lot of wasted material during their



Original content from this work may be used under the terms of the [Creative Commons Attribution 4.0 licence](#). Any further distribution of this work must maintain attribution to the author(s) and the title of the work, journal citation and DOI.

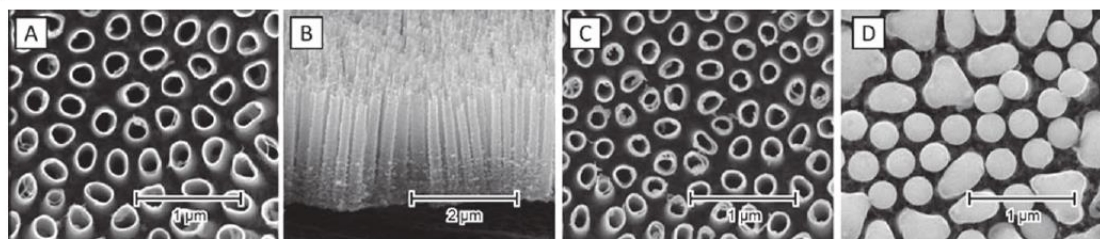


Figure 1. SEM images presenting top (A) and side (B) view of the anodized and calcined titania nanotubes, as well as representative sample of TNTs sputtered with 5 nm nickel layer (C) and treated with laser (D).

synthesis. Moreover, typical wet-chemistry route makes the upscaling difficult and even outstanding results are contained to the laboratory scale. These difficulties incentivize the use of techniques feasible outside laboratory and chemical compounds free of precious elements.

Known for their corrosion resistance, the titania nanotubes (TNTs) with highly developed surface are often synthesized via a scalable electrochemical anodization process [1]. Moreover, through the adjustments in the process parameters, such as electrolyte composition, temperature, and potential applied, their geometry can be tailored, changing their properties depending on the specific needs [2, 3]. Furthermore, due to the bandgap of 3.2 eV the TNTs exhibit photoactive properties in the UV light, which may further improve their catalytic properties under illumination [4]. Although the width of their bandgap hampers their efficiency under the visible light, the TNTs can be regarded as an excellent material for further modification since the nanostructure is already formed onto the stable, conducting substrate which is important for applications in water-splitting devices.

The transition metal oxides, as a part of the non-noble family, are becoming increasingly popular due to vast availability and, thanks to the tailored synthesis pathways, are often almost as feasible as more expensive alternatives [5–10]. The transition metals from the 4th period especially, are one of the most abundant elements on Earth, and although iron, cobalt, nickel, and copper have all been used as catalysts for water splitting, the obtained results vary significantly depending on the synthesis pathways. It is known, however, that the activity of both titania and the transition metal oxides benefits from the presence of defects, such as oxygen vacancies [11–13], therefore, to achieve a simple and efficient synthesis pathway, methods promoting structural disordering should be considered.

We, therefore, propose a titania-based electrode modified with 4th group transition metals (Fe, Co, Ni, Cu) treated with pulsed laser radiation (Nd:YAG, 355 nm) in a vacuum. The proposed approach eliminates the usage of metal liquid precursors, while each fabrication step is already well-controlled on a technological scale. Moreover, the performance of the electrodes towards water splitting in alkaline media is presented, and the reaction overpotential is calculated for the best-performing samples. Furthermore, the selected electrodes underwent a thorough analysis of their morphology (SEM, TEM) as well as optical (UV–vis), physical (Raman, GI-

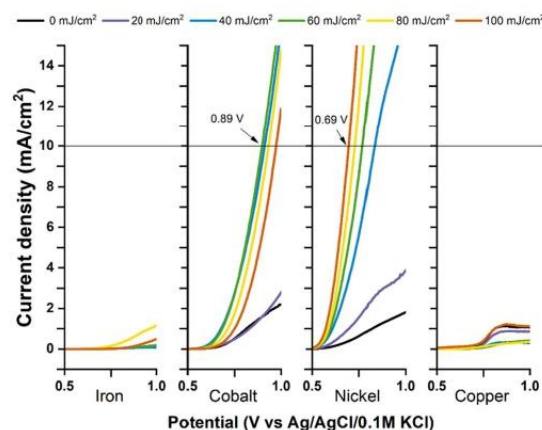


Figure 2. Anodic linear voltammetric sweeps of the Fe, Co, Ni, and Cu-modified titania nanotubes after laser-treatment with 0–100 mJ cm⁻².

XRD), and electrochemical (voltammetry and impedance spectroscopy) properties, based on which an energy diagram showing possible reaction pathway has been created.

2. Experimental section

2.1. Synthesis

The titanium foil (99.7% pure, 0.127 mm thick, Strem) was cut into rectangular (20 × 35 mm) pieces which were degreased ultrasonically in acetone (p.a. Protolab), ethanol (96%, Chempur), and deionized water (0.05 μS, Hydrolab). To obtain laterally spaced titania nanotubes, they underwent chemical anodization in a temperature-controlled (40 °C, Julabo F-12) cylindrical cell, where titanium acted as an anode and platinum net (20 × 25 mm) as a cathode. The electrolyte consisted of 0.3 wt% NH₄F (Chempur), 0.5 wt% HF (Chempur), and 7 wt% deionized water in diethylene glycol (Chempur). The potential was controlled by in-house built hardware which increased it linearly over 400 s up to 40 V, kept constant for 2 h, and decreased it at the same rate. After the process, the samples were submerged in ethanol for approximately 1 h to wash out the remaining electrolyte. The crystalline, anatase phase was obtained via furnace annealing at 450 °C for 2 h

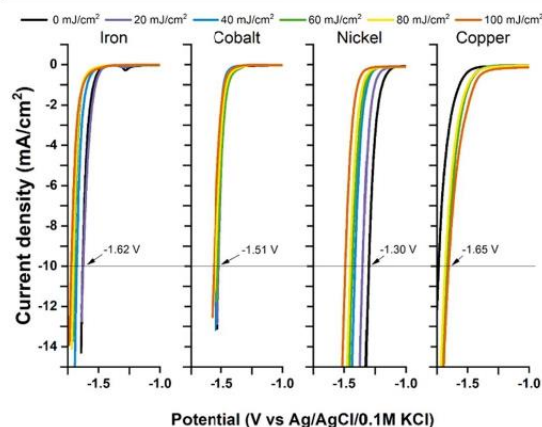


Figure 3. Cathodic linear voltammetric sweeps of the Fe, Co, Ni, and Cu-modified titania nanotubes after laser-treatment with 0–100 mJ cm⁻².

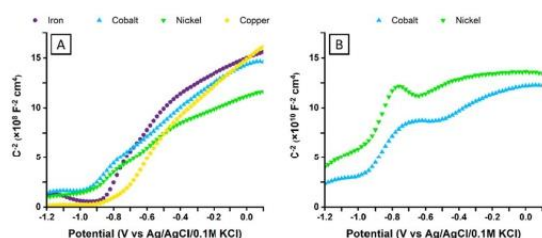


Figure 4. Mott-Schottky diagrams of the modified electrodes in the steady-state (A) as well as Co and Ni electrodes on their first run (B).

(Nabertherm), where the heating rate was set to 2 °C min⁻¹. The samples were sputtered (Quorum Technologies, Q150T S) with 5 nm of iron (Micro to Nano), cobalt, nickel, and copper (Quorum Technologies) and treated with 355 nm laser pulses (Quantel, Nd:YAG, 3ω) in a vacuum (<5 × 10⁻⁸ bar, Pfeiffer) with fluence in the range of 0–100 mJ cm⁻².

2.2. Characterization

The scanning electron microscope (SEM) images were taken by FE-SEM FEI Quanta FEG 250, whereas transmission electron microscope (TEM) pictures were done using JEOL ARM 200F (200 eV) equipped with an energy-dispersive x-ray spectrometer (EDX). The grazing incidence x-ray diffraction patterns (GI-XRD) were obtained via PANalytical X'pert MRD diffractometer with Kα radiation, operating at 45 mA and 40 kV. The dual-beam UV-vis spectrometer (Lambda 35, Perkin-Elmer) equipped with diffuse reflectance accessory was used to obtain reflectance UV-vis spectra, whereas a confocal Raman spectrometer (InVia Renishaw) equipped with a 514 nm laser and a ×50 lens was used to extract the Raman spectra. The x-ray photoelectron spectra (XPS) were obtained via Escalab250Xi calibrated for adventitious C1s (284.6 eV) [14]. The electrochemical performance of the samples was determined using Autolab

PGStat 302 N potentiostat-galvanostat in a three-electrode system, where the investigated sample was immersed in 0.5 M NaOH electrolyte (Stanlab) and acted as a working electrode whereas Ag/AgCl/0.1 M KCl and platinum mesh were used as a reference- and counter-electrodes respectively. Before the measurements, the electrolyte was deaerated with argon (5 N), while during the test a constant flow of the inert gas above the solution was kept. The simulated solar radiation was provided by Oriel LS0500 equipped with AM 1.5 filter. The radiation intensity was set to 100 mW cm⁻² and verified using Si reference cell (Rera). The electrochemical cell was equipped with a quartz window transparent to the UV light. The cyclic voltammetry (CV) sweeps in the -0.6 to +0.6 V range at 50 mV s⁻¹ were performed before other measurements both in the dark and under illumination ensuring penetration of the electrolyte into the pores of the material. To investigate hydrogen- and oxygen evolution reactions (HER/OER), the polarization was applied from 0 V versus Ag/AgCl/0.1 M KCl at 0.1 mV s⁻¹ rate in the anodic and cathodic regions respectively, up to a point where current densities over 10 mA cm⁻² could be detected. The impedance investigation was conducted in the galvanostatic mode in the dark and under simulated irradiation at current densities of 1 and 10 mA cm⁻² in the 20 000–1 Hz range at 20 points per decade and amplitude of 10 μA. The Mott-Schottky (MS) analysis was done from +0.1 to -1.2 V at 1 kHz, with 10 mV amplitude. Before recording the impedance data, the electrode was polarized for 15 min and for 1 min between each data point. The charge carrier density was calculated according to the formula [15]

$$N_d = \frac{2}{\varepsilon_0 \varepsilon q} \left[\frac{d \frac{1}{C^2}}{dE} \right]^{-1},$$

where ε_0 is the electric permittivity of vacuum, ε is a relative permittivity of anatase [16], and q stands for the charge of the electron. The expression in the square brackets stands for the slope of the MS plot.

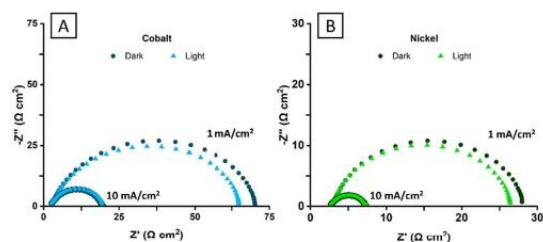
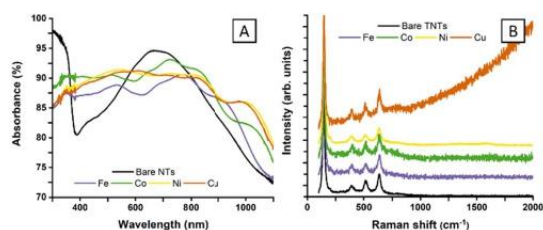
3. Results and discussion

The parameters of the nanotubes were chosen based on previous research [3, 17] to maximize the photoactivity of the substrate material. Figure 1(A) shows the SEM images of the anatase TiO₂ nanotubes from the top, whereas figure 1(B) shows their cross-section. The obtained morphology is characterized by the distinct lateral spacing between the nanotubes (ca. 140 nm), which is only slightly lower than their diameter (ca. 190 nm). Their average wall thickness is 14 nm, and they reach 2 μm in length. The SEM images after sputtering show the thickening of the nanotube rims, as it is where most of the metal is being deposited (figure 1(C)) [18], whereas the representative picture of the laser-treated nanotubes is shown in figure 1(D).

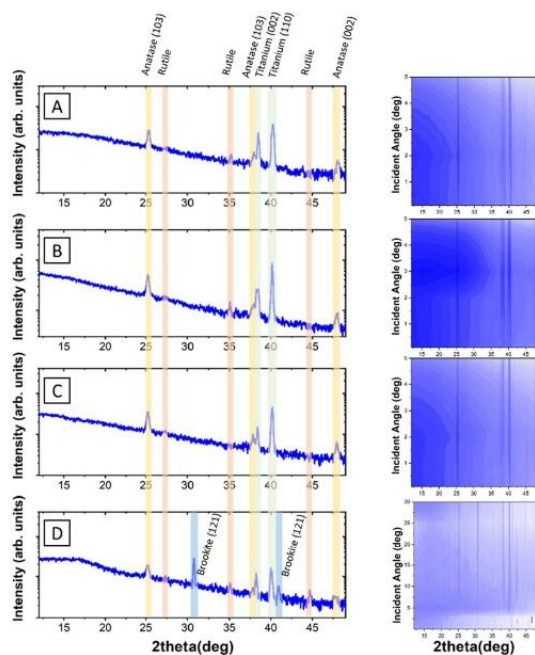
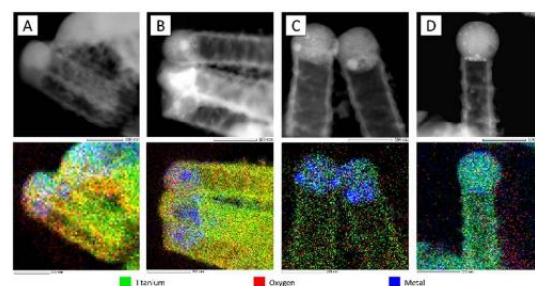
The performance of the prepared electrodes was determined based on their oxygen evolution reaction overpotentials at 10 mA cm⁻² [19, 20]. The linear voltammetric

Table 1. The values of the flatband potentials and charge carrier densities for the selected samples.

Parameter\Metal	E_{fb} versus Ag/AgCl/0.1 M KCl (V)	E_{fb} versus RHE (V)	N_d ($\times 10^{19} \text{ cm}^{-3}$)	N_{di} ($\times 10^{19} \text{ cm}^{-3}$)
Iron	− 0.87 V	0.22 V	1.14	1.14
Cobalt	− 1.02 V	0.07 V	2.03	0.0136
Nickel	− 1.01 V	0.08 V	2.37	0.0094
Copper	− 0.77 V	0.32 V	1.34	1.30

**Figure 5.** Nyquist representation of the impedance spectra for the electrodes modified with Co and Ni under constant load of 1 and 10 mA cm^{-2} in the dark and under the simulated AM 1.5 illumination.**Figure 6.** UV-vis absorbance (A) and Raman (B) spectra of the selected samples.

sweeps in the anodic region for all of the prepared substrates are shown in figure 2. In comparison to the sputtered-only samples, most of the laser-treated specimen exhibit higher current densities in the OER region. In the case of iron-enriched samples, the treatment with 80 mJ cm^{-2} contributed to the highest current density increase, but it only barely passed 1.1 mA cm^{-2} at 1 V. Cobalt, on the other hand, peaked after irradiation with 60 mJ cm^{-2} pulses, reaching 10 mA cm^{-2} at +0.89 V. The most promising results were, however, obtained for electrodes with added nickel and irradiated with 100 mJ cm^{-2} , as the threshold was reached at only +0.69 V. In the case of copper though, the laser treatment had a reverse effect, where treatment with up to 80 mJ cm^{-2} lowered obtained current densities. Irradiation with 100 mJ cm^{-2} , however, had little effect in comparison with the sputtered-only sample. Nonetheless, the samples reached a plateau at +0.85 V at a maximum current density of only 1.2 mA cm^{-2} , not reaching the expected breakpoint of 10 mA cm^{-2} . Interestingly though, the laser treatment resulted in a reverse trend when investigated for hydrogen evolution reaction. Polarization in the cathodic region revealed the lowest overpotentials for sputtered-only samples (0 mJ cm^{-2}) in the case of Fe, Co, and Ni and for Cu irradiated with

**Figure 7.** Grazing incidence diffractograms of the electrodes modified with iron (A), cobalt (B), nickel (C), and copper (D).**Figure 8.** TEM (top) and EDX (bottom) images of the titania nanotubes with 5 nm Fe (A), Co (B), Ni (C), and Cu (D) after laser-induced re-solidification of the titania cap.

100 mJ cm^{-2} (figure 3). The 12 h stability test of the best electrodes show potential change below 3%, indicating good stability under load (ESI (available online at stacks.iop.org/NANO/33/205401/mmedia)). Furthermore, from all of the investigated samples, four best-performing in the OER region (one from each metal) were chosen for further investigation.

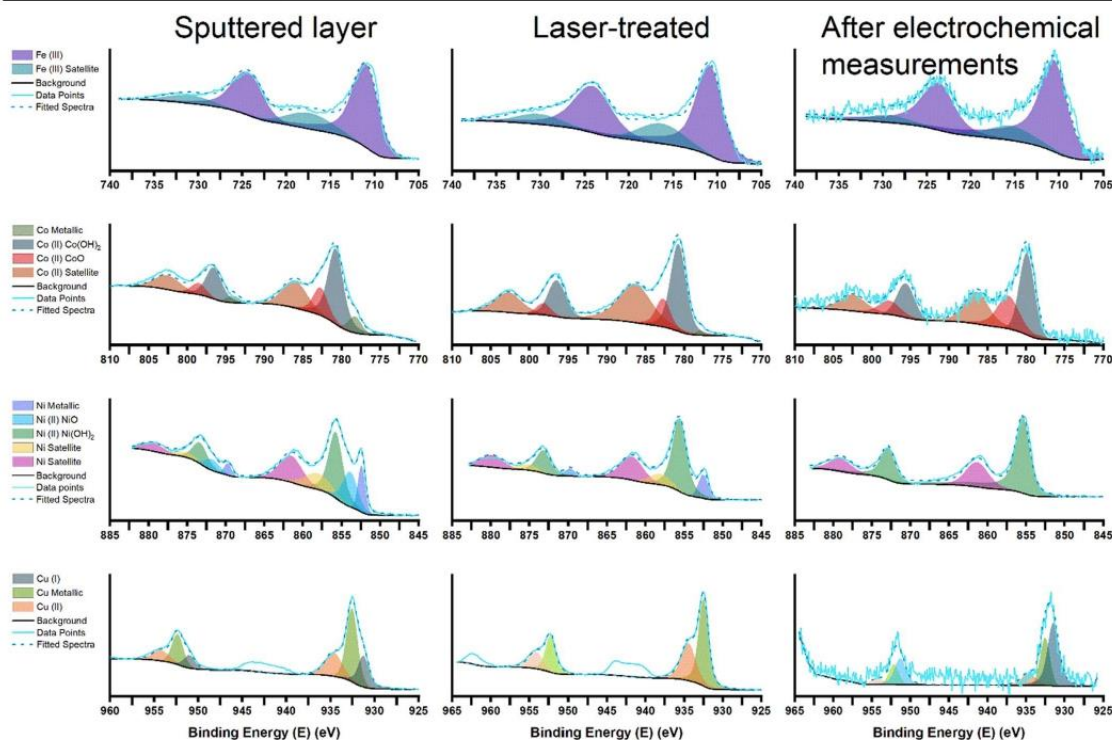


Figure 9. The deconvoluted XPS spectra of the investigated electrodes in their respective metal energy ranges after each modification step.

Although the investigation of the electrodes under AM 1.5 illumination was done alongside the measurements in the dark, the change in overpotential values was within the margin of error (below 0.01 V).

During the investigation, the repeated Mott–Schottky measurements were done, but in the case of nickel- and cobalt-coated electrodes, the initial results varied significantly from the ones obtained in the 2nd and 3rd run. As there should be no reactions occurring on the electrode in the investigated range, this phenomenon was deemed worthy of analysis. Therefore, figure 4(A) presents MS plots for the selected samples in their steady-state (3rd run), whereas figure 4(B) shows the initial run of the Co- and Ni-modified electrodes. It is worth noting, that although the curves obtained from electrodes containing iron and copper did not change their course over three consecutive runs, others underwent a significant transformation which might be attributed to the presence of trap states being filled or oxyhydroxides formed on the surface [21]. The steady-state flat band potential (E_{fb}) was determined based on the intersection of the tangent to the linear part with the potential axis and subsequently the density of charge carriers (N_d) was calculated from its slope (table 1) [22, 23]. The obtained values show, that the best performing electrodes (Co, Ni) share a similar position of the Fermi level, while the analysis of the slope indicates slightly higher carrier density in a nickel electrode. Both Fe- and Cu-modified substrates exhibit nearly

halved charge carrier density and positively shifted E_{fb} levels relative to Ni and Co. Interestingly, the initial number of charge carriers (N_{di}) for the electrodes containing cobalt and nickel was over two orders of magnitude lower.

Based on the performance of the electrodes towards OER (figure 2) and the charge carrier density (table 1), a further electrochemical investigation was done only for the most promising samples. Therefore, figure 5 shows Nyquist representation of the impedance spectra of the samples modified with cobalt and nickel. Although the shapes of the semicircles are very similar in both cases, the values measured in each case differ substantially. Under the 1 mA cm^{-2} load, the semicircles indicate a drop in resistance under simulated solar light in the low-frequency range ($\sim 9\%$ for Co, $\sim 6\%$ for Ni). However, under an applied load of 10 mA cm^{-2} , the resistance increased by about 1%. Nevertheless, the bulk resistance of the nickel electrode was about 2.5 times lower than for their cobalt counterparts.

The absorbance spectra of the selected specimen are shown in figure 6(A). The reference sample exhibits strong absorption in the UV region, with the cutoff according to its bandgap (3.23 eV), followed by an absorption maximum at ca. 670 nm, most likely from the titanium foil underneath the nanotubes. However, all of the laser-treated samples exhibit decreased UV absorbance due to the creation of oxygen vacancies [24]. On the other hand, despite overall much flatter absorption characteristics, interference fringes are visible

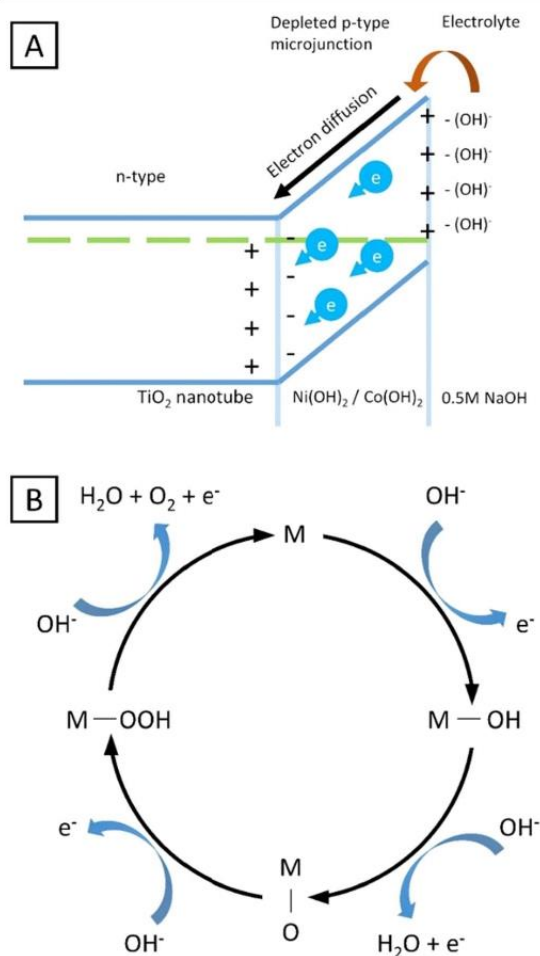


Figure 10. Schematic representation of the micro p-n junction facilitating efficient OER mechanism (A), and the mechanism of oxygen generation through metal oxides in alkaline media (B) [41].

throughout the spectrum. They are caused by the interference of the light reflected from the semi-transparent nanotube seals in their upper region and the titanium sheet underneath. As it is a purely geometrical phenomenon, Chiarello *et al* [25] have proposed an equation, in which the height of the nanotubes can be approximated from the distance of the respective fringes. It is noteworthy, that the two samples modified with 100 mJ cm⁻² laser pulses (Ni, Cu) show nearly identical absorbance spectrum, proving that the changes in absorbance are driven primarily by the laser irradiation.

The figure 6(B) shows normalized Raman spectra of the investigated samples, with all the peaks expected for anatase: 144 (*E_{g(1)}*), 197 (*E_{g(2)}*), 395 (*B_{1g}*), 519 (*B_{1g}*), and 635 (*E_{g(3)}*) cm⁻¹ [26], but no signal from any of the metal species. Furthermore, the GI-XRD studies were done to investigate the differences in crystal structure after the laser treatment (figure 7). Despite some artifacts from bending of the sample,

contributions from titanium (002), (110) and anatase (101), (103), (002) were found, with a very faint addition of rutile [27]. Interestingly, a relatively strong reflection characteristic to brookite (121) was found in a sample with copper, but neither absorbance, Raman, nor XRD investigation revealed the identifiable presence of metal species on the surface, likely due to their low amount.

The TEM-EDX revealed the distribution of the elements in the modified nanotubes (figure 8). The red color represents the position of oxygen atoms, titanium is marked green, and the sputtered metal is marked blue. Although the Ti and O are distributed evenly through the samples, the Fe, Co, Ni, and Cu are mostly confined to the nanotube cap. The images also indicate, that the nanotube remains empty inside and only the upper part of the nanotube was re-solidified during laser processing, resembling a match head. In the case of cobalt and nickel, the metal is localized in the form of nanoparticles, whereas more uniform distributions of iron and copper within the nanotube can be observed.

Figure 9 shows deconvoluted high-resolution XPS spectra of the electrodes in the energy range of their respective metal which were taken after each modification step. The iron-infused electrode shows Fe (III) contribution at 710.9 with its satellite at 716.6 eV and does not change significantly during the modification process. The cobalt species indicate a small metallic contribution (777.9 eV), cobalt hydroxide (780.7 eV), cobalt oxide (782.7 eV), and the satellite peak (786.5 eV). During the laser- and electrochemical-treatment, the contribution of the metallic cobalt decreases in favor of CoO and Co(OH)₂. Similarly, although sample sputtered with nickel shows a strong metallic peak at 852.5 eV, oxide at 853.9 eV, oxyhydroxide at 855.6 eV, and two related satellites at 858.2 and 862.0 eV, the contribution from nickel oxide disappears during the laser-treatment, followed by metallic contribution after electrochemical analysis. In the final electrode, only contributions from nickel oxyhydroxide and its satellite are visible. Lastly, the copper gives a weak Cu₂O signal at 951.0 eV, a strong metallic signal at 932.5 eV, and the Cu (II) at 934.6 with its broad satellite centered at 942.3 eV. Although the Cu (I) transforms into Cu (II) during the laser treatment, the process is reversed when the electrode is polarized in the alkaline electrolyte, which results in Cu (I) being the major factor in the electrode. Interestingly, the Fe, Co, and Cu electrodes exhibit a lower signal-to-noise ratio after measurements in the electrolyte, suggesting that they may dissolve in the electrolyte [28–33]. The two best electrodes (with cobalt and nickel) show similar evolution of the oxidation states, as both of them favor oxyhydroxide creation, which plays an important role in catalytic charge transfer [21, 34, 35]. The progressive hydroxylation of the metallic species in those two electrodes also explains the change of the Mott–Schottky graphs (figure 4(B)), as even though the initial cyclic voltammetric sweeps were performed, the electrodes stabilized only after two impedance sweeps in lower potentials.

Given the results, the mechanism of the charge transfer at the metal-infused titania electrode can be derived (figure 10). Due to the presence of the oxygen vacancies, the anatase TiO₂ is an intrinsic n-type semiconductor [36], the same as iron [37] and copper oxide [38], whereas the CoO, and NiO₂, are

of the p-type [39, 40]. Because the metal species are confined to the uppermost nanotube region (figure 8), we can model the nanotubes sputtered with cobalt and nickel as a p-n junction where, in the steady-state, electrons diffuse from the cap to the nanotube body. The depletion of the cap region accelerates the formation of the double-layer through the binding with hydroxyl groups, which then are transformed into gaseous oxygen. In the alkaline electrolyte, the metal nanoparticles act as trap states for the (OH⁻) groups (figure 4(B)), bind with them (figure 9), and act as an efficient channels for charge transport. As the electrodes' performance is dependent on the laser fluence used in modification, it can be responsible for creating additional oxygen vacancies within titania structure. Similarly, exposure to alkaline media facilitates oxidation of the metallic nickel, promoting formation of the p-type layer. As a result of the modification, the potential difference within the depleted micro p-n junction is elevated. Therefore, the same effects are responsible for lowering overpotentials of the oxygen generation and increasing potential required for HER.

4. Conclusions

In this work, the performance of the laser-treated, metal-sputtered titania electrodes towards HER and OER was investigated. Although the irradiation with laser improves the activity towards OER, it has an inverse effect when investigated towards HER (Cu being the exception). The electrochemical and physical investigation allows to conclude, that the improved photocatalytic activity towards OER can be attributed to the micro p-n junction, formed between the nanotube and embedded p-type metal oxides, which allows for easier oxyhydroxide formation on the surface of the electrode. Furthermore, the encapsulation of the nanotubes resulted in an appearance of the interference fringes, which is overall much more uniform than for unmodified material. Although the changes in the impedance spectra indicate photoactivity of the electrodes, illumination with AM 1.5 radiation does not change the obtained overpotential values, which itself appears to be connected to the number of charge carriers present in modified electrodes.

Acknowledgments

This work received financial support from the Polish National Science Centre: Grant No. 2017/26/E/ST5/00416. E.C. Acknowledges the partial financial support from the National Science Centre (NCN) of Poland by the OPUS grant 2019/35/B/ST5/00248.

Data availability statement

All data that support the findings of this study are included within the article (and any supplementary files).

ORCID iDs

Jakub Wawrzyniak  <https://orcid.org/0000-0001-7664-9584>

Jakub Karczewski  <https://orcid.org/0000-0001-9322-7842>

Emerson Coy  <https://orcid.org/0000-0002-4149-9720>

Jacek Ryl  <https://orcid.org/0000-0002-0247-3851>

Katarzyna Grochowska  <https://orcid.org/0000-0001-7577-3399>

Katarzyna Siuzdak  <https://orcid.org/0000-0001-7434-6408>

References

- [1] Xiang C, Sun L, Wang Y, Wang G, Zhao X and Zhang S 2017 Large-scale, uniform, and superhydrophobic titania nanotubes at the inner surface of 1000 mm long titanium tubes *J. Phys. Chem. C* **121** 15448–55
- [2] Ozkan S, Nguyen N T, Mazare A and Schmuki P 2018 Optimized spacing between TiO₂ nanotubes for enhanced light harvesting and charge transfer *ChemElectroChem* **5** 3183–90
- [3] Wawrzyniak J, Grochowska K, Karczewski J, Kupracz P, Ryl J, Dołęga A and Siuzdak K 2020 The geometry of free-standing titania nanotubes as a critical factor controlling their optical and photoelectrochemical performance *Surf. Coat. Technol.* **389** 125628
- [4] Wawrzyniak J, Karczewski J, Coy E, Iatsunskyi I, Ryl J, Gazda M, Grochowska K and Siuzdak K 2021 Spectacular oxygen evolution reaction enhancement through laser processing of the nickel-decorated titania nanotubes *Adv. Mater. Interfaces* **8** 2001420
- [5] Wang Z, Zhang L, Schülli T U, Bai Y, Monny S A, Du A and Wang L 2019 Identifying copper vacancies and their role in the CuO based photocathode for water splitting *Angew. Chem. Int. Ed.* **58** 17604–9
- [6] Wang J, Cui W, Liu Q, Xing Z, Asiri A M and Sun X 2016 Recent progress in cobalt-based heterogeneous catalysts for electrochemical water splitting *Adv. Mater.* **28** 215–30
- [7] Jang J-W et al 2015 Enabling unassisted solar water splitting by iron oxide and silicon *Nat. Commun.* **6** 7447
- [8] Artero V, Chavarot-Kerlidou M and Fontecave M 2011 Splitting water with cobalt *Angew. Chem. Int. Ed.* **50** 7238–66
- [9] Tsai H-C, Vedhanarayanan B and Lin T-W 2019 Freestanding and hierarchically structured au-dendrites/3D-graphene scaffold supports highly active and stable Ni₃S₂ electrocatalyst toward overall water splitting *ACS Appl. Energy Mater.* **2** 3708–16
- [10] Vedhanarayanan B, Shi J, Lin J-Y, Yun S and Lin T-W 2021 Enhanced activity and stability of MoS₂ through enriching 1T-phase by covalent functionalization for energy conversion applications *Chem. Eng. J.* **403** 126318
- [11] Domaschke M, Zhou X, Wergen L, Romeis S, Miehl M E, Meyer K, Peukert W and Schmuki P 2019 Magnéli-phases in anatase strongly promote cocatalyst-free photocatalytic hydrogen evolution *ACS Catal.* **9** 3627–32
- [12] Wang Y, Liang Z, Zheng H and Cao R 2020 Recent progress on defect-rich transition metal oxides and their energy-related applications *Chem.—Asian J.* **15** 3717–36
- [13] Xiong X et al 2018 A highly-efficient oxygen evolution electrode based on defective nickel-iron layered double hydroxide *Sci. China Mater.* **61** 939–47
- [14] Swift P 1982 Adventitious carbon? The panacea for energy referencing? *Surf. Interface Anal.* **4** 47–51

- [15] Haryński Ł, Grochowska K, Karczewski J, Ryl J and Siuzdak K 2020 Scalable route toward superior photoresponse of UV-laser-treated TiO₂ nanotubes *ACS Appl. Mater. Interfaces* **12** 3225–35
- [16] Park B H, Li L S, Gibbons B J, Huang J Y and Jia Q X 2001 Photovoltaic response and dielectric properties of epitaxial anatase-TiO₂ films grown on conductive La_{0.5}Sr_{0.5}CoO₃ electrodes *Appl. Phys. Lett.* **79** 2797–9
- [17] Ozkan S, Mazare A and Schmuki P 2018 Critical parameters and factors in the formation of spaced TiO₂ nanotubes by self-organizing anodization *Electrochim. Acta* **268** 435–47
- [18] Grochowska K, Ryl J, Karczewski J, Śliwiński G, Cenian A and Siuzdak K 2019 Non-enzymatic flexible glucose sensing platform based on nanostructured TiO₂–Au composite *J. Electroanal. Chem.* **837** 230–9
- [19] McCrory C C L, Jung S, Peters J C and Jaramillo T F 2013 Benchmarking heterogeneous electrocatalysts for the oxygen evolution reaction *J. Am. Chem. Soc.* **135** 16977–87
- [20] Weber M F and Dignam M J 1984 Efficiency of splitting water with semiconducting photoelectrodes *J. Electrochem. Soc.* **131** 1258–65
- [21] Xu Z J 2020 Transition metal oxides for water oxidation: all about oxyhydroxides? *Sci. China Mater.* **63** 3–7
- [22] Beranek R 2011 (Photo)electrochemical methods for the determination of the band edge positions of TiO₂-based nanomaterials *Adv. Phys. Chem.* **2011** 1–20
- [23] Tsuchiya H, Macak J M, Ghicov A, Räder A S, Taveira L and Schmuki P 2007 Characterization of electronic properties of TiO₂ nanotube films *Corros. Sci.* **49** 203–10
- [24] Pasikhani J V, Gilani N and Pirbazari A E 2018 Improvement the wastewater purification by TiO₂ nanotube arrays: the effect of etching-step on the photo-generated charge carriers and photocatalytic activity of anodic TiO₂ nanotubes *Solid State Sci.* **84** 57–74
- [25] Chiarello G L, Zuliani A, Ceresoli D, Martinazzo R and Selli E 2016 Exploiting the photonic crystal properties of TiO₂ nanotube arrays to enhance photocatalytic hydrogen production *ACS Catal.* **6** 1345–53
- [26] Chen X and Mao S S 2007 Titanium dioxide nanomaterials: synthesis, properties, modifications, and applications *Chem. Rev.* **107** 2891–959
- [27] Haryński Ł, Grochowska K, Kupracz P, Karczewski J, Coy E and Siuzdak K 2020 The in-depth studies of pulsed UV laser-modified TiO₂ nanotubes: the influence of geometry, crystallinity, and processing parameters *Nanomaterials* **10** 430
- [28] Uhlig I, Szargan R, Nesbitt H W and Laajalehto K 2001 Surface states and reactivity of pyrite and marcasite *Appl. Surf. Sci.* **179** 222–9
- [29] Biesinger M C, Payne B P, Grosvenor A P, Lau L W M, Gerson A R and Smart R S C 2011 Resolving surface chemical states in XPS analysis of first row transition metals, oxides and hydroxides: Cr, Mn, Fe, Co and Ni *Appl. Surf. Sci.* **257** 2717–30
- [30] Graat P C J and Somers M A J 1996 Simultaneous determination of composition and thickness of thin iron-oxide films from XPS Fe 2p spectra *Appl. Surf. Sci.* **100–101** 36–40
- [31] Wu C-K, Yin M, O'Brien S and Koberstein J T 2006 Quantitative analysis of copper oxide nanoparticle composition and structure by x-ray photoelectron spectroscopy *Chem. Mater.* **18** 6054–8
- [32] Khan M A, Nayan N, Shadiullah S, Ahmad M K and Soon C F 2020 Surface study of CuO nanopetals by advanced nanocharacterization techniques with enhanced optical and catalytic properties *Nanomaterials* **10** 1298
- [33] Pourbaix M 1974 *Atlas of Electrochemical Equilibria in Aqueous Solutions* (Houston, Texas: National Association of Corrosion Engineers (NACE))
- [34] Dionigi F et al 2020 *In-situ* structure and catalytic mechanism of NiFe and CoFe layered double hydroxides during oxygen evolution *Nat. Commun.* **11** 2522
- [35] Chen T-Y, Vedhanarayanan B, Lin S-Y, Shao L-D, Sofer Z, Lin J-Y and Lin T-W 2020 Electrodeposited NiSe on a forest of carbon nanotubes as a free-standing electrode for hybrid supercapacitors and overall water splitting *J. Colloid Interface Sci.* **574** 300–11
- [36] Coronado J M and Hernández-Alonso M D 2013 The keys of success: TiO₂ as a benchmark photocatalyst *Design of Advanced Photocatalytic Materials for Energy and Environmental Applications* ed J M Coronado et al (London: Springer London) pp 85–101
- [37] Kobayashi S and Ichimura M 2018 Electrochemical deposition of Cu-doped p-type iron oxide thin films *Semicond. Sci. Technol.* **33** 105006
- [38] Xiong L, Huang S, Yang X, Qiu M, Chen Z and Yu Y 2011 p-type and n-type Cu₂O semiconductor thin films: controllable preparation by simple solvothermal method and photoelectrochemical properties *Electrochim. Acta* **56** 2735–9
- [39] Vladimirova S, Krivetskiy V, Rumyantseva M, Gaskov A, Mordvinova N, Lebedev O, Martyshev M and Forsh P 2017 Co₃O₄ as p-type material for CO sensing in humid air *Sensors* **17** 2216
- [40] Irwin M D, Buchholz D B, Hains A W, Chang R P H and Marks T J 2008 p-type semiconducting nickel oxide as an efficiency-enhancing anode interfacial layer in polymer bulk-heterojunction solar cells *Proc. Natl Acad. Sci.* **105** 2783–7
- [41] Yan Z, Liu H, Hao Z, Yu M, Chen X and Chen J 2020 Electrodeposition of (hydro)oxides for an oxygen evolution electrode *Chem. Sci.* **11** 10614–25

Summary

The presented cycle of publications contains a comprehensive study of all the synthesis steps required to create an efficient electrode for water electrolysis. The mechanism of nanotube formation as well as the most important factors determining nanotube growth were given in chapter one. Furthermore, based on the available literature data, an optimal electrolyte composition was designed to yield titania nanotubes with a distinct spacing between them. Attachment 1 showcases the influence of the anodization voltage on the size and spatial distribution of the titania nanotubes. The linear voltamperograms revealed that the structures showing the most photoactivity were anodized at 40 V, which was also the point where absorbance, optical bandgap, and flat-band potential have all reached a plateau. Furthermore, a first hint of the self-induced oxygen vacancies created during anodization was found [66] in the form of shallow surface states which were filled by polarizing the sample under simulated solar radiation.

Chapter two describes the mechanism of light absorption and discusses the effects of the nanosecond laser interactions with matter. In Attachment 2, the effects of three wavelengths of pulsed laser radiation on the anodized titania nanotubes are shown. Although the 532 nm radiation did not induce any meaningful changes in the investigated fluence range, the irradiation with both 266 and 355 nm result in the melting of the topmost part of the nanotubes. The absorption and photoluminescence spectra suggest that the majority of the changes happen at the 20 mJ/cm² mark and indicate an elevated number of oxygen vacancies in the material post-treatment [6,32,43]. Their presence did not, however, translate into higher photoactivity as indicated in Figure 4. Nonetheless,

work two presents an innovative method of creating multi-purpose hollow titania nanopillars from the spaced TiO₂ nanotube arrays.

Chapter three points out the importance of developing novel electrode materials for water electrolysis, describes the principles of efficient water-splitting electrodes, and outlines the most important factors affecting their performance. Work three (Attachment 3) investigated the properties of the TiO₂ nanotube-based electrode covered with metallic nickel and irradiated with various fluences of 355 nm pulsed laser. Although no improvement towards oxygen evolution reaction was detected after sputtering nickel, it was significant after laser irradiation. Consistently with work two, the most notable changes were induced at the 20 mJ/cm² mark. The structural analysis has revealed that in the best-performing sample sputtered nickel transformed into nickel oxide and oxyhydroxide, which can be responsible for improved reaction kinetics [46]. Work four (Attachment 4) included an investigation of hydrogen- as well as oxygen evolution mechanisms and included four sputtered metal species (Fe, Co, Ni, and Cu), all of which can form metal oxyhydroxides. However, the investigation revealed that only the cobalt- and nickel-covered electrodes have shown improvements toward OER. They are also the only metal oxides showing intrinsic p-type conductivity, contrary to the titanium, iron, and copper oxides [60–64]. Therefore, a new mechanism has been proposed based on a depleted p-n junction, where the sputtered cobalt and nickel oxides serve as a depleted p-type region. It creates a potential difference between them and the n-type titania underneath, forcing electrons to diffuse into the electrode and away from the electrolyte. Furthermore, the depletion of the electrode surface lowers the adsorption energy of the negatively charged (OH⁻) groups, allowing them to bind more easily. The depleted p-n junction theory explains both the laser-induced improvements toward the OER and the lower efficiency in HER. Furthermore, as the number of p- and n-type

carriers is dependent on the number of oxygen vacancies in the metal oxides, it explains the relation between laser fluence used for modification and the electrodes' performance.

Overall, the presented cycle of publications encompasses all of the processing steps necessary to create a titania-based electrode for water electrolysis. It takes into the account geometrical complexity of the substrate, laser interactions with titania, and mechanisms responsible for water-splitting. The established theory agrees with all the experimental data and can be used to further improve existing electrode materials, using already widely utilized technologies.

List of references

1. Tang, H.; Berger, H.; Schmid, P.E.; Lévy, F.; Burri, G. Photoluminescence in TiO₂ Anatase Single Crystals. *Solid State Communications* **1993**, *87*, 847–850, doi:10.1016/0038-1098(93)90427-O.
2. Shan, C.X.; Hou, X.; Choy, K.-L. Corrosion Resistance of TiO₂ Films Grown on Stainless Steel by Atomic Layer Deposition. *Surface and Coatings Technology* **2008**, *202*, 2399–2402, doi:10.1016/j.surfcoat.2007.08.066.
3. Wang, Y.; Wen, C.; Hodgson, P.; Li, Y. Biocompatibility of TiO₂ Nanotubes with Different Topographies. *J. Biomed. Mater. Res.* **2014**, *102*, 743–751, doi:10.1002/jbm.a.34738.
4. Roy, P.; Kim, D.; Lee, K.; Spiecker, E.; Schmuki, P. TiO₂ Nanotubes and Their Application in Dye-Sensitized Solar Cells. *Nanoscale* **2010**, *2*, 45–59, doi:10.1039/B9NR00131J.
5. Assefpour-Dezfuly, M.; Vlachos, C.; Andrews, E.H. Oxide Morphology and Adhesive Bonding on Titanium Surfaces. *J Mater Sci* **1984**, *19*, 3626–3639, doi:10.1007/BF02396935.
6. Pasikhani, J.V.; Gilani, N.; Pirbazari, A.E. Improvement the Wastewater Purification by TiO₂ Nanotube Arrays: The Effect of Etching-Step on the Photo-Generated Charge Carriers and Photocatalytic Activity of Anodic TiO₂ Nanotubes. *Solid State Sciences* **2018**, *84*, 57–74, doi:10.1016/j.solidstatesciences.2018.08.003.
7. Ghicov, A.; Albu, S.P.; Hahn, R.; Kim, D.; Stergiopoulos, T.; Kunze, J.; Schiller, C.-A.; Falaras, P.; Schmuki, P. TiO₂ Nanotubes in Dye-Sensitized Solar Cells: Critical Factors for the Conversion Efficiency. *Chem. Asian J.* **2009**, *4*, 520–525, doi:10.1002/asia.200800441.
8. Ma, M.; Kazemzadeh-Narbat, M.; Hui, Y.; Lu, S.; Ding, C.; Chen, D.D.Y.; Hancock, R.E.W.; Wang, R. Local Delivery of Antimicrobial Peptides Using Self-Organized TiO₂ Nanotube Arrays for Peri-Implant Infections. *J. Biomed. Mater. Res.* **2012**, *100A*, 278–285, doi:10.1002/jbm.a.33251.
9. Ali, S.; Granbohm, H.; Lahtinen, J.; Hannula, S.-P. Titania Nanotubes Prepared by Rapid Breakdown Anodization for Photocatalytic Decolorization of Organic Dyes

- under UV and Natural Solar Light. *Nanoscale Res Lett* **2018**, *13*, 179, doi:10.1186/s11671-018-2591-5.
10. Galstyan, V.; Vomiero, A.; Comini, E.; Faglia, G.; Sberveglieri, G. TiO₂ Nanotubular and Nanoporous Arrays by Electrochemical Anodization on Different Substrates. *RSC Adv.* **2011**, *1*, 1038, doi:10.1039/c1ra00077b.
 11. Zhang, J.; Huang, W.; Zhang, K.; Li, D.; Xu, H.; Zhu, X. Bamboo Shoot Nanotubes with Diameters Increasing from Top to Bottom: Evidence against the Field-Assisted Dissolution Equilibrium Theory. *Electrochemistry Communications* **2019**, *100*, 48–51, doi:10.1016/j.elecom.2019.01.019.
 12. Zhao, S.; Lu, S.; Cui, H.; Yu, D.; Zhang, S.; Kong, J.; Zhu, X. A Mathematical Model for the Growth of Anodic TiO₂ Nanotubes under Higher Current Density. *J. Electrochem. Soc.* **2017**, *164*, E401–E407, doi:10.1149/2.1131713jes.
 13. Jin, R.; Fan, H.; Liu, Y.; Ma, W.; Lu, H.; Yang, P.; Ma, W. Formation Mechanism of Lotus-Root-Shaped Nanostructure during Two-Step Anodization. *Electrochimica Acta* **2016**, *188*, 421–427, doi:10.1016/j.electacta.2015.12.027.
 14. Gong, T.; Li, C.; Li, X.; Yue, H.; Zhu, X.; Zhao, Z.; Lv, R.; Zhu, J. Evidence of Oxygen Bubbles Forming Nanotube Embryos in Porous Anodic Oxides. *Nanoscale Adv.* **2021**, *3*, 4659–4668, doi:10.1039/D1NA00389E.
 15. Lu, H.; Fan, H.; Jin, R.; Chong, B.; Shen, X.; Yan, S.; Zhu, X. Formation and Morphology Evolution of Anodic TiO₂ Nanotubes under Negative Pressure. *Electrochimica Acta* **2016**, *215*, 380–387, doi:10.1016/j.electacta.2016.08.128.
 16. Siuzdak, K.; Haryński, Ł.; Wawrzyniak, J.; Kupracz, P.; Grochowska, K. Self-Standing Nanoarchitectures. In *Self-standing Substrates*; Inamuddin, Boddula, R., Asiri, A.M., Eds.; Springer International Publishing: Cham, 2020; pp. 1–56 ISBN 978-3-030-29521-9.
 17. Regonini, D.; Bowen, C.R.; Jaroenworarluck, A.; Stevens, R. A Review of Growth Mechanism, Structure and Crystallinity of Anodized TiO₂ Nanotubes. *Materials Science and Engineering: R: Reports* **2013**, *74*, 377–406, doi:10.1016/j.mser.2013.10.001.
 18. Paulose, M.; Prakasam, H.E.; Varghese, O.K.; Peng, L.; Popat, K.C.; Mor, G.K.; Desai, T.A.; Grimes, C.A. TiO₂ Nanotube Arrays of 1000 Mm Length by Anodization of Titanium Foil: Phenol Red Diffusion. *J. Phys. Chem. C* **2007**, *111*, 14992–14997, doi:10.1021/jp075258r.

19. Cui, L.; Hui, K.N.; Hui, K.S.; Lee, S.K.; Zhou, W.; Wan, Z.P.; Thuc, C.-N.H. Facile Microwave-Assisted Hydrothermal Synthesis of TiO₂ Nanotubes. *Materials Letters* **2012**, *75*, 175–178, doi:10.1016/j.matlet.2012.02.004.
20. Albu, S.P.; Ghicov, A.; Macak, J.M.; Schmuki, P. 250 Mm Long Anodic TiO₂ Nanotubes with Hexagonal Self-Ordering. *phys. stat. sol. (RRL)* **2007**, *1*, R65–R67, doi:10.1002/pssr.200600069.
21. Xiang, C.; Sun, L.; Wang, Y.; Wang, G.; Zhao, X.; Zhang, S. Large-Scale, Uniform, and Superhydrophobic Titania Nanotubes at the Inner Surface of 1000 Mm Long Titanium Tubes. *J. Phys. Chem. C* **2017**, *121*, 15448–15455, doi:10.1021/acs.jpcc.7b03124.
22. Gong, D.; Grimes, C.A.; Varghese, O.K.; Hu, W.; Singh, R.S.; Chen, Z.; Dickey, E.C. Titanium Oxide Nanotube Arrays Prepared by Anodic Oxidation. *Journal of Materials Research* **2001**, *16*, 3331–3334, doi:10.1557/JMR.2001.0457.
23. Taveira, L.; Macak, J.; Tsuchiya, H.; Dick, L.; Schmuki, P. Initiation and Growth of Self-Organized TiO₂ Nanotubes Anodically Formed in NH₄F/(NH₄)₂SO₄ Electrolytes. *Journal of the Electrochemical Society* **2005**, *152*, B405–B410.
24. Shankar, K.; Mor, G.K.; Prakasam, H.E.; Yoriya, S.; Paulose, M.; Varghese, O.K.; Grimes, C.A. Highly-Ordered TiO₂ Nanotube Arrays up to 220 Mm in Length: Use in Water Photoelectrolysis and Dye-Sensitized Solar Cells. *Nanotechnology* **2007**, *18*, 065707, doi:10.1088/0957-4484/18/6/065707.
25. Binns, C. *Introduction to Nanoscience and Nanotechnology: Introduction to Nanoscience*; John Wiley & Sons, Inc.: Hoboken, NJ, USA, 2010; ISBN 978-0-470-61883-7.
26. Ozkan, S.; Mazare, A.; Schmuki, P. Critical Parameters and Factors in the Formation of Spaced TiO₂ Nanotubes by Self-Organizing Anodization. *Electrochimica Acta* **2018**, *268*, 435–447, doi:10.1016/j.electacta.2018.02.120.
27. Ozkan, S.; Nguyen, N.T.; Mazare, A.; Cerri, I.; Schmuki, P. Controlled Spacing of Self-Organized Anodic TiO₂ Nanotubes. *Electrochemistry Communications* **2016**, *69*, 76–79, doi:10.1016/j.elecom.2016.06.004.
28. Nguyen, N.T.; Ozkan, S.; Hwang, I.; Zhou, X.; Schmuki, P. Spaced TiO₂ Nanotube Arrays Allow for a High Performance Hierarchical Supercapacitor Structure. *J. Mater. Chem. A* **2017**, *5*, 1895–1901, doi:10.1039/C6TA10179H.
29. Kaselouris, E.; Nikolos, I.K.; Orphanos, Y.; Bakarezos, E.; Papadogiannis, N.A.; Tatarakis, M.; Dimitriou, V. A Review of Simulation Methods of Laser Matter

- Interactions Focused on Nanosecond Laser Pulsed Systems. *J. Multiscale Modelling* **2013**, *05*, 1330001, doi:10.1142/S1756973713300013.
30. Pelant, I.; Valenta, J. *Luminescence Spectroscopy of Semiconductors*; Oxford University Press, 2012; ISBN 978-0-19-958833-6.
 31. Hannay, N.B.; Colombo, U. *Electronic Materials*; Springer US: Boston, MA, 1973; ISBN 978-1-4615-6890-2.
 32. Brown, M.S.; Arnold, C.B. Fundamentals of Laser-Material Interaction and Application to Multiscale Surface Modification. In *Laser Precision Microfabrication*; Sugioka, K., Meunier, M., Piqué, A., Eds.; Springer Series in Materials Science; Springer Berlin Heidelberg: Berlin, Heidelberg, 2010; Vol. 135, pp. 91–120 ISBN 978-3-642-10522-7.
 33. Steen, W.M.; Mazumder, J. *Laser Material Processing*; Springer London: London, 2010; ISBN 978-1-84996-061-8.
 34. Van Overschelde, O.; Wautelet, M. Diffraction-Aided Laser-Induced Microstructuring of Thin TiO₂ Films on Glass. *Appl. Phys. Lett.* **2006**, *89*, 161114, doi:10.1063/1.2364462.
 35. Kim, J.; Kim, J.; Lee, M. Laser Welding of Nanoparticulate TiO₂ and Transparent Conducting Oxide Electrodes for Highly Efficient Dye-Sensitized Solar Cell. *Nanotechnology* **2010**, *21*, 345203, doi:10.1088/0957-4484/21/34/345203.
 36. Liu, Y.; Zhu, B.; Wang, L.; Dai, Y.; Ma, H.; Lakshminarayana, G.; Qiu, J. Femtosecond Laser Direct Writing of TiO₂ Crystalline Patterns in Glass. *Appl. Phys. B* **2008**, *93*, 613–617, doi:10.1007/s00340-008-3166-4.
 37. Ardakani, H.K. Electrical and Optical Properties of in Situ “Hydrogen-Reduced” Titanium Dioxide Thin Films Deposited by Pulsed Excimer Laser Ablation. *Thin Solid Films* **1994**, *248*, 234–239, doi:10.1016/0040-6090(94)90017-5.
 38. Hsu, M.-Y.; Van Thang, N.; Wang, C.; Leu, J. Structural and Morphological Transformations of TiO₂ Nanotube Arrays Induced by Excimer Laser Treatment. *Thin Solid Films* **2012**, *520*, 3593–3599, doi:10.1016/j.tsf.2011.12.036.
 39. Haryński, Ł.; Grochowska, K.; Kupracz, P.; Karczewski, J.; Coy, E.; Siuzdak, K. The In-Depth Studies of Pulsed UV Laser-Modified TiO₂ Nanotubes: The Influence of Geometry, Crystallinity, and Processing Parameters. *Nanomaterials* **2020**, *10*, 430, doi:10.3390/nano10030430.
 40. Xu, Y.; Melia, M.A.; Tsui, L.; Fitz-Gerald, J.M.; Zangari, G. Laser-Induced Surface Modification at Anatase TiO₂ Nanotube Array Photoanodes for

- Photoelectrochemical Water Oxidation. *J. Phys. Chem. C* **2017**, *121*, 17121–17128, doi:10.1021/acs.jpcc.7b05368.
41. Haryński, Ł.; Grochowska, K.; Karczewski, J.; Ryl, J.; Siuzdak, K. Scalable Route toward Superior Photoresponse of UV-Laser-Treated TiO₂ Nanotubes. *ACS Appl. Mater. Interfaces* **2020**, *12*, 3225–3235, doi:10.1021/acsami.9b19206.
 42. Chiarello, G.L.; Zuliani, A.; Ceresoli, D.; Martinazzo, R.; Selli, E. Exploiting the Photonic Crystal Properties of TiO₂ Nanotube Arrays To Enhance Photocatalytic Hydrogen Production. *ACS Catal.* **2016**, *6*, 1345–1353, doi:10.1021/acscatal.5b02817.
 43. Sarkar, A.; Khan, G.G. The Formation and Detection Techniques of Oxygen Vacancies in Titanium Oxide-Based Nanostructures. *Nanoscale* **2019**, *11*, 3414–3444, doi:10.1039/C8NR09666J.
 44. Ritchie, H.; Roser, M. CO₂ and Greenhouse Gas Emissions Available online: <https://ourworldindata.org/greenhouse-gas-emissions> (accessed on 22 February 2022).
 45. Chen, S.; Wang, L.-W. Thermodynamic Oxidation and Reduction Potentials of Photocatalytic Semiconductors in Aqueous Solution. *Chem. Mater.* **2012**, *24*, 3659–3666, doi:10.1021/cm302533s.
 46. Xu, Z.J. Transition Metal Oxides for Water Oxidation: All about Oxyhydroxides? *Sci. China Mater.* **2020**, *63*, 3–7, doi:10.1007/s40843-019-9588-5.
 47. Ha, Y.; Shi, L.; Chen, Z.; Wu, R. Phase-Transited Lysozyme-Driven Formation of Self-Supported Co₃O₄@C Nanomeshes for Overall Water Splitting. *Adv. Sci.* **2019**, 1900272, doi:10.1002/advs.201900272.
 48. Chi, K.; Tian, X.; Wang, Q.; Zhang, Z.; Zhang, X.; Zhang, Y.; Jing, F.; Lv, Q.; Yao, W.; Xiao, F.; et al. Oxygen Vacancies Engineered CoMoO₄ Nanosheet Arrays as Efficient Bifunctional Electrocatalysts for Overall Water Splitting. *Journal of Catalysis* **2020**, *381*, 44–52, doi:10.1016/j.jcat.2019.10.025.
 49. Zhang, Y.; Fu, J.; Zhao, H.; Jiang, R.; Tian, F.; Zhang, R. Tremella-like Ni₃S₂/MnS with Ultrathin Nanosheets and Abundant Oxygen Vacancies Directly Used for High Speed Overall Water Splitting. *Applied Catalysis B: Environmental* **2019**, *257*, 117899, doi:10.1016/j.apcatb.2019.117899.
 50. Yao, N.; Li, P.; Zhou, Z.; Meng, R.; Cheng, G.; Luo, W. Nitrogen Engineering on 3D Dandelion-Flower-Like CoS₂ for High-Performance Overall Water Splitting. *Small* **2019**, *15*, 1901993, doi:10.1002/smll.201901993.

51. Lin, J.; Wang, P.; Wang, H.; Li, C.; Si, X.; Qi, J.; Cao, J.; Zhong, Z.; Fei, W.; Feng, J. Defect-Rich Heterogeneous MoS₂/NiS₂ Nanosheets Electrocatalysts for Efficient Overall Water Splitting. *Adv. Sci.* **2019**, *6*, 1900246, doi:10.1002/advs.201900246.
52. Liu, C.; Jia, D.; Hao, Q.; Zheng, X.; Li, Y.; Tang, C.; Liu, H.; Zhang, J.; Zheng, X. P-Doped Iron–Nickel Sulfide Nanosheet Arrays for Highly Efficient Overall Water Splitting. *ACS Appl. Mater. Interfaces* **2019**, *11*, 27667–27676, doi:10.1021/acsami.9b04528.
53. Corrigan, D.A. The Catalysis of the Oxygen Evolution Reaction by Iron Impurities in Thin Film Nickel Oxide Electrodes. *J. Electrochem. Soc.* **1987**, *134*, 377–384, doi:10.1149/1.2100463.
54. Kibria, M. Electrochemical Studies of the Nickel Electrode for the Oxygen Evolution Reaction. *International Journal of Hydrogen Energy* **1996**, *21*, 179–182, doi:10.1016/0360-3199(95)00066-6.
55. Song, F.; Busch, M.M.; Lassalle-Kaiser, B.; Hsu, C.-S.; Petkucheva, E.; Bensimon, M.; Chen, H.M.; Corminboeuf, C.; Hu, X. An Unconventional Iron Nickel Catalyst for the Oxygen Evolution Reaction. *ACS Cent. Sci.* **2019**, *5*, 558–568, doi:10.1021/acscentsci.9b00053.
56. Domaschke, M.; Zhou, X.; Wergen, L.; Romeis, S.; Miehlich, M.E.; Meyer, K.; Peukert, W.; Schmuki, P. Magnéli-Phases in Anatase Strongly Promote Cocatalyst-Free Photocatalytic Hydrogen Evolution. *ACS Catal.* **2019**, *9*, 3627–3632, doi:10.1021/acscatal.9b00578.
57. Wang, Y.; Liang, Z.; Zheng, H.; Cao, R. Recent Progress on Defect-rich Transition Metal Oxides and Their Energy-Related Applications. *Chem. Asian J.* **2020**, *15*, 3717–3736, doi:10.1002/asia.202000925.
58. Xiong, X.; Cai, Z.; Zhou, D.; Zhang, G.; Zhang, Q.; Jia, Y.; Duan, X.; Xie, Q.; Lai, S.; Xie, T.; et al. A Highly-Efficient Oxygen Evolution Electrode Based on Defective Nickel-Iron Layered Double Hydroxide. *Sci. China Mater.* **2018**, *61*, 939–947, doi:10.1007/s40843-017-9214-9.
59. Wawrzyniak, J.; Grochowska, K.; Karczewski, J.; Kupracz, P.; Ryl, J.; Dołęga, A.; Siuzdak, K. The Geometry of Free-Standing Titania Nanotubes as a Critical Factor Controlling Their Optical and Photoelectrochemical Performance. *Surface and Coatings Technology* **2020**, *389*, 125628, doi:10.1016/j.surfcoat.2020.125628.
60. Coronado, J.M.; Hernández-Alonso, M.D. The Keys of Success: TiO₂ as a Benchmark Photocatalyst. In *Design of Advanced Photocatalytic Materials for*

Energy and Environmental Applications; Coronado, J.M., Fresno, F., Hernández-Alonso, M.D., Portela, R., Eds.; Green Energy and Technology; Springer London: London, 2013; pp. 85–101 ISBN 978-1-4471-5060-2.

61. Kobayashi, S.; Ichimura, M. Electrochemical Deposition of Cu-Doped p-Type Iron Oxide Thin Films. *Semicond. Sci. Technol.* **2018**, *33*, 105006, doi:10.1088/1361-6641/aad76a.
62. Xiong, L.; Huang, S.; Yang, X.; Qiu, M.; Chen, Z.; Yu, Y. P-Type and n-Type Cu₂O Semiconductor Thin Films: Controllable Preparation by Simple Solvothermal Method and Photoelectrochemical Properties. *Electrochimica Acta* **2011**, *56*, 2735–2739, doi:10.1016/j.electacta.2010.12.054.
63. Vladimirova, S.; Krivetskiy, V.; Rumyantseva, M.; Gaskov, A.; Mordvinova, N.; Lebedev, O.; Martyshov, M.; Forsh, P. Co₃O₄ as p-Type Material for CO Sensing in Humid Air. *Sensors* **2017**, *17*, 2216, doi:10.3390/s17102216.
64. Irwin, M.D.; Buchholz, D.B.; Hains, A.W.; Chang, R.P.H.; Marks, T.J. P-Type Semiconducting Nickel Oxide as an Efficiency-Enhancing Anode Interfacial Layer in Polymer Bulk-Heterojunction Solar Cells. *Proceedings of the National Academy of Sciences* **2008**, *105*, 2783–2787, doi:10.1073/pnas.0711990105.
65. Yan, Z.; Liu, H.; Hao, Z.; Yu, M.; Chen, X.; Chen, J. Electrodeposition of (Hydro)Oxides for an Oxygen Evolution Electrode. *Chem. Sci.* **2020**, *11*, 10614–10625, doi:10.1039/D0SC01532F.
66. Mueller, D.N.; Machala, M.L.; Bluhm, H.; Chueh, W.C. Redox Activity of Surface Oxygen Anions in Oxygen-Deficient Perovskite Oxides during Electrochemical Reactions. *Nat Commun* **2015**, *6*, 6097, doi:10.1038/ncomms7097.

Statements of contribution

mgr inż. Jakub Wawrzyniak
Physical Aspects of EcoEnergy Department
Institute of Fluid-Flow Machinery
Polish Academy of Sciences
jwawrzyniak@imp.gda.pl

Statement of contribution

In the article

- Wawrzyniak, J.; Grochowska, K.; Karczewski, J.; Kupracz, P.; Ryl, J.; Dołęga, A.; Siuzdak, K. *The Geometry of Free-Standing Titania Nanotubes as a Critical Factor Controlling Their Optical and Photoelectrochemical Performance*. Surface and Coatings Technology 2020, 389, 125628, doi:10.1016/j.surfcoat.2020.125628.

I have planned the experiment, optimized the contents of the electrolyte, and synthesized titania nanostructures. Furthermore, I have performed the Raman, UV-vis, and electrochemical measurements. I was responsible for the description of the physical properties of the titania nanostructures and estimating their surface area. I have also prepared most of the graphical contents of the manuscript, written the majority of the manuscript and most of the revision.

In the article

- Wawrzyniak, J.; Karczewski, J.; Kupracz, P.; Grochowska, K.; Coy, E.; Mazikowski, A.; Ryl, J.; Siuzdak, K. *Formation of the Hollow Nanopillar Arrays through the Laser-Induced Transformation of TiO₂ Nanotubes*. Sci Rep 2020, 10, 20235, doi:10.1038/s41598-020-77309-2.

I have planned parts of the experiment, synthesized the substrates with titania nanotubes, and performed their laser modification. I have performed UV-vis measurements and described the physical properties of the obtained structures in the manuscript. I have also prepared all of the figures and written most of the revision.

In the article

- Wawrzyniak, J.; Karczewski, J.; Coy, E.; Iatsunskyi, I.; Ryl, J.; Gazda, M.; Grochowska, K.; Siuzdak, K. *Spectacular Oxygen Evolution Reaction Enhancement*

through Laser Processing of the Nickel-Decorated Titania Nanotubes. Adv. Mater. Interfaces 2021, 8, 2001420, doi:10.1002/admi.202001420.

I have planned parts of the experiment, synthesized the substrates, and performed the UV-vis and electrochemical measurements. I have analyzed the results, prepared all of the graphical content of the manuscript, written the manuscript, and the majority of the revision.

In the article

- Wawrzyniak, J.; Karczewski, J.; Coy, E.; Ryl, J.; Grochowska, K.; Siuzdak, K. *Nanostructure of the Laser-Modified Transition Metal Nanocomposites for Water Splitting*. Nanotechnology 2022, 33, 205401, doi:10.1088/1361-6528/ac512a.

I have planned parts of the experiment, synthesized the electrodes, performed UV-vis, Raman, and electrochemical experiments. I have analyzed the results and proposed the mechanism responsible for the observed effects, which include the role of the deposited metal species and laser modification. I have prepared all of the graphical content of the manuscript, written the manuscript, and the revision.

J. Wawrzyniak

Gdansk, 22.04.2022

dr hab. Katarzyna Grochowska
Physical Aspects of EcoEnergy Department
Institute of Fluid-Flow Machinery
Polish Academy of Sciences
kgrochowska@imp.gda.pl

Statement of contribution

In the article

- Wawrzyniak, J.; Grochowska, K.; Karczewski, J.; Kupracz, P.; Ryl, J.; Dołęga, A.; Siuzdak, K. *The Geometry of Free-Standing Titania Nanotubes as a Critical Factor Controlling Their Optical and Photoelectrochemical Performance*. Surface and Coatings Technology 2020, 389, 125628, doi:10.1016/j.surfcoat.2020.125628.

I took part in planning of the experiments and discussion of the results concerning the morphology, structural and optical properties of studied materials. I wrote part of the original draft and part of the response to reviewers with required revision of the manuscript.

In the articles

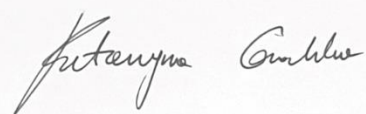
- Wawrzyniak, J.; Karczewski, J.; Kupracz, P.; Grochowska, K.; Coy, E.; Mazikowski, A.; Ryl, J.; Siuzdak, K. *Formation of the Hollow Nanopillar Arrays through the Laser-Induced Transformation of TiO₂ Nanotubes*. Sci Rep 2020, 10, 20235, doi:10.1038/s41598-020-77309-2.
- Wawrzyniak, J.; Karczewski, J.; Coy, E.; Iatsunskyi, I.; Ryl, J.; Gazda, M.; Grochowska, K.; Siuzdak, K. *Spectacular Oxygen Evolution Reaction Enhancement through Laser Processing of the Nickel-Decorated Titania Nanotubes*. Adv. Mater. Interfaces 2021, 8, 2001420, doi:10.1002/admi.202001420.

I took part in planning of the experiments and discussion of the results concerning the optical properties of studied materials and correction of the manuscript.

In the article

- Wawrzyniak, J.; Karczewski, J.; Coy, E.; Ryl, J.; Grochowska, K.; Siuzdak, K. *Nanostructure of the Laser-Modified Transition Metal Nanocomposites for Water Splitting*. Nanotechnology 2022, 33, 205401, doi:10.1088/1361-6528/ac512a.

I took part in the revision of the manuscript.

A handwritten signature in black ink, reading "Katarzyna Gmchwa". The signature is written in a cursive style with a large, stylized initial 'K'.

dr hab. inż. Jakub Karczewski
Institute of Nanotechnology and Materials Science
Gdańsk University of Technology
jakub.karczewski@pg.edu.pl

Statement of contribution

In the articles

- Wawrzyniak, J.; Grochowska, K.; Karczewski, J.; Kupracz, P.; Ryl, J.; Dołęga, A.; Siuzdak, K. *The Geometry of Free-Standing Titania Nanotubes as a Critical Factor Controlling Their Optical and Photoelectrochemical Performance*. Surface and Coatings Technology 2020, 389, 125628, doi:10.1016/j.surfcoat.2020.125628.
- Wawrzyniak, J.; Karczewski, J.; Coy, E.; Iatsunskyi, I.; Ryl, J.; Gazda, M.; Grochowska, K.; Siuzdak, K. *Spectacular Oxygen Evolution Reaction Enhancement through Laser Processing of the Nickel-Decorated Titania Nanotubes*. Adv. Mater. Interfaces 2021, 8, 2001420, doi:10.1002/admi.202001420.
- Wawrzyniak, J.; Karczewski, J.; Coy, E.; Ryl, J.; Grochowska, K.; Siuzdak, K. *Nanostructure of the Laser-Modified Transition Metal Nanocomposites for Water Splitting*. Nanotechnology 2022, 33, 205401, doi:10.1088/1361-6528/ac512a.

I have performed the SEM analysis.

In the article

- Wawrzyniak, J.; Karczewski, J.; Kupracz, P.; Grochowska, K.; Coy, E.; Mazikowski, A.; Ryl, J.; Siuzdak, K. *Formation of the Hollow Nanopillar Arrays through the Laser-Induced Transformation of TiO₂ Nanotubes*. Sci Rep 2020, 10, 20235, doi:10.1038/s41598-020-77309-2.

I have performed the SEM and XRD analysis.

dr hab. inż. Jacek Ryl, prof. GUT
Institute of Nanotechnology and Materials Science
Gdańsk University of Technology
jacryl@pg.edu.pl

Statement of contribution

In the articles

- Wawrzyniak, J.; Grochowska, K.; Karczewski, J.; Kupracz, P.; Ryl, J.; Dołęga, A.; Siuzdak, K. *The Geometry of Free-Standing Titania Nanotubes as a Critical Factor Controlling Their Optical and Photoelectrochemical Performance*. Surface and Coatings Technology 2020, 389, 125628, doi:10.1016/j.surfcoat.2020.125628.
- Wawrzyniak, J.; Karczewski, J.; Kupracz, P.; Grochowska, K.; Coy, E.; Mazikowski, A.; Ryl, J.; Siuzdak, K. *Formation of the Hollow Nanopillar Arrays through the Laser-Induced Transformation of TiO₂ Nanotubes*. Sci Rep 2020, 10, 20235, doi:10.1038/s41598-020-77309-2.
- Wawrzyniak, J.; Karczewski, J.; Coy, E.; Iatsunskyi, I.; Ryl, J.; Gazda, M.; Grochowska, K.; Siuzdak, K. *Spectacular Oxygen Evolution Reaction Enhancement through Laser Processing of the Nickel-Decorated Titania Nanotubes*. Adv. Mater. Interfaces 2021, 8, 2001420, doi:10.1002/admi.202001420.
- Wawrzyniak, J.; Karczewski, J.; Coy, E.; Ryl, J.; Grochowska, K.; Siuzdak, K. *Nanostructure of the Laser-Modified Transition Metal Nanocomposites for Water Splitting*. Nanotechnology 2022, 33, 205401, doi:10.1088/1361-6528/ac512a.

I have performed the XPS measurements coupled with the fitting procedure.



Signed by /
Podpisano przez:

Jacek Ryl
Politechnika
Gdańska

Date / Data:
2022-04-22 14:42

dr hab. inż. Emerson Coy, prof. UAM

NanoBioMedical Centre

Adam Mickiewicz University

coyeme@amu.edu.pl

Statement of contribution

In the articles

- Wawrzyniak, J.; Karczewski, J.; Kupracz, P.; Grochowska, K.; Coy, E.; Mazikowski, A.; Ryl, J.; Siuzdak, K. *Formation of the Hollow Nanopillar Arrays through the Laser-Induced Transformation of TiO₂ Nanotubes*. Sci Rep 2020, 10, 20235, doi:10.1038/s41598-020-77309-2.
- Wawrzyniak, J.; Karczewski, J.; Coy, E.; Iatsunskyi, I.; Ryl, J.; Gazda, M.; Grochowska, K.; Siuzdak, K. *Spectacular Oxygen Evolution Reaction Enhancement through Laser Processing of the Nickel-Decorated Titania Nanotubes*. Adv. Mater. Interfaces 2021, 8, 2001420, doi:10.1002/admi.202001420.

I have performed the HR-TEM-EDX measurements and analyzed the results.

In the article

- Wawrzyniak, J.; Karczewski, J.; Coy, E.; Ryl, J.; Grochowska, K.; Siuzdak, K. *Nanostructure of the Laser-Modified Transition Metal Nanocomposites for Water Splitting*. Nanotechnology 2022, 33, 205401, doi:10.1088/1361-6528/ac512a.

I have performed the HR-TEM-EDX and the GI-XRD measurements and analyzed the results.



Signed by /
Podpisano przez:
Luis Emerson Coy
Romero
Date / Data:
2022-04-22 14:25

dr inż. Piotr Kupracz
Physical Aspects of EcoEnergy Department
Institute of Fluid-Flow Machinery
Polish Academy of Sciences
pkupracz@imp.gda.pl

Statement of contribution

In the article

- Wawrzyniak, J.; Grochowska, K.; Karczewski, J.; Kupracz, P.; Ryl, J.; Dołęga, A.; Siuzdak, K. *The Geometry of Free-Standing Titania Nanotubes as a Critical Factor Controlling Their Optical and Photoelectrochemical Performance*. Surface and Coatings Technology 2020, 389, 125628, doi:10.1016/j.surfcoat.2020.125628.

I have reviewed the manuscript.

In the article

- Wawrzyniak, J.; Karczewski, J.; Kupracz, P.; Grochowska, K.; Coy, E.; Mazikowski, A.; Ryl, J.; Siuzdak, K. *Formation of the Hollow Nanopillar Arrays through the Laser-Induced Transformation of TiO₂ Nanotubes*. Sci Rep 2020, 10, 20235, doi:10.1038/s41598-020-77309-2.

I have performed the photoluminescence investigation.



Prof. Anna Dołęga
Department of Inorganic Chemistry
Gdańsk University of Technology
E-mail: anna.dolega@pg.edu.pl

Gdańsk, 22nd April 2022

Statement of contribution

In the article

- Wawrzyniak, J.; Grochowska, K.; Karczewski, J.; Kupracz, P.; Ryl, J.; Dołęga, A.; Siuzdak, K. *The Geometry of Free-Standing Titania Nanotubes as a Critical Factor Controlling Their Optical and Photoelectrochemical Performance*. Surface and Coatings Technology 2020, 389, 125628, doi:10.1016/j.surfcoat.2020.125628.

I have performed the FTIR measurements and took part in the analysis of the spectra.

Anna Dołęga

dr inż. Adam Mazikowski
Department of Metrology and Optoelectronics
Gdańsk University of Technology
adamazik@pg.edu.pl

Statement of contribution

In the article

- Wawrzyniak, J.; Karczewski, J.; Kupracz, P.; Grochowska, K.; Coy, E.; Mazikowski, A.; Ryl, J.; Siuzdak, K. *Formation of the Hollow Nanopillar Arrays through the Laser-Induced Transformation of TiO₂ Nanotubes*. Sci Rep 2020, 10, 20235, doi:10.1038/s41598-020-77309-2.

I have performed the colorimetric analysis.

Adam Mazikowski



Poznań, dnia 01.03.2022

dr hab Igor Iatsunskyi, prof. UAM

NanoBioMedical Centre

Adam Mickiewicz University

igoyat@amu.edu.pl

Statement of contribution

In the article

- Wawrzyniak, J.; Karczewski, J.; Coy, E.; Iatsunskyi, I.; Ryl, J.; Gazda, M.; Grochowska, K.; Siuzdak, K. *Spectacular Oxygen Evolution Reaction Enhancement through Laser Processing of the Nickel-Decorated Titania Nanotubes*. Adv. Mater. Interfaces 2021, 8, 2001420, doi:10.1002/admi.202001420.

I have assisted in the HR-TEM sample preparation and experiment.

 Igor Iatsunskyi

ul. Umultowska 85, 61-614 Poznań
NIP 777 00 06 350, REGON 000001293
tel. +48 61 829 6704, tel. /fax. +48 61 829 51 59
cnbmadm@amu.edu.pl

www.cnbm.amu.edu.pl

prof. dr hab. inż. Maria Gazda
Institute of Nanotechnology and Materials Science
Gdańsk University of Technology
maria.gazda@pg.edu.pl

Statement of contribution

In the article

- Wawrzyniak, J.; Karczewski, J.; Coy, E.; Iatsunskyi, I.; Ryl, J.; Gazda, M.; Grochowska, K.; Siuzdak, K. *Spectacular Oxygen Evolution Reaction Enhancement through Laser Processing of the Nickel-Decorated Titania Nanotubes*. Adv. Mater. Interfaces 2021, 8, 2001420, doi:10.1002/admi.202001420.

I have performed the XRD measurement and analysis.

M. Gazda

22. 04. 2022, Gdańsk

dr hab inż. Katarzyna Siuzdak, prof. IMP PAN
Physical Aspects of EcoEnergy Department
Institute of Fluid-Flow Machinery
Polish Academy of Sciences
ksiuzdak@imp.gda.pl

Statement of contribution

In the article

- Wawrzyniak, J.; Grochowska, K.; Karczewski, J.; Kupracz, P.; Ryl, J.; Dołęga, A.; Siuzdak, K. *The Geometry of Free-Standing Titania Nanotubes as a Critical Factor Controlling Their Optical and Photoelectrochemical Performance*. Surface and Coatings Technology 2020, 389, 125628, doi:10.1016/j.surfcoat.2020.125628.

I have planned the experiments, analyzed electrochemical results, written part of the manuscript and the revision. I have provided funding and guidance.

In the articles

- Wawrzyniak, J.; Karczewski, J.; Kupracz, P.; Grochowska, K.; Coy, E.; Mazikowski, A.; Ryl, J.; Siuzdak, K. *Formation of the Hollow Nanopillar Arrays through the Laser-Induced Transformation of TiO₂ Nanotubes*. Sci Rep 2020, 10, 20235, doi:10.1038/s41598-020-77309-2.
- Wawrzyniak, J.; Karczewski, J.; Coy, E.; Iatsunskyi, I.; Ryl, J.; Gazda, M.; Grochowska, K.; Siuzdak, K. *Spectacular Oxygen Evolution Reaction Enhancement through Laser Processing of the Nickel-Decorated Titania Nanotubes*. Adv. Mater. Interfaces 2021, 8, 2001420, doi:10.1002/admi.202001420.
- Wawrzyniak, J.; Karczewski, J.; Coy, E.; Ryl, J.; Grochowska, K.; Siuzdak, K. *Nanostructure of the Laser-Modified Transition Metal Nanocomposites for Water Splitting*. Nanotechnology 2022, 33, 205401, doi:10.1088/1361-6528/ac512a.

I took part in planning of the experiments and the analysis of the electrochemical results. I have provided funding and guidance. I have also reviewed the manuscripts.

dr hab. inż. Katarzyna Siuzdak
prof. IMP PAN

Katarzyna Siuzdak
Pracownik Kierownik
Materiałów Funkcjonalnych

Scientific contribution of the candidate

Research papers

1. **Wawrzyniak, J.**; Karczewski, J.; Coy, E.; Ryl, J.; Grochowska, K.; Siuzdak, K. Nanostructure of the Laser-Modified Transition Metal Nanocomposites for Water Splitting. *Nanotechnology* **2022**, 33, 205401, doi:10.1088/1361-6528/ac512a. IF = 3.874, 100 pkt.
2. **Wawrzyniak, J.**; Karczewski, J.; Coy, E.; Iatsunskyi, I.; Ryl, J.; Gazda, M.; Grochowska, K.; Siuzdak, K. Spectacular Oxygen Evolution Reaction Enhancement through Laser Processing of the Nickel-Decorated Titania Nanotubes. *Adv. Mater. Interfaces* **2021**, 8, 2001420, doi:10.1002/admi.202001420. IF = 6.147, 100 pkt.
3. **Wawrzyniak, J.**; Karczewski, J.; Kupracz, P.; Grochowska, K.; Coy, E.; Mazikowski, A.; Ryl, J.; Siuzdak, K. Formation of the Hollow Nanopillar Arrays through the Laser-Induced Transformation of TiO₂ Nanotubes. *Sci Rep* **2020**, 10, 20235, doi:10.1038/s41598-020-77309-2. IF = 4.379, 140 pkt.
4. **Wawrzyniak, J.**; Karczewski, J.; Ryl, J.; Grochowska, K.; Siuzdak, K. Laser-Assisted Synthesis and Oxygen Generation of Nickel Nanoparticles. *Materials* **2020**, 13, 4068, doi:10.3390/ma13184068. IF = 3.623, 140 pkt.
5. **Wawrzyniak, J.**; Grochowska, K.; Karczewski, J.; Kupracz, P.; Ryl, J.; Dołęga, A.; Siuzdak, K. The Geometry of Free-Standing Titania Nanotubes as a Critical Factor Controlling Their Optical and Photoelectrochemical Performance. *Surface and Coatings Technology* **2020**, 389, 125628, doi:10.1016/j.surfcoat.2020.125628. IF = 4.158, 100 pkt.
6. **Wawrzyniak, J.**; Karczewski, J.; Kupracz, P.; Grochowska, K.; Załęski, K.; Pshyk, O.; Coy, E.; Bartmański, M.; Szkodo, M.; Siuzdak, K. Laser-Assisted Modification of Titanium Dioxide Nanotubes in a Tilted Mode as Surface Modification and Patterning Strategy. *Applied Surface Science* **2020**, 508, 145143, doi:10.1016/j.apsusc.2019.145143. IF = 6.707, 140 pkt.

7. Pawłowski, Ł.; **Wawrzyniak, J.**; Banach-Kopeć, A.; Cieřlik, B.M.; Jurak, K.; Karczewski, J.; Tylingo, R.; Siuzdak, K.; Zieliński, A. Antibacterial Properties of Laser-Encapsulated Titanium Oxide Nanotubes Decorated with Nanosilver and Covered with Chitosan/Eudragit Polymers. *Biomaterials Advances* **2022**, *138*, 212950, doi:10.1016/j.bioadv.2022.212950. IF = 7.328, 140 pkt.
8. Kupracz, P.; Grochowska, K.; **Wawrzyniak, J.**; Siuzdak, K. The Interaction of the Pulsed Laser Irradiation with Titania Nanotubes - Theoretical Studies on the Thermal Effect. *International Journal of Thermal Sciences* **2021**, *162*, 106800, doi:10.1016/j.ijthermalsci.2020.106800. IF = 3.744, 140 pkt.
9. Siuzdak, K.; Haryński, Ł.; **Wawrzyniak, J.**; Grochowska, K. Review on Robust Laser Light Interaction with Titania – Patterning, Crystallisation and Ablation Processes. *Progress in Solid State Chemistry* **2020**, *62*, 100297, doi:10.1016/j.progsolidstchem.2020.100297. IF = 5.682, 200 pkt.
10. Kupracz, P.; Grochowska, K.; Karczewski, J.; **Wawrzyniak, J.**; Siuzdak, K. The Effect of Laser Re-Solidification on Microstructure and Photo-Electrochemical Properties of Fe-Decorated TiO₂ Nanotubes. *Materials* **2020**, *13*, 4019, doi:10.3390/ma13184019. IF = 3.623, 140 pkt.
11. Siuzdak, K.; Haryński, Ł.; **Wawrzyniak, J.**; Kupracz, P.; Grochowska, K. Self-Standing Nanoarchitectures. In *Self-standing Substrates*; Inamuddin, Boddula, R., Asiri, A.M., Eds.; Springer International Publishing: Cham, 2020; pp. 1–56 ISBN 978-3-030-29521-9. 80 pkt.

Conference appearances

1. Oral presentation *Laser-treated Transition Metal Oxides for Water Splitting*, Spring Meeting of the Materials Research Society, Honolulu 2022.
2. Oral presentation *Laser-based Modification of the Titania Nanotubes*, Spring Meeting of the European Materials Research Society, Online 2021.
3. Poster *Laser-modified TiO₂ Nanotube Arrays Decorated with Rare Earth Based Compounds – Towards Unique Marking*, Spring Meeting of the European Materials Research Society, Online 2021.
4. Oral presentation *Laser-modified Transition Metal Oxides for Water Splitting*, 29th Topical Meeting of the International Society of Electrochemistry, Online 2021
5. Poster *Pulsed Laser Treatment of the Amorphous Titania Nanotubes: Towards fast modification approach*, Nanophotonics and Micro/Nano Optics International Conference, Munich 2019

Patents and utility models

1. **Wawrzyniak, J.**; Grochowska, K.; Siuzdak, K. Utility model *Diode* no. 072509, 2022

Stipends and awards

1. PhD Scholarship of the IMP PAN for year 2020/2021
2. PhD Pro-quality Scholarship of the Gdańsk University of Technology 2020/2021
3. Rector's Scholarship for the best PhD Students of Gdańsk University of Technology 2020/2021
4. Young Scientist Award for oral presentation during 2021 Spring Meeting of the European Materials Research Society
5. PhD Scholarship of the IMP PAN for year 2021/2022
6. PhD Pro-quality Scholarship of the Gdańsk University of Technology 2021/2022
7. Rector's Scholarship for the best PhD Students of Gdańsk University of Technology 2021/2022